Dissertation

submitted to the
Combined Faculty of Natural Sciences and Mathematics
of the Ruperto Carola University Heidelberg, Germany
for the degree of
Doctor of Natural Sciences

Presented by
Steffie Revia, M.Sc.
Born in: Medan, Indonesia
Oral examination: 24th June 2020

KDM6A is an epigenetic gatekeeper of mTORC1 signaling in cancer

Referees: Prof. Dr. Ralf Bartenschlager

Dr. med. Darjus Felix Tschaharganeh

Summary

Kdm6a is a histone H3K27-specific demethylase and a component of the highly conserved MLL3/4-COMPASS-like complex. Genomic sequencing studies of human tumor samples revealed frequent deletions and/or loss-of-function mutations of Kdm6a in various human cancer types, suggesting an important role in tumorigenesis. Yet, despite its frequent alterations in human cancer, biological functions mediated by Kdm6a during malignant transformation and progression remain poorly understood.

To gain further insights to these questions, we generated mouse models with liver-specific deletion or downregulation of Kdm6a by CRISPR/Cas9 or inducible RNA-interference, respectively. Disruption of Kdm6a by both approaches led to formation of aggressive hepatocellular carcinomas (HCC) in a short time frame. Conversely, endogenous re-expression of Kdm6a in Kdm6a-deficient tumors significantly reduced tumor progression and prolonged survival *in vivo.*

Transcriptional profiling linked the apparent Kdm6a tumor suppressor activity to regulation of mTOR signaling and epigenetic profiling using Cut&Run analyses revealed control of Deptor and Tsc2, two known negative regulators of mTOR signaling, by Kdm6a. Interestingly, the observed expression changes occurred in the absence of changes in H3K27me3 deposition. Immediate biochemical validation reaffirmed aberrant up-regulation of mTORC1 signaling upon Kdm6a loss. mTOR activation appeared to be critical to suppress cell death as blunting mTOR signaling by Kdm6a re-expression promoted caspases-3/7 activation *in vitro* and *in vivo*. Notably, CRISPR-mediated Deptor deletion rescued the Kdm6a phenotype, while Deptor overexpression abrogated Kdm6a-induced liver tumorigenesis. Moreover, we also found a strong sensitivity of Kdm6a-deficent tumors to mTOR inhibitors. Finally, analyses of human HCCs showed a strong positive correlation between KDM6A and DEPTOR expression, further suggesting a direct relationship in human tumorigenesis. In addition, utilizing a pancreatic ductal adenocarcinoma (PDAC) mouse model we could demonstrate that shRNA-mediated silencing of Kdm6a synergizes with oncogenic $Kras^{G12D}$ to drive pancreatic tumor formation and we could recapitulate the tumor-suppressive function of Kdm6a via mTOR regulation this tumor model and tumor type.

Hence, our results link KDM6A-dependent epigenetic remodeling to mTOR signaling and provide a potential therapeutic strategy for KDM6A-deficient tumors.

Zusammenfassung

Kdm6a ist eine Histon-H3K27-spezifische Demethylase und Teil des hoch konservierten MLL3/4-COMPASS-like Komplexes. Jüngste Sequenzierungsdaten humaner Tumorproben verschiedener Krebsarten zeigten häufige Deletionen und Loss-of-Function-Mutationen von Kdm6a. Dies lässt auf eine wichtige Rolle von Kdm6a in der Tumorgenese schließen. Trotz der häufigen genomischen Veränderungen von Kdm6a in humanen Krebsarten ist seine biologische Funktion während der malignen Transformation und Progression noch immer unzureichend geklärt.

Zur genaueren Untersuchung wurden Mausmodelle generiert, um mittels CRISPR/Cas9 oder induzierbarer RNA-Interferenz leberspezifische Deletionen und Knockdowns von Kdm6a zu erzeugen. Beide Ansätze führten in relativ kurzer Zeit zur Entstehung aggressiver hepatozellulärer Karzinome (HCC). Wohingegen die endogene Re-Expression von Kdm6a in etablierten Kdm6a-defizienten Tumoren zu einem signifikanten Rückgang der Tumorprogression und längerem Überleben *in vivo* führte.

Durch die Untersuchung des transkriptionellen Profils konnte die tumorsuppressive Funktion von Kdm6a mit einer Suppression des mTOR Signalweges in Verbindung gebracht werden. Eine genauere Untersuchung des epigenetischen Profils durch Cut&Run-Analysen offenbarte eine Regulation von Deptor und Tsc2, zweier negativer Regulatoren des mTOR-Signalweges, durch Kdm6a. Interessanterweise fand die Kdm6a-vermittelte Regulation ohne Änderungen der H3K27me3-Einlagerung statt. Die sofortige biochemische Validierung bestätigte eine verstärkte Hochregulierung des mTOC1-Signalweges nach Verlust von Kdm6a. Die Aktivierung von mTOR scheint entscheiden zu sein, um den Zelltod zu unterdrücken, da die Herabregulierung von mTOR als Folge der Re-Expression von Kdm6a *in vitro* und *in vivo* die Aktivierung von Caspase-3/7 zur Folge hatte. Die CRISPR-vermittelte Deletion von Deptor führte zur Wiederherstellung des Kdm6a vermittelten Phänotyps, während die Überexpression von Deptor eine von Kdm6a verursachte Tumorgenese in der Leber verhinderte. Darüber hinaus konnten wir eine starke Anfälligkeit von KDM6A-defizienten Tumoren gegenüber mTOR-Inhibitoren feststellen. Letztlich zeigten Auswertungen von humanen HCCs eine starke positive Korrelation zwischen der Expression von KDM6A und DEPTOR, was einen direkten

Zusammenhang zur humanen Tumorgenese nahelegt. Zusätzlich konnte in einem Mausmodell für Pankreaskarzinome gezeigt werden, dass eine shRNA-vermittelte Suppression von Kdm6a zusammen mit onkogenem $Kras^{G12D}$ zur Bildung von Pankreastumoren führt, und dadurch die tumor-suppressive Funktion von Kdm6a via mTOR-Regulation in einem unabhängigen Tumormodell und -typ rekapitulieren.

Somit stellen unsere Ergebnisse einen neuen Zusammenhang zwischen KDM6A-abhängiger epigenetischer Remodellierung und dem mTOR-Signalweg da und zeigen neue Therapiemöglichkeiten für KDM6A-defiziente Tumoren auf.

Table of Contents

Summary i

Zusammenfassung iii

List of Figures viii

List of Tables x

List of Abbreviation xi

1. Introduction 1

1.1 Cancer is caused by genetic changes 1

1.1.1 Proto-oncogene activation 1

1.1.2 Tumor suppressor genes 3

1.2 Epigenetic regulation 3

1.2.1 Epigenetic alterations in cancer 4

1.2.2 MLL3/MLL4 COMPASS-like complex 7

1.2.3 The histone H3K27-demethylase KDM6A 9

1.3 Liver and mouse models of liver cancer 11

1.3.1 Liver physiology and pathology 11

1.3.2 Mouse models of liver cancer 13

1.4 Pancreas and mouse models of pancreatic cancer 15

1.4.1 Pancreas physiology and pathology 15

1.4.2 Mouse model of pancreatic cancer 16

2. Objective 19

3. Materials and Methods 20

3.1 Molecular cloning 20

3.1.1 CRISPR/Cas9 guide 21

3.1.2 Short hairpin RNA (shRNA) 21

3.2 Animal experiments 22

3.2.1 ESC-based pancreatic cancer 23

3.2.2 Magnetic Resonance Imaging (MRI) 23

3.3 Immunohistochemistry (IHC) 23
3.4 Derivation of primary liver tumor cell lines 24
3.5 Derivation of primary pancreatic tumor cell lines 24
3.6 Cell culture 25
3.7 Virus production 25
3.8 Transduction 25
3.9 Immunoblotting 26
3.17 Mutation detection by T7 assay 27
3.18 Clonogenic assay 27
3.19 Competition assay 28
3.20 Apoptosis assay 28
3.21 Drug treatment and cell viability assay 28
3.22 Quantitative reverse transcription PCR (qRT-PCR) 28
3.23 RNA sequencing and differential expression analysis 29
3.24 CUT&RUN 29
3.18 Human patient samples 30
3.18.1 Immunohistochemistry 31
3.18.2 Quantitative Reverse Transcription Real-Time PCR (qRT-PCR) 31
3.19 Cell lines, virus production for pooled CRISPR/Cas9 screening 31
3.19.1 Pooled CRISPR/Cas9 screening 32
4. Results 34
4.1 KDM6A cooperates with c-MYC to drive liver tumorigenesis 34
4.2 Sustained Kdm6a loss is important for liver tumor maintenance 38
4.3 Pro-apoptotic effect of Kdm6a 40
4.3.1 Endogenous Kdm6a re-expression induces apoptosis 40
4.3.2 Kdm6a overexpression cause apoptosis *in vitro* 42

4.4 Deciphering molecular function of Kdm6a as tumor suppressor 44
4.4.1 Loss of KDM6A leads to transcriptional and epigenetic changes 44
4.4.2 KDM6A-deficient cells show hyperactivation of mTORC1 signaling 47
4.4.3 Kdm6a regulates mTORC1 signaling through Deptor 51
4.4.4 KDM6A expression correlates with DEPTOR expression in human HCC 52
4.5 Kdm6a-deficient tumors are susceptible to mTOR inhibition 55
4.6 Epigenetic vulnerabilities of Kdm6a-deficient cells 56
4.6.1 pooled CRISPR/Cas9 screening 56
4.6.2 Hits validation 57
4.7 Loss of KDM6A with $Kras^{G12D}$ leads to PDAC 59
5. Discussion 62
5.1 Kdm6a is a tumor suppressor in liver cancer 62
5.2 Molecular function of Kdm6a in tumor suppression 63
5.2 Loss of Kdm6a is essential for c-MYC driven tumorigenesis 64
5.3 Kdm6a re-expression induces apoptosis 65
5.4 Therapeutic possibilities of Kdm6a-deficient tumors 66
5.5 Loss of Kdm6a exerts specific vulnerability towards Hdac3 67
5.6 Tumor suppressive function of Kdm6a beyond liver cancer 69
6. Supplementary Data 70
7. Bibliography 72
Acknowledgement 81

List of Figures

Figure 1.1 Epigenetic mechanisms in mammalian cells. 4
Figure 1.2 Alterations in DNA methylation and histone modifications during cancer progression. 5
Figure 1.3 Genetic alterations in enhancer regions. 7
Figure 1.4 The MLL3/MLL4 COMPASS-like complex. 8
Figure 1.5 Structure and domain of human KDM6A (UTX) and KDM6C (UTY) proteins 9
Figure 1.6 KDM6A Mutations in Human Cancers. 11
Figure 1.7 Hierarchical structure of the liver consist of different cell types serve the diverse functional roles of the liver; 12
Figure 1.8 Mechanism of hydrodynamics-based gene delivery to the mouse liver; ..14
Figure 1.9 Mechanism of action of Sleeping beauty Transposons. 15
Figure 1.10 PDAC initiation and progression. 16
Figure 1.11 ES cell approach for modeling pancreatic cancer. 18

Figure 4.1 CRISPR/Cas9-mediated editing of Kdm6a. 35
Figure 4.2 Kdm6a constrains c-MYC-driven tumorigenesis. 37
Figure 4.3 RNAi-mediated suppression of Kdm6a also promotes c-MYC-driven hepatocarcinogenesis. 38
Figure 4.4 Endogenous Kdm6a re-expression restrains tumor progression. 40
Figure 4.5 Kdm6a re-expression induces apoptosis. 41
Figure 4.6 Kdm6a overexpression causes apoptosis in Kdm6a-deficient cells. 43
Figure 4.7 Kdm6a loss leads to distinct transcriptional changes. 46
Figure 4.8 Genome wide profiling of histone modifications and Kdm6a. 49
Figure 4.9 Kdm6a loss hyperactivates mTOR signaling. 50
Figure 4.10 Deptor disruption can partially rescue apoptosis caused by Kdm6a expression. 52
Figure 4.11 KDM6A expression correlates with DEPTOR expression in human HCC. 54
Figure 4.12 Kdm6a-deficient tumors are susceptible to mTOR inhibition. Dose response curve of different mTOR inhibitors 55
Figure 4.13 Pooled CRISPR/Cas9 screening. 57
Figure 4.14 Kdm6a-deficient cells are vulnerable to Hdac3 depletion. 58

Figure 4.15 Loss of Kdm6a with KrasG12D leads to PDAC. 60
Figure 4.16 Kdm6a loss with KrasG12D activates mTOR signaling and is accompanied with sensitivity to mTOR inhibitors. 61

Suppl. Figure 1 Binding sites of Kdm6a genome-wide based on Cut&Run profiling. 70
Suppl. Figure 2 The mTOR complexes and signaling pathway of mTORC1 and mTORC2; 71

List of Tables

Table 1: Plasmids generated and used in this study 20
Table 2: sgRNA sequences for CRISPR/Cas9 mediated genome editing 21
Table 3: 97-mer hairpin and cloning primer sequences 22
Table 4: Antibodies for Immunoblotting 26
Table 5: T7 primer sequences 27
Table 6: qRT-PCR primer sequences 29
Table 7: Antibodies for Cut&Run 30
Table 8: PCR primer sequences for CRISPR/Cas9 screening 32

List of Abbreviation

3’-UTR	3’-untranslated region
Akt	Protein Kinase B
ALL	Acute lymphoblastic leukemia
AML	Acute myeloid leukemia
COMPASS	Complex Proteins Associated with Set1
CpG island	Repetitive cytosine-phosphat-guanine nucleotide sequences
Cut&Run	Cleavage under targets and release using nuclease
DEPTOR	DEP domain-containing mTOR-interacting protein
DMEM	Dulbecco's Modified Eagle's Medium
DNMT	DNA methyltransferase
Dox	Doxycyclin
DR	Direct repeat
ESC	Embryonic stem cell
FBS	Fetal bovine serum
FC	Fold change
Flp	Flippase
FRT	Flippase recognition target
GEMM	Genetically-engineered mouse model
GFP	Green fluorescence protein
GSEA	Gene set enrichment analysis
GTP	Guanosine triphosphate
HAT	Histone acetyltransferase
HCC	Hepatocellular carcinoma
HDAC	Histone deacetylase
HDM	Histone demethylase
HDTVi	Hydrodynamic tail vein injection
HE	Haematoxylin and Eosin staining
HMT	Histone methyltransferase
HPV	Human papilloma virus
IHC	Immunohistochemistry
Indel	Insertion and deletion

IPA	Ingenuity pathway analysis
JNK	c-Jun N-terminal kinase
KDM6A	Lysine demethylase 6A
KRAS	Kirsten Rat Sarcoma
MLL	Mixed lineage leukemia
MM	Multiple myeloma
MRI	Magnetic Resonance Imaging
mTOR	Mamalian target of rapamycin
mTORC1	Mamalian target of rapamycin complex 1
PanIN	Pancreatic intraepithelial neoplasia
PBS	Phosphate buffered saline
PDAC	Pancreatic ductal adenocarcinoma
PEI	Polyethylenimine
PI3K	Phosphoinositide 3-kinase
PRC2	Protein Regulator of cytokinesis 2
qRT-PCR	Quantitative real-time polymerase chain reaction
RFP	Red fluorescence protein
RNA-seq	Next generation RNA sequencing
rtTA	Reverse tetracycline transactivator
S6K	S6 Kinase
S6RP	S6 Ribosomal Protein
SB	Sleeping beauty transposon system
sgRNA	Single guide RNA
shRNA	Short hairpin RNA
TCGA	The Cancer Genome Atlas
TGF	Transforming growth factor
TMA	Tissue microarray
TRE	Tetracycline Response Element
tRFP	Turbo RFP
TSC	Tuberous sclerosis complex
TSS	Transcription start site
UTX	Ubiquitously transcribed tetratricopeptide repeat on chromosome X

1. Introduction

1.1 Cancer is caused by genetic changes

Cancer can be loosely defined as a genetic diseases, which involves uncontrolled growth of undifferentiated cells that develop across time and have the potential to spread to surrounding tissues and/or other parts of the body [1-3]. While cancer can arise from various tissue types, it commonly arises from transformation of normal cells through successive accumulation of genetic alterations, which remain unrepaired [1, 4]. Specifically, these alterations include single nucleotide variations, small insertions and deletions (indels), copy number alterations, chromosomal rearrangements, and large structural variations [5, 6], which can be caused by internal or external mutagens. Some of these genetic alterations enable cells to acquire different cancer hallmarks that together fuel malignant growth of transformed cells [1]. These cancer traits or hallmarks were first comprehensively summarized by Douglas Hanahan and Robert Weinberg in 2000 [7] and were consequently extended afterwards [8]. These hallmarks include evading apoptosis, sustaining proliferative signaling, evading growth suppression, unlimited replicative potential, sustained angiogenesis, activating invasion and metastasis, avoiding immune destruction, tumor-promoting inflammation, deregulating cellular energetics, genome instability, and mutations [7, 8]. Thus, depending on their function, individual genes altered in cancer cells may be intimately linked to certain hallmarks during cancer development and/or progression and can act as either an oncogene or a tumor suppressor gene [9, 10] depending if they promote or suppress these activities.

1.1.1 Proto-oncogene activation

A proto-oncogene refers to a gene that is involved in growth-promoting pathways under normal circumstance and which upon gain-of-function mutation or increased expression can act as a driver for uncontrolled cell growth [1, 11]. Increased expression of c-MYC in hepatocellular carcinoma (HCC) [12, 13] or expression of Kras activating mutants in pancreatic ductal adenocarcinoma (PDAC) [14, 15] are two examples of bona-fide oncogenes, which clearly demonstrate the oncogenic nature of genes otherwise involved in physiological cellular functions.

As a transcription factor, c-MYC mediates various biological functions such as cell cycle progression, proliferation [16], differentiation and apoptosis [17, 18] via transcriptional regulation of nearly 15% of the human genome [13]. Not surprisingly, aberrant c-MYC expression is frequently correlates with increased cell proliferation and aggressive, poorly differentiated tumors [16].

Molecularly MYC is a key integrator of growth-regulatory and oncogenic signaling pathways and can be induced by Notch, WNT, Hedgehog and JAK-STAT signaling. MYC forms a heterodimer with MAX and MYC-MAX heterodimers can then bind to open chromatin and function as a transcriptional activator or repressor of selected gene subsets [19]. For example, MYC can influence the cell cycle where MYC downregulates cell cycle inhibitors like p15, p21, p27 but also upregulates cyclins and therefore positively drives the cell cycle and proliferation [19]. In some oncogenic contexts, c-MYC activation also induces DNA damage indirectly through this cell cycle entry and progression under inappropriate conditions and cause genetic instability, which contributes to tumorigenesis [20, 21] Of note, however, multiple studies have established that c-MYC over-expression alone is insufficient to overcome intrinsic barrier for tumor transformation such as cellular senescence or apoptosis [22-24]. For example acute enforced expression MYC was shown to upregulate pro-apoptotic genes such as BAX, NOXA and BIM subsequently leading to cell death [19].

Unlike c-MYC, the oncogenicity of Kras is linked to its molecular function as a small GTPase. Under physiological conditions, KRAS is predominantly GDP-bound and only bound to GTP upon stimulation, such as growth factors. KRAS binding to GTP amplifies the GTPase activity of Kras, which then feeds into different downstream pathways including, but not limited to the PI3K/Akt/mTOR and the RAS/RAF/MEK/ERK pathway [14, 25, 26]. Activation of those pathways are known to promote cell survival, proliferation, cytokine secretion and to support cancer development.

In contrast to wild-type Kras, point mutations of KRAS, such as the G12D and the G12V, which are detected in up to 95% of PDAC cases, have been shown to lead to sustained GTPase activity and thus sustained activation of downstream molecular effectors driving cell proliferation, transformation, adhesion, and survival [25, 27].

1.1.2 Tumor suppressor genes

In contrast to oncogenes, tumor suppressor genes constrain tumor transformation and progression [28] through activating diverse cellular processes including induction of cell cycle checkpoint responses, detection of DNA damage and repair, ubiquitination and degradation of mitogenic signaling, induction of apoptosis, and inhibition of tumor angiogenesis [28-30]. Deletion or loss-of-function mutations of tumor suppressor genes allow cells to escape inhibitory signals, which counterbalance growth-stimulating pathways, and result in the onset and progression of cancer [1]. For example, the TP53 gene, which regulates cell cycle and initiates apoptosis, is a very prominent tumor suppressor gene and consequently frequently inactivated by mutation or deletion in many different human cancers [31, 32].

1.2 Epigenetic regulation

Apart from genetic regulation of gene expression und subsequent gene function, there also exists epigenetic regulation that can also control distinct gene expression patterns. These epigenetic regulatory mechanisms involve post-translational histone modifications, DNA methylation, and/or expression of non-coding RNAs (ncRNAs), including microRNAs (miRNAs), small interfering RNAs, and long ncRNAs (lncRNAs) in the absence of DNA sequence alteration (genotype) (Figure 1.1) [33-35]

DNA methylation is preferentially found on promoter elements and was shown to silence transcription of adjacent genes [36] while at chromatin level, epigenetic modifications of histone by acetylation, methylation, phosphorylation, or ubiquitination at different histone residues may either increase or decrease accessibility of the DNA wrapped around the nucleosome [37]. Finally, miRNAs inhibit translation by complementing sequences in the 3' untranslated region of target mRNAs [33, 38], while lncRNAs regulate gene expression by different mechanisms, including chromatin remodelling, protein inhibition, post-transcriptional modifications, and transcriptional co-activation or repression [33, 39]. In summary, all of these epigenetic modifications influence gene expression in different ways and play an important role for gene regulation in mammalian cells.

Not surprisingly, recent studies have found both alterations in the epigenetic landscape and recurrent mutations in epigenetic regulatory genes in numerous human cancer types [10, 40, 41]. These results suggest that cancer initiation and progression

are not only controlled by genetic events but also involve various epigenetic alterations for neoplastic transformation [42].

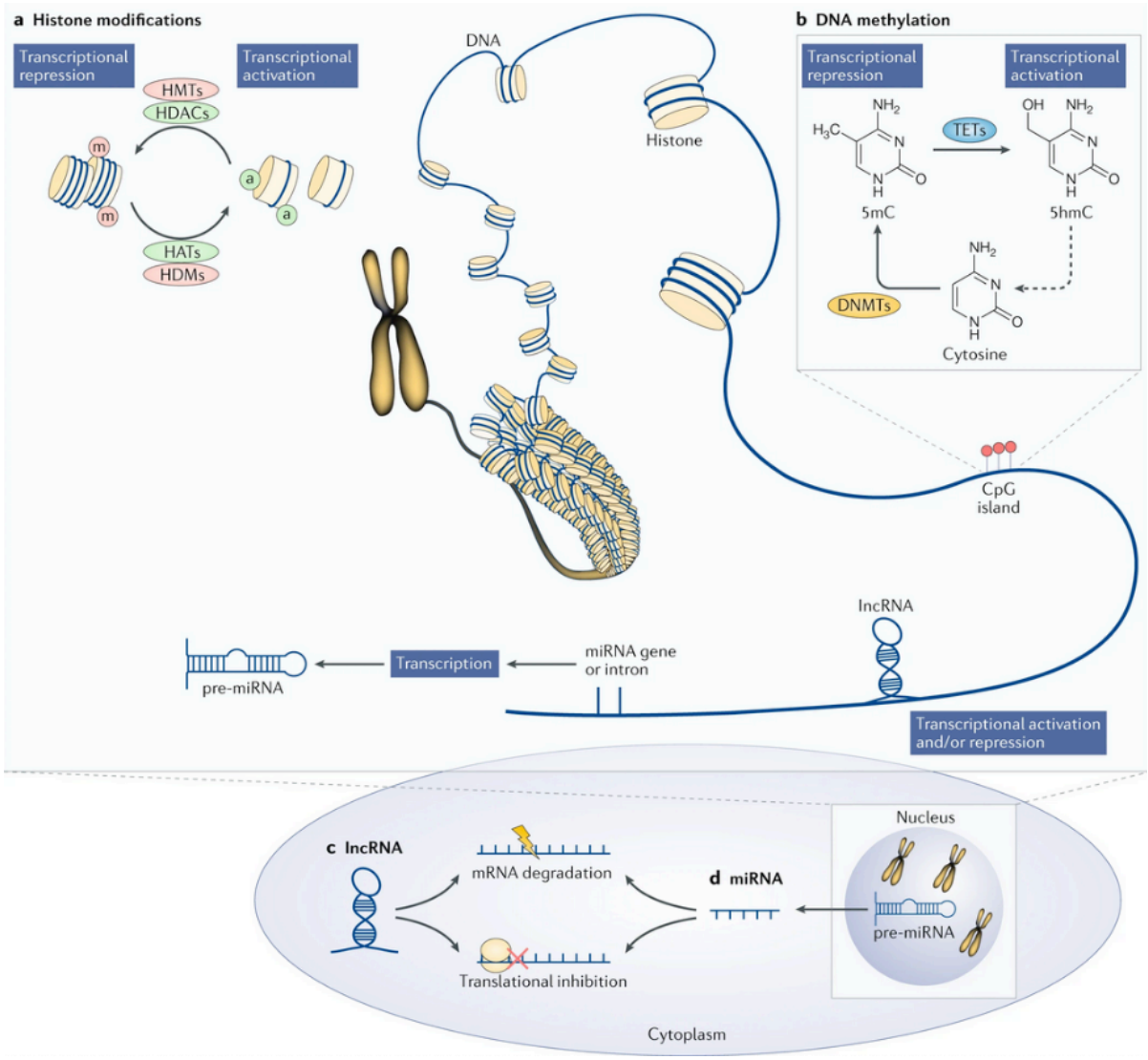

Figure 1.1 Epigenetic mechanisms in mammalian cells. Epigenetic modification can take place either on DNA level, where methyl groups are add to cytosine nucleotides. On the protein level histones, a core component of the nucleosome can get altered by different modifications leading to either activation or repression of genes. Finally on RNA level, lncRNA and miRNA can control transcriptional initiation or repression; Unmodified taken from Angiolilli et al. [35].

1.2.1 Epigenetic alterations in cancer

Ranges of epigenetic dysregulations affecting proto-oncogenes and/or tumor suppressors have also been implicated to oncogenesis as depicted in Figure 1.2. These include, but not limited to, DNA methylation, histone modifications and enhancer deregulation.

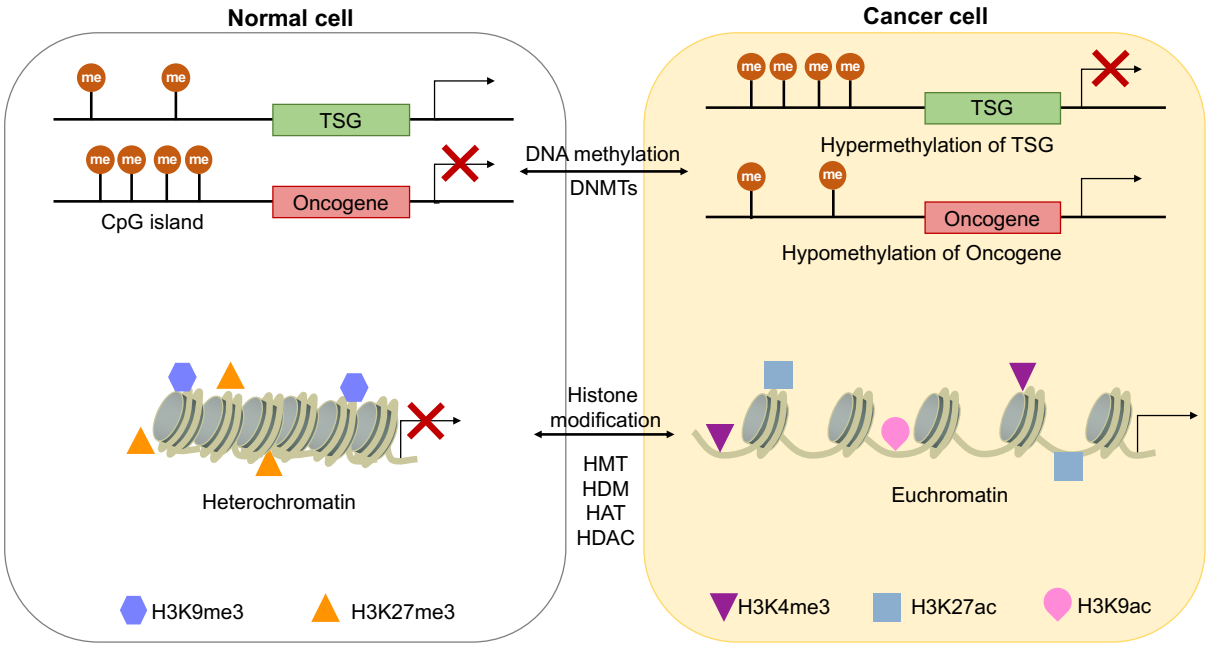

Figure 1.2 Alterations in DNA methylation and histone modifications during cancer progression. Upper panel, hypomethylation of CpG island promoters induces active transcription of while hypermethylation silence gene expression. Lower panel, modification of histone tails at different positions have different chromatin state and consequences. Adapted from Khan et al. [43].

1.2.1.1 DNA methylation

DNA methylation is known as a mechanism of gene silencing that usually takes place in CpG-rich DNA stretches called ‘CpG islands’ located in the promoter regions of genes [44]. The methylation is catalyzed by the DNA methyltransferases (DNMTs) [45] and alterations of DNMT activity by mutations or upregulation can induce the onset of cancer [46]. For instance, hypermethylation in promoter regions of tumor suppressor genes including DNA repair genes, MLH1 or cell cycle regulator, CDKN2A, provides tumor cells with a growth advantage and increase their genetic instability [47]. In contrast, hypomethylation in tumor cells is primarily associated with oncogenes such as c-MYC, which is one of the widely reported hypomethylated genes in cancers [47].

1.2.1.2 Histone modification

In addition to changes in DNA methylation, histone modification patterns are also altered in human cancers. The majority of histone modifications occur towards the N-terminal histone tails preferably in lysine, arginine and serine residues [43]. Histone modifications are reversible and are controlled by a group of enzymes including histone acetyltransferases (HATs) and deacetylases (HDACs) for acetylation,

methyltransferases (HMTs) and demethylases (HDMs) for methylation, kinases and phosphatases for phosphorylation, ubiquitin ligases and deubiquitinases for ubiquitination, SUMO ligases and proteases for SUMOylation, which add and remove such modifications as shown in Figure 1.2 [47, 48]. These histone modifications lead to different states of chromatin, either heterochromatin or euchromatin. Heterochromatin is usually densely compacted and transcriptionally inert, whereas euchromatin is loosely packed, less condensed, and transcriptionally active (Figure 1.2). In addition, these histone modifications also directly activate or repress gene expression. For example, gene activation is characterized by high levels of H3K4me3, H3K36me3, H3K79me3 and acetylation, while gene repression is known to be associated with high level of H3K9, H3K27 and H4K20 methylation [49].

In cancer, aberrant expression of those histone modifying enzymes are frequently observed [41]. For example, loss of acetylation is mediated by HDACs that have been found to be over-expressed or mutated in multiple gastric carcinomas. Moreover, inactivating mutations in the histone methyltransferase SETD2, histone demethylase KDM6A and JARID1C are found in renal carcinomas [50].

1.2.1.3 Deregulation of enhancers in cancer

Regulation of gene transcription does not only occur in transcription start sites but also in the so called enhancer regions. Enhancers are regulatory non-coding DNA sequences that can activate genes across a long distance and are decorated by specific epigenetic marks. Enhancer mutations and hijacking was recently demonstrated to cause deregulation of transcriptional programs and to drive tumorigenesis [51]. Enhancer hijacking is a process where the repositioning of inter- or intra-chromosomal enhancers to close proximity of proto-oncogenes leads to the activation of these genes and contributes to oncogenesis [51]. Besides, mutations in enhancer sequences can result in activation of proto-oncogenes or inactivation of tumor suppressor genes (Figure 1.3).

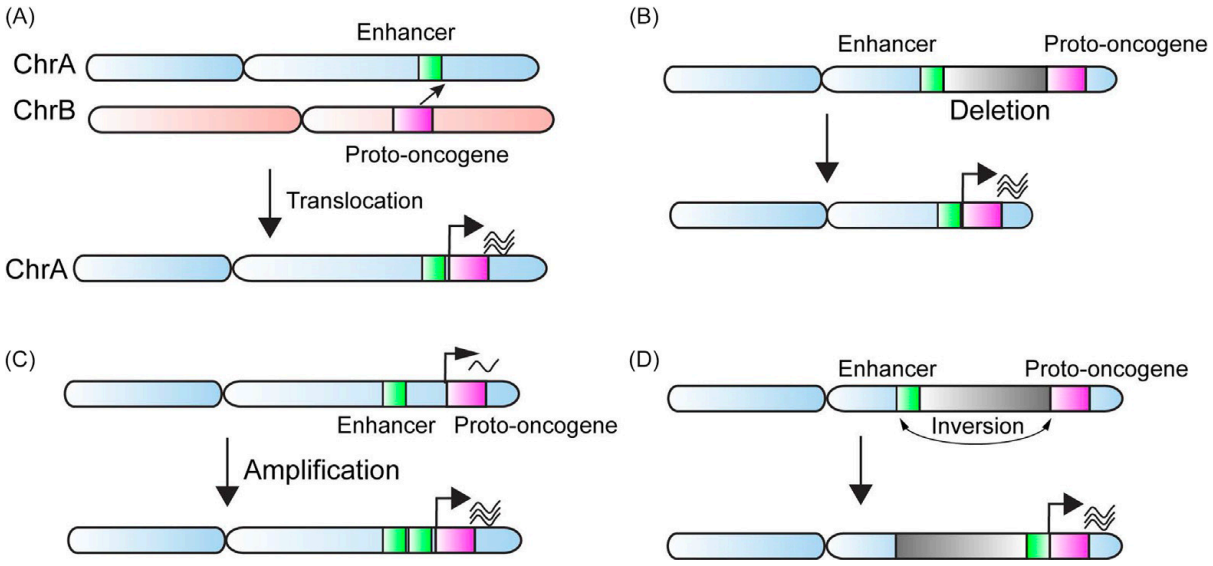

Figure 1.3 Genetic alterations in enhancer regions. (A) Inter-chromosomal translocation of enhancer to drive expression of a proto-oncogene. Enhancers activate proto-oncogenes through intra-chromosomal deletion **(B)**, amplification **(C)**, and inversion **(D)**.

1.2.1.4 Oncohistones

The definition of an 'oncohistone' is a missense mutation that occurs in the N-terminal tail of histone H3 where lysine-methionine substitutions affect the function of lysine methyltransferase such as polycomb repressor complexes 1 and 2 (PRC1 and PRC2) [52]. For example, H3.3K36M mutations in chondroblastomas and H3K27M mutations in high-grade gliomas are some of the currently known oncohistones that induce oncogenesis. Recent analyses of cancer genomes show that mutations in histones do not only affect dysregulation of gene expression but also alter the nucleosome three-dimensional structure and stability, providing a novel mechanism by which oncohistones contribute to tumorigenesis [53, 54]. Studies also showed that mutations do not only happen in histone H3 but in all four core histones, in both the N-terminal tails and globular histone fold domains, and at or near residues that contain important post-translational modifications [54].

1.2.2 MLL3/MLL4 COMPASS-like complex

The mammalian MLL3/4 COMPASS-like complex is known to methylate lysine 4 (K4) of histone H3 protein around enhancer elements [55-57]. This complex contains two histone H3K4 methyltransferases – MLL3 (KMT2C) and MLL4 (KMT2D), a H3K27 demethylase – UTX (KDM6A), scaffold proteins (ASH2, WDR5, RBBP5, and hDPY30), and other less characterized proteins (Figure 1.4) [57, 58]. Importantly,

genome sequencing revealed frequent mutations of KMT2C, KMT2D, and KDM6A in several tumor types [59-61], including liver tumors [62, 63].

Enhancer activation of tumor suppressor genes by the MLL3/MLL4 COMPASS-like complex may be a general mechanism in repressing cancer development which has been described previously [64]. In Drosophila, Trr, a homolog of MLL3/MLL4, was demonstrated to suppress cell proliferation and consequently Trr mutation causes tissue overgrowth [65]. Lee et al. described MLL3/MLL4 as a p53 coactivator that induced expression of p53 target genes involved in DNA damage response. They also observed MLL3 deletion in p53 heterozygous background mice shortened the onset of tumorigenesis, further suggesting a role of MLL3/MLL4 in p53 mediated DNA damage repair [66]. Consistently, other studies has also implicated the MLL4 mutation in genomic instability [67]. However, it remains to be established whether these mutations act as driver or passenger events during the course of tumorigenesis in different tumor types.

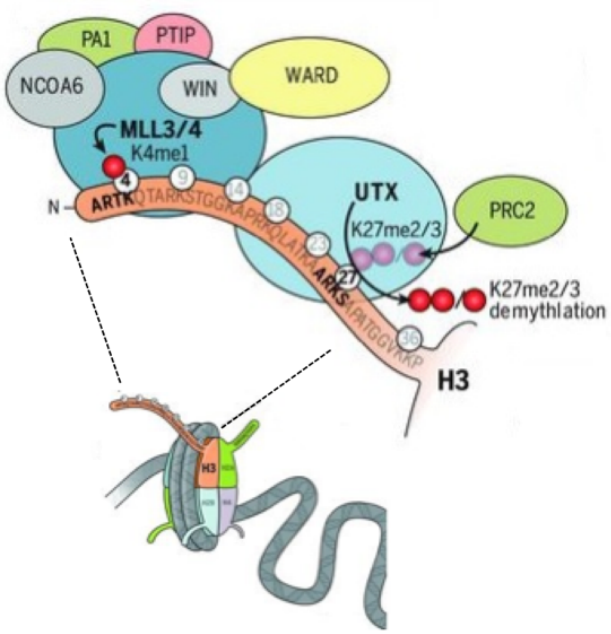

Figure 1.4 The MLL3/MLL4 COMPASS-like complex. The complex consists of several scaffold proteins as well as the histone H3K4 methyltransferases KMT2C and KMT2D, KDM6A a H3K27 demethylase, and NcoA6 a nuclear co-activator receptor; modified from Piunti et al. [57].

1.2.3 The histone H3K27-demethylase KDM6A

As shown in Figure 1.4, MLL3 and MLL4 co-exist in a multimeric composition within COMPASS including the ubiquitously transcribed tetratricopeptide repeat on chromosome X (UTX, also known as KDM6A). KDM6A comprises 1401 amino acids with JmjC catalytic domain and 6 protein interaction-mediating tetratricopetide repeat domains [68, 69] (Figure 1.5). While KDM6A is located on the X chromosome, both copies of this gene escape from X-chromosome inactivation in females [70-72]. The Paralog to KDM6A, the ubiquitously transcribed tetratricopeptide repeat gene on the Y chromosome (UTY, encoded by KDM6C) shares 83% of sequence and structural similarity with KDM6A (Figure 1.4) [58]. But KDM6C was found to have significantly lower histone demethylase activity *in vitro* in comparison to KDM6A [73, 74].

To date, KDM6A is known as a histone lysine demethylase that specifically removes methyl groups from di- and trimethylated H3K27, a histone mark known to be associated with gene repression and chromatin condensation [64, 75]. Methylation of H3K27 has been described to be deposited by PRC2 at both enhancers and promoters to silence transcription [57]. Thus, histone demethylase activity of KDM6A can antagonize the Polycomb-mediated repression. Previous studies have also shown that while MLL3 deposits H3K4me1 activation marks, KDM6A within the same complex is able to remove H3K27me repressive marks simultaneously without interfering enzymatic activity of the other protein [58, 76]. This enzymatic activity of KDM6A is abrogated as a consequence of H1146A and E1148A point mutations within the Fe(II)-binding motif of the catalytic JmjC domain [77, 78].

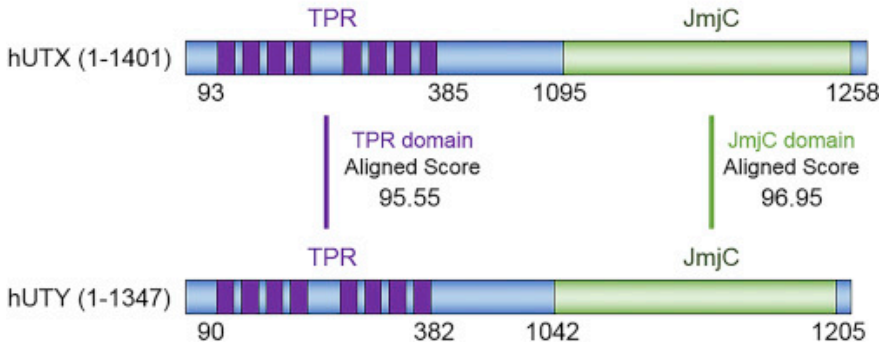

Figure 1.5 Structure and domain of human KDM6A (UTX) and KDM6C (UTY) proteins; modified from Want et al. [58]

In addition, the function of KDM6A in development has also been described to be independent of its demethylase capability [79-82]. KDM6A was described by Wang

et al. as a enhancer modulator that facilitates the conversion of conversion of inactive enhancers to an active state by recruiting and coupling the functions of MLL4 and p300 in a demethylase-independent manner [79]. Recruitment of MLL4 and p300 into enhancer region leads to deposition of H3K4me1 and H3K27ac and thus establishing an “active enhancer landscape”. It was also shown to facilitate the interaction between SWI/SNF complex and T-box factors, a family of transcription factor, in chromatin remodeling during developmental stages [82].

In this regard, KDM6A does not only play a role in normal development and differentiation [80, 83-86] but also in cancer development [87, 88]. It is frequently mutated in a number of cancers (Figure 1.6), including acute lymphoblastic leukemia (ALL) [88, 89], chronic myelomonocytic leukemia (CMML) [90], colorectal adenocarcinoma, renal cell carcinoma, multiple myeloma [91, 92], bladder cancer [93], pancreatic cancer [94, 95] and liver tumors [62, 63]. Its tendency of biallelic KDM6A inactivation in females and the two-hit KDM6A-KDM6C loss in males that contribute to oncogenesis, indicates that KDM6a is a classical two-hit tumor suppressor function of KDM6A [96]. Thus, the role of KDM6A as tumor suppressor has been increasingly investigated and was so far best studied in T-cell lymphomas, as summarized by Van der Meulen et al. [87]. There, KDM6A was described to regulate cell growth in Notch-dependent manner that has been also confirmed by another study [88].

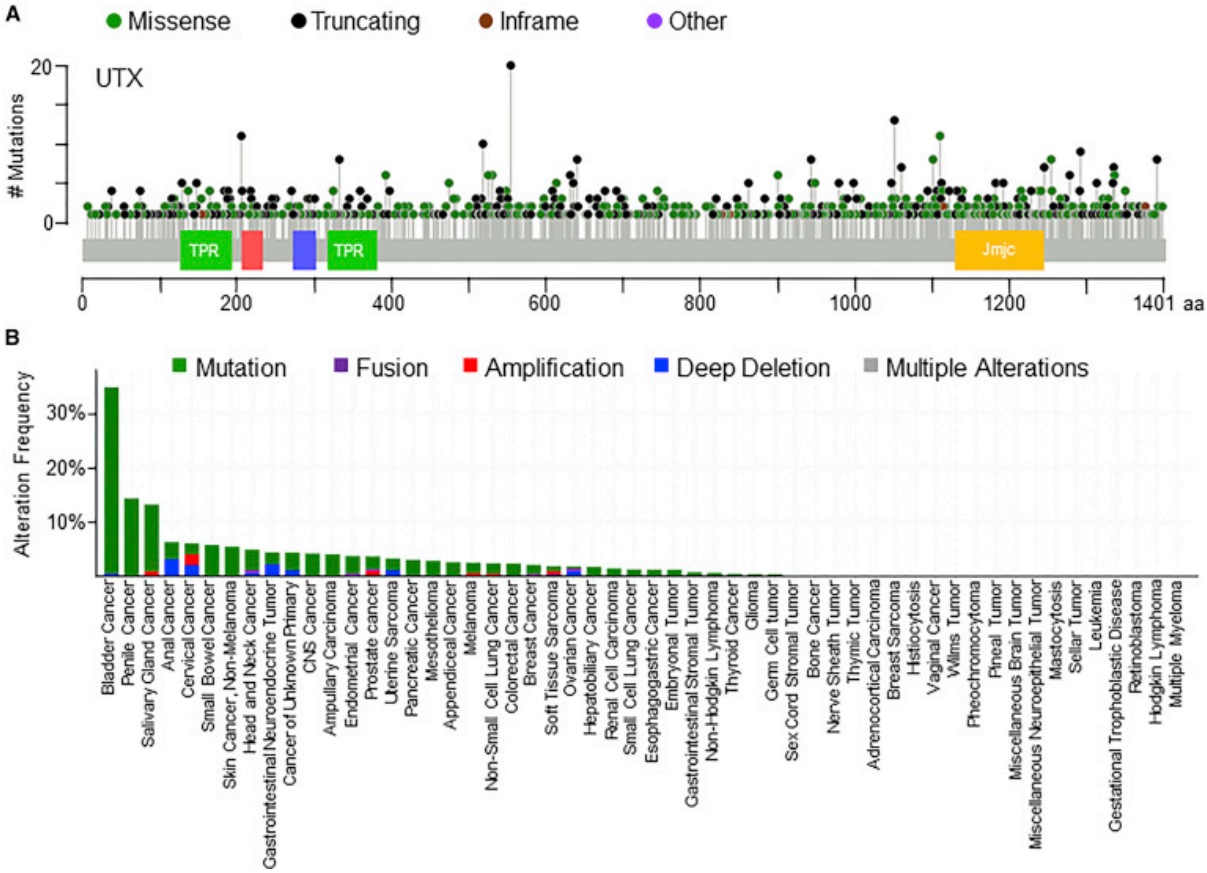

Figure 1.6 KDM6A Mutations in Human Cancers. (A) KDM6A mutations in the protein coding region from cBioPortal. The red, green, and blue boxes indicate computationally identified TPR motifs while the yellow box indicates the JmjC domain. **(B)** KDM6A mutation frequencies across various human cancer types as obtained from cBioPortal; modified from Wang et al. [58].

1.3 Liver and mouse models of liver cancer

1.3.1 Liver physiology and pathology

The Liver is one of the largest organs in mammals and plays an important role in metabolism, glycogen storage, protein synthesis as well as detoxification [97]. Liver tissue consists of two major parenchymal cell types, hepatocytes and cholangiocytes (biliary epithelial cells), with distinct morphology and functions [98]. Hepatocytes are big cells with large cytoplasm and are mainly responsible for metabolic function, whereas cholangiocytes are smaller cells, lining the bile ducts, which transport bile into the intestine (Figure 1.7). The prevalence of liver diseases and associated mortality have risen markedly within recent decades due to viral hepatitis, excessive alcohol consumption, obesity and metabolic disorders, such as type 2 diabetes mellitus [99]. Malignancies of the liver, hepatocellular carcinoma (HCC) and intrahepatic cholangiocarcinoma (CC), can be distinguished histologically and by

assessing expression of lineage-specific markers. HCC typically consists of polygonal cells growing in a solid-trabecular growth pattern, whereas CC often displays a ductal morphology with a substantial stromal reaction.

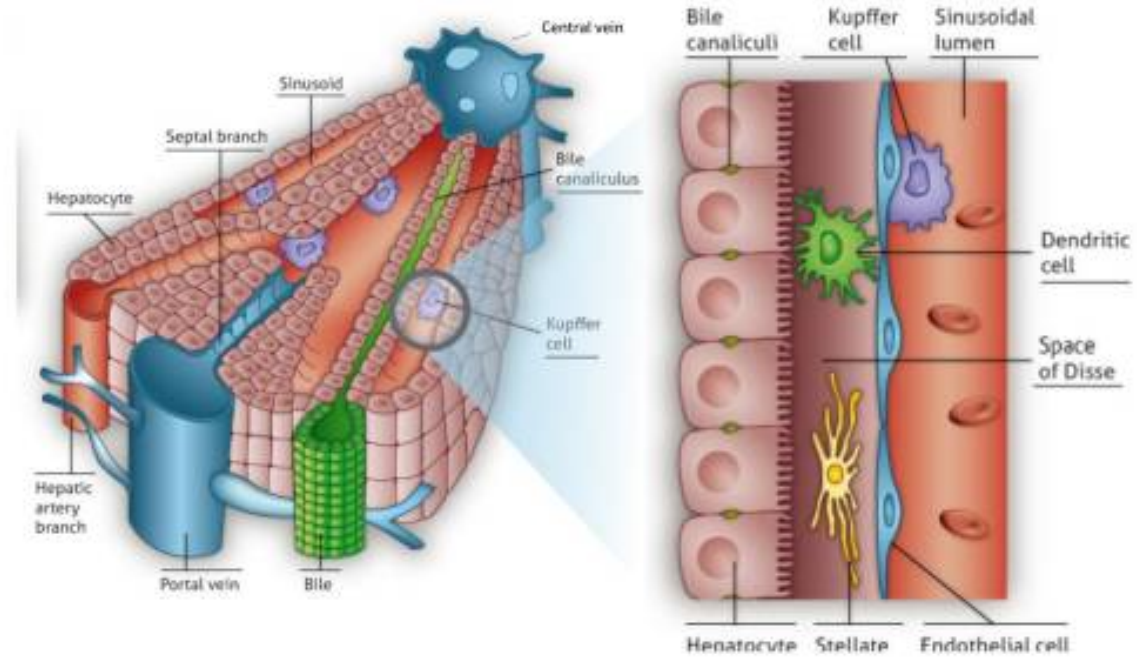

Cell Type	Functions
Hepatocyte	Protein storage and synthesis, carbohydrate metabolism, secretion of urea and bile, detoxification
Sinusoidal endothelial cell	Mediate nutrient transport, cell extravasation, blood protein scavenging
Hepatic stellate cell	Lipid and vitamin A storage
Kupffer cell	Mononuclear phagocyte system
Biliary epithelial cells	Regulate ductular transport of bile from the liver
Dendritic cell	Antigen presentation, regulate T cell activation and tolerance

Figure 1.7 Hierarchical structure of the liver consist of different cell types serve the diverse functional roles of the liver; unmodified from Bhatia et al. [97].

There is a magnitude of evidence that liver cancer progression is, as in other cancer types, associated with epigenetic changes. For example, methylation profiling of liver cancers revealed an increased number of methylated genes along the progression of liver malignancy [100-102]. Moreover, several histone marks, e.g. H3K4me3 and H3K27me3 were aberrantly distributed on chromatin of liver tumor tissue, further suggesting that epigenetic deregulation plays an important role in human liver cancer [103].

1.3.2 Mouse models of liver cancer

In the last 30 years, technological advances have facilitated the generation of different mouse models to mimic the alterations frequently observed in human cancers or to conduct intervention studies to assess the relevance of candidate gene networks in tumor establishment, progression, and maintenance. Amongst different liver malignancies, hepatocellular carcinoma (HCC) is by far the most common type, accounting for 70–80% of cases [104]. To date, mouse models to study HCC are largely available and can be subcategorized into chemically induced models, transplantation models/xenograft, different GEMMs including the hepatitis virus transgenic mice and transgenic models that allow genetic manipulation to express proto-oncogenes or inactivate tumor suppressor genes either in inducible or constitutive manner. Moreover, liver-specific promoter element such as albumin are used to achieve tissue-specific expression. For example, Murakami and colleagues developed a transgenic mouse model that co-express c-MYC and transforming growth factor alpha (TGF- α) in murine livers and led to hepatic oncogenesis within 2 months [105].

Utilizing these technologies, sophisticated multi-allelic mouse were generated where conditional expression can be achieved in a space and time-restricted fashion [104]. Although GEMMs provide us the tool to study and investigate role of specific genes and interaction of different genes related to HCC development, the approaches are known to be very time-consuming and resource-demanding.

Hence our group is taking advantage of the previously established hydrodynamic tail vein injection (HDTVi) technique to generate a mosaic GEMMs of aggressive hepatocellular carcinoma within a shorter time. Principally, this technique involves rapid mechanical delivery of approximately 2 mL of physiological saline solution containing genetic material of interest via injection into the tail vein within 5-7 seconds [106-108]. The rapid tail vein injection of such volume is expected to saturate the hepatic vein due to initial cardiac congestion [106, 108]. As a result, a build-up hydrodynamic pressure within the hepatic vein promotes invagination of the hepatocyte cellular membrane and therefore absorption of the injected solution and its content by the liver (Figure 1.8). Using this technique, we are able to generate genetically defined, mosaic tumors in wild-type mice.

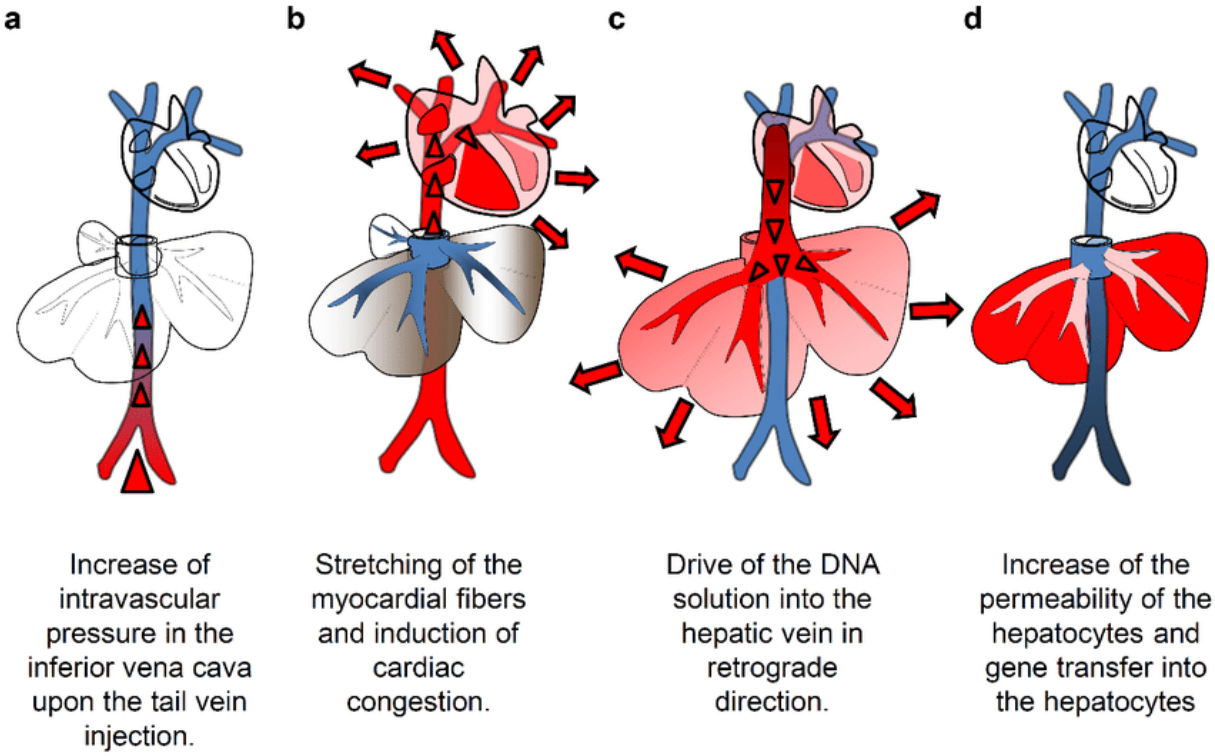

Figure 1.8 Mechanism of hydrodynamics-based gene delivery to the mouse liver; unmodified from Kamimura et al. [108].

Combination of this technique and SB transposon-based system allows stable integration of a genetic cargo of interest into the genome of murine liver following hydrodynamic tail vein injection of plasmid DNA. Sleeping Beauty (SB), a member of the Tc1/mariner class of transposons, is an active DNA-transposon system for genetic transformation and insertional mutagenesis that consist of the transposase and transposon vector [109, 110]. This transposon vector usually contain the genetic cargo of interest which is flanked by the binding sites for the SB transposase, the so-called inverted repeats/direct repeats (IRDRL (left) and IRDRR (right)) . In principle, SB mediates the precise cut-and-paste transposition from transposon vector into TA-rich genomic DNA regions (Figure 1.9).

However, not only expression plasmids can be delivered into murine liver but also CRISPR/Cas9 system or RNAi-based system can be used to mimic the genetic features found in liver cancer patients and serve as a tool to investigate the roles of genetic alterations in liver carcinogenesis.

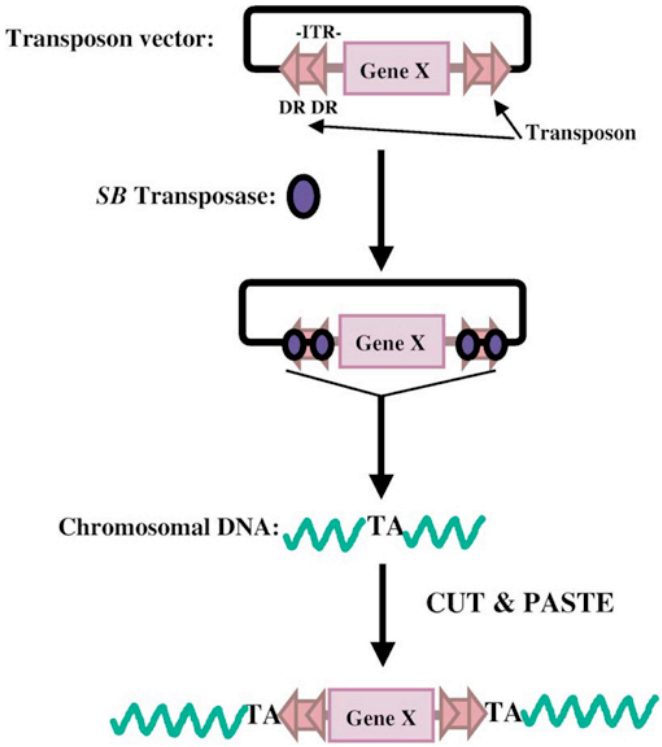

Figure 1.9 Mechanism of action of Sleeping beauty Transposons. Expression of Sleeping beauty Transposon vector in combination with Sleeping beauty Transposase leads to integration of genetic cargo into TA-rich genomic DNA regions.

1.4 Pancreas and mouse models of pancreatic cancer

1.4.1 Pancreas physiology and pathology

The Pancreas as an organ functions as both an endocrine gland secreting peptide hormones, such as insulin, into blood to maintain glucose homeostasis, and as an exocrine gland secreting digestive enzymes into duodenum for nutrients digestion and absorption [111, 112]. The endocrine pancreas consists of multiple secretory islet cells (Islets of Langerhans) including the β cells that secrete insulin, whereas the exocrine pancreas consists of pancreatic acinar and duct cells. Endocrine and exocrine functions in the pancreas are tightly regulated and inappropriate activation or inactivation of the pathways mediating the pancreas's fine regulatory mechanisms have considerable impacts on health and disease [112]. The most common type of pancreas malignancies is pancreatic ductal adenocarcinoma (PDAC) [113], which is characterized by mutations in KRAS and frequent deregulation of embryonic signaling pathways [114]. Histologically precursor stages of PDAC are categorized into mucinous cystic neoplasm (MCN), intraductal papillary mucinous neoplasm (IPMN) and pancreatic intraepithelial neoplasia (PanIN) [115]. PanIN is the most commonly

observed and well-characterized premalignant lesion that can further develop into pancreatic tumors such as PDAC [116] (Figure 1.10).

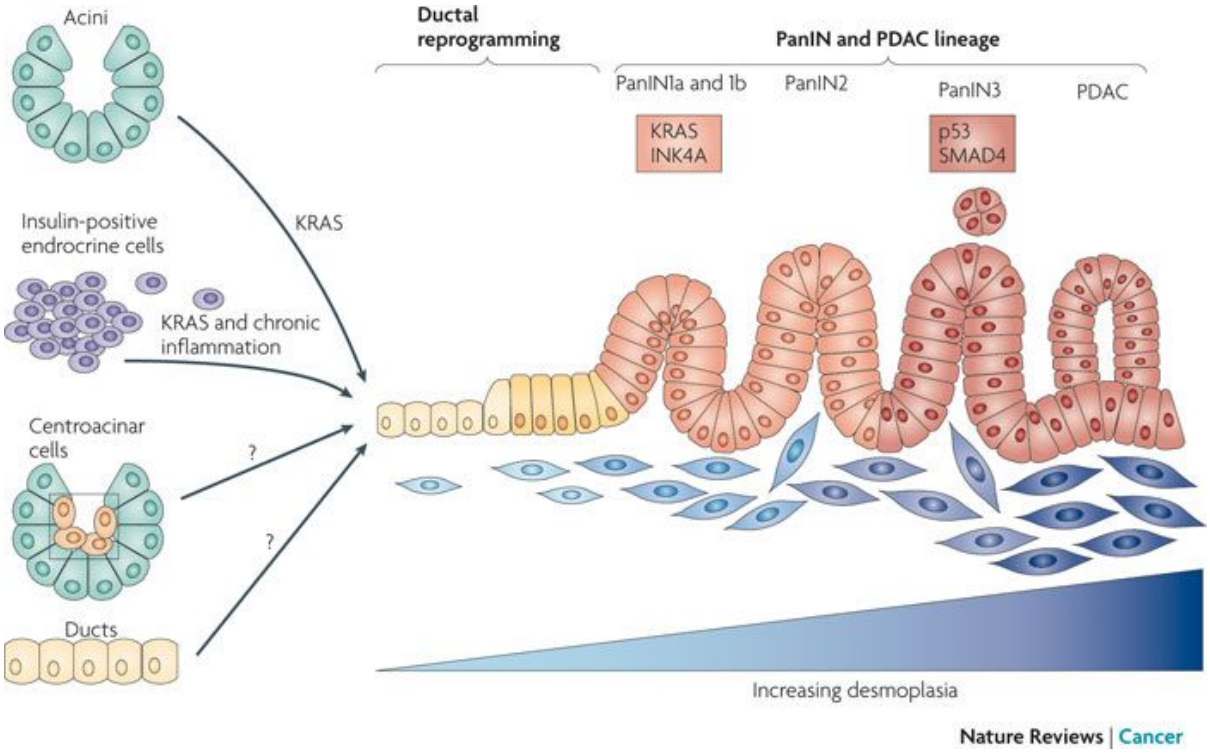

Figure 1.10 PDAC initiation and progression. The Kras G12D or G12V mutations in normal pancreatic ductal epithelial cells lead to constant activation of Kras and initiate the development of PanIN and PDAC; unmodified from Morris et al. [114].

1.4.2 Mouse model of pancreatic cancer

Prior to the development of PDAC GEMMs, xenograft were the main model used to study the PDAC *in vivo* [117]. The GEMM mouse model of PDAC, LSL-Kras$^{G12D/+}$; PdxCre model (now referred to as the KC model), recapitulates the step-wise development of cancer and was developed by the groups of David Tuveson and Ronald DePinho in 2003 taking advantage of the already established LSL-Kras$^{G12D/+}$ mouse [118, 119]. This KC model was then further advanced by addition of conditional alleles of different frequent mutated genes in PDAC including TP53, SMAD4, CDKN2A, and ARID1A [120]. One of the best studied GEMM of PDAC is the LSL-Kras$^{G12D/+}$;LSL-Trp53$^{R172H/+}$;Pdx-1-Cre (KPC) mouse model [121]. This KPC model was shown to accelerate PanIN development and to develop PDAC with a median survival of 5.5 months. Tumors arising from KPC model were found to recapitulate many of the clinical and histopathological features of human disease such as ascites development, poor vascularity, fibrosis, and metastatic spread [117].

To evaluate the molecular function of KDM6A in pancreas, we generated GEMM with the combination of $Kras^{G12D}$ activation and Kdm6a repression/deletion. Previously, transgenic mice to ablate Kdm6a expression in the pancreas with activation of $Kras^{G12D}$ has been developed by Andricovich et al. where loss of Kdm6a in pancreatic cancer leads to aberrant activation of super-enhancers regulating ΔNp63, MYC, and RUNX3 oncogenes. Furthermore, Kalisz et al. also established the similar transgenic mice where they observed both HNF1A and KDM6A regulate a common transcriptional program that is defective in non-classical human PDAC. Altogether, studies of KDM6A in pancreatic malignancies shown that loss of Kdm6a contributes to poor prognosis and increased aggressiveness in disease development.

In light of this, we generated an embryonic stem cell (ESC)-based mouse model of PDAC. To this end, we employed ESC harboring pancreas specific Cre-expression (p48-Cre), a conditional LSL-$Kras^{G12D}$ allele, as well as LSL-rtTA (CAGs-LSL-RIK) allele to generate a mouse model of PDAC [122] (Figure 1.11). Furthermore, the targeting cassette for shRNA constructs at the ColA1 locus (CHC) in ES cells have a frt-hygro-pA “homing” cassette, so that in the presence of FLPe recombinase, flippase recognition target (FRT) site at the ColA1 locus recombine with those present in the targeting vector and only correct integration of targeting vector and homing cassette confers hygromycin resistance. The targeting vector used in the study express GFP as shRNA expression reporter followed by the miR-30 based shRNA targeting KDM6A or control shRNA targeting Renilla luciferase under TRE promoter (Figure 1.11).

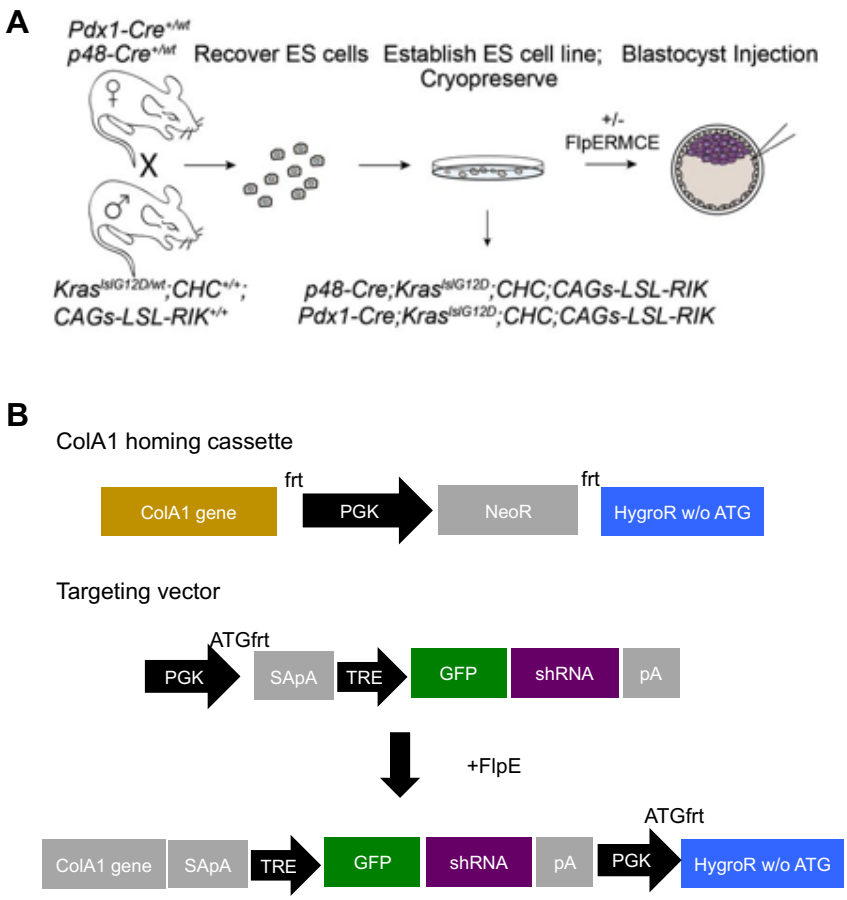

Figure 1.11 ES cell approach for modeling pancreatic cancer. (A) ES cells are rederived from p48- Cre, LSL-Kras^{G12D}, LSL-RIK, CHC mice and cultured. ES cells can integrate a targeting construct at the CHC locus by recombinase mediated cassette exchange (RMCE). Finally, targeted ES cells will be subjected to Blastocyst injection. **(B)** Schematic vectors used for the RMCE. Adapted from Saborowski et al. [122]

2. Objective

KDM6A is reported to be highly mutated in different human cancers. However, its precise role in tumorigenesis, in particular in solid cancers, is poorly understood. Thus, the objectives of this PhD project were to address the role of the KDM6A in tumor suppression along three major milestones:

First, the molecular function of KDM6A was studied in context of different oncogenic stimuli and in different tumor types. To this end, MYC-driven liver tumors with inducible suppression of KDM6A were generated by HDTVi and effects of endogenous reactivation of KDM6A in tumor progression was evaluated both *in vitro* and *in vivo*. Furthermore, the role of KDM6A suppression was also investigated in an ESC-based mouse model for pancreatic cancer with an oncogenic KRAS G12D background. This allowed to distinguish tumor-type specific differences of KDM6A suppression and to reveal also potential common traits in tumorigenesis.

Second, genome-wide transcriptional and epigenetic changes associated with loss and/or low KDM6A expression in presence of defined oncogenes were characterized using RNA-seq and cleavage under targets and release using nuclease (Cut&Run). Differentially expressed genes were subjected to gene ontology and gene set enrichment analysis in order to identify biological processes that contribute to transformation driven by loss of KDM6A. Additionally, the Cut&Run data revealed not only specific chromatin binding sites of KDM6A across the genome but also potential correlations with changes in histone modifications.

Finally, having identified the aforementioned epigenetic and transcriptional changes, we aimed to define specific pathway-dependencies of KDM6A-deficient cancer cells. Additionally, using a focused pooled CRISPR/Cas9 screening approach based on a sgRNA library targeting all known epigenetic modifiers precise epigenetic vulnerabilities of KDM6A-deficient tumors were identified and a number of essential genes of KDM6A-deficient cells were validated.

3. Materials and Methods

3.1 Molecular cloning

Table 1: Plasmids generated and used in this study

Plasmid	Description	Origin
pX330-U6-Chimeric_BB-CBh-hSpCas9	SpCas9 and chimeric guide RNA expression plasmid	Addgene, #42230
pLentiCRISPR v2	Lentiviral backbone expressing SpCas9 and sgRNA under U6 promoter	Addgene, #52961
pLKO.U6-EFs-GFP-P2A-Blasticidin	Lentiviral backbone expressing SpCas9 and sgRNA under U6 promoter	AG Tschaharganeh, DKFZ, Heidelberg
pT3-EF1a-MYC	Transposon based c-MYC expression plasmid	AG Tschaharganeh, DKFZ, Heidelberg
pT3-cMYC-IRES-rtTA3	Transposon based c-MYC and rtTA3 expression plasmid	AG Tschaharganeh, DKFZ, Heidelberg
pT3-EF1a-GFP-miR-E	Transposon based shRNA expression plasmid	AG Tschaharganeh, DKFZ, Heidelberg
pT3-EF1a-linker-IRES-GFP	Transposon based expression plasmid for overexpression	AG Tschaharganeh, DKFZ, Heidelberg
pT3-NRAS	Transposon based NRAS expression plasmid	AG Tschaharganeh, DKFZ, Heidelberg
pT3-ßCat	Transposon based ß-Catenin expression plasmid	AG Tschaharganeh, DKFZ, Heidelberg
pT3-TRE-tRFP-miR-E	Transposon based plasmid for doxycycline-inducible shRNA expression	AG Tschaharganeh, DKFZ, Heidelberg
pCol-TGM	Targeting vector for ESC	AG Tschaharganeh, DKFZ, Heidelberg
pCAGs-FLPe	Flpe-recombinase expression vector	AG Tschaharganeh, DKFZ, Heidelberg
pMSCV-rtTA3-PGK-Puro	Retroviral vector for rtTA3 expression	AG Tschaharganeh, DKFZ, Heidelberg
pSIN-TRE-KDM6A-PGK-Venus	Retroviral vector for doxycycline-inducible expression	AG Tschaharganeh, DKFZ, Heidelberg
pSIN-TRE-linker-PGK-Venus	Retroviral vector for doxycycline-inducible expression (control)	AG Tschaharganeh, DKFZ, Heidelberg
MLPe (MSCV-LTR-miR-E-PGK-Puro-IRES-GFP)	Retroviral vector for shRNA expression	AG Tschaharganeh, DKFZ, Heidelberg

psPAX2	Lentiviral packaging plasmid	Addgene, #12260
pMD.2G	VSV-G envelope expressing plasmid	Addgene, #12259
CMV-SB13	Sleeping beauty transposase expression vector	AG Tschaharganeh, DKFZ, Heidelberg
LentiCas9-Blast	Lentiviral vector expressing SpCas9	Addgene, #52962
pUiSEPR	Lentiviral vector expressing improved sgRNA under U6 promoter	AG Tschaharganeh, DKFZ, Heidelberg

3.1.1 CRISPR/Cas9 guide

For CRISPR/Cas9-mediated genome editing, sgRNAs were subcloned into pX330 or pLentiCRISPR v2 according to Feng Zhang protocol [123]. Briefly, BbsI-digested pX330 or pLentiCRISPR v2 were ligated to the annealed and phosphorylated sgRNA. All constructs were subjected to Sanger sequencing with humanU6 primer before used in the study.

Table 2: sgRNA sequences for CRISPR/Cas9 mediated genome editing

Name	**Sequence (5' – 3')**
mKDM6A.1 guide	TCATCACCGAAAGCGGCGG
mKDM6A.2 guide	CCCAGCTTTTGTCGAGCCA
mTP53 guide	ACCCTGTCACCGAGACCCC
mDEPTOR.1 guide	TGCAGAAATTAGCCGACCG
mDEPTOR.2 guide	CAGAATGAACTTCCGTCGG

3.1.2 Short hairpin RNA (shRNA)

The test the knockdown efficacy of shRNAs targeting KDM6A, potent shRNAs were predicted using the algorithm by Pelossof et al. [124] and cloned into the MLPe vector (MSCV-LTR-miR-E-PGK-Puro-IRES-GFP) as described before [125]. The hairpins was ordered as 97-mer oligos and were PCR amplified with miRE-XhoI and miRE-EcoRI primer. The PCR product was then digested with EcoRI-HF and XhoI and purified before ligated to the EcoRI-HF/XhoI-digested MLPe backbone. To evaluate the knockdown efficiency of the shRNAs, target cells were transduced with a MOI<0.7 to achieve single copy integration. After Puromycin selection cells were harvested and

subjected to western blot. Knockdown efficiency was compared to cells transduced with Renilla luciferase, a non-targeting control.

Two most potent shRNAs against KDM6A were chosen and further cloned into pT3-TRE-tRFP-miR-E and pCol-TGM. Both plasmids were also digested with EcoRI-HF and XhoI, and ligated to the EcoRI-HF/XhoI-digested PCR amplicons (hairpin). All plasmids were sequenced with miR-E primer before used in the study.

Table 3: 97-mer hairpin and cloning primer sequences

Name	Sequence (5' – 3')
shKDM6A.1 (mouse)	TGCTGTTGACAGTGAGCGATGCTACGAATCTCTAATCTTATAGTGAAGC CACAGATGTATAAGATTAGAGATTCGTAGCAGTGCCTACTGCCTCGGA
shKDM6A.2 (mouse)	TGCTGTTGACAGTGAGCGAACAGACTATGAGTCTAGTTTATAGTGAAGC CACAGATGTATAAACTAGACTCATAGTCTGTGTGCCTACTGCCTCGGA
shRenilla (mouse)	TGCTGTTGACAGTGAGCGCAGGAATTATAATGCTTATCTATAGTGAAGC CACAGATGTATAGATAAGCATTATAATTCCTATGCCTACTGCCTCGGA
miRE-XhoI	TACAATACTCGAGAAGGTATATTGCTGTTGACAGTGAGCG
miRE-EcoRI	TTAGATGAATTCTAGCCCCTTGAAGTCCGAGGCAGTAGGCA
miR-E primer	TGTTTGAATGAGGCTTCAGTAC

3.2 Animal experiments

For hydrodynamic tail vein injections, 8 weeks old female C57Bl/6 animals were purchased from Envigo. 5µg DNA of pT3-EF1a-MYC, 20µg of pX330 expressing indicated sgRNAs together with CMV-SB13 Transposase (1:5 ratio); 20µg of pT3-TRE-tRFP-shRNA, 5µg of pT3-myc-IRES-rtTA3 and CMV-SB13 were prepared in a sterile 0.9% NaCl solution and injected into the lateral tail vein with a total volume corresponding 10 % of body weight in 5-7 seconds as described before.

All animals were monitored daily and animal experiments were performed in compliance with all relevant ethical regulations determined in the animal permit. Upon euthanasia, relevant organs from experimental mice were visually inspected, harvested, and photographed. Tumor samples were taken to obtain genomic DNA, RNA, protein and the rest were incubated in 4% PFA for at least 24 h for further use. All animal experiments were approved by the regional board Karlsruhe, Germany.

3.2.1 ESC-based pancreatic cancer

ESCs harboring disease predisposing alleles as described before were used to introduce the conditional KDM6A knockdown by generating pCol-TGM plasmids containing the shRNA. Two shRNAs against KDM6A and one control shRNA against Renilla luciferase were cloned into pCol-TGM plasmid and were electroporated into the ESCs together with pCAGs-FLPe to mediate recombinase-mediated cassette exchange. After electroporation ESCs were selected for Hygromycin resistance and only ESCs with successful integration of the targeting construct at the ColA1a locus confer Hygromycin resistance. After selection, resistant clones were picked and expanded. Targeted clones were used for Blastocyst injections (in cooperation with the DKFZ transgenic core facility) to generate cohorts of chimeric mice, which were directly used for further experiments. Mice received doxycyclin-containing diet at the age of 4 weeks in order to activate shRNA expression and thus KDM6A knockdown. Disease onset was monitored by weekly palpation.

3.2.2 Magnetic Resonance Imaging (MRI)

MRI was carried out by our small animal imaging core facility in DKFZ using a Bruker BioSpec 1Tesla (Ettlingen, Germany). For the imaging, mice were anesthetized with 3% sevoflurane in air. T2 weighted imaging were performed using a T2_RARE_ sequence axial: TE = 84 ms, TR = 4806.1582 ms, FOV 30x30 mm, slice thickness 1mm, averages = 4, Scan Time 461.39 s, echo spacing 8 ms, rare factor 10, slices 20, image size 192x192, flip angle 180. If liver lesions can be observed in T2, contrast-enhanced T1 measurement (80 µl ProHance, 0.5 mmol/kg, Bracco, i.p. injection) were carried out to visualize and quantify tumor growth. Unfortunately the liver tumors did not accumulate the contrast reagent and thus a volumetric size determination with T1 was not possible. The size determination was then performed using T2-weighted MRI images. The region of interest (ROI) were drawn manually in each layer and total volume of the lesion from the individual ROI was calculated with ParaVision software (Bruker). The evaluation was carried out by the same person throughout the study.

3.3 Immunohistochemistry (IHC)

All samples were fixed in 4% paraformaldehyde for at least 72h, embedded in paraffin and sliced into 3 µm thick sections for IHC staining. Slides were deparaffinized with

xylene, rehydrated through a descending alcohol series and washed in water. For antigen retrieval, slides was put in sodium citrate buffer (pH 6.0) and boiled in a pressure cooker for 8 min followed by cooling down under running water for 5 min. Subsequently slides were blocked with 3% hydrogen peroxide for endogenous peroxidase activity, washed for 1min under running water and twice with phosphate-buffered saline (PBS) and blocked with 5% BSA in PBS with 0.05% Triton X-100 at room temperature for 1 hour. Slides were incubated with the rabbit monoclonal anti-KDM6A (# 33510; Cell Signaling Technology; dilution 1:200), anti-tRFP (AB233; Evrogen; dilution 1:750), and anti-Deptor (NBP1-49674; Novus Biological; dilution 1:500) overnight at 4 °C. Slides were then washed three times with PBS+0.05% Triton X-100, incubated with ImmPRESS goat anti rabbit or mouse IgG Polymer Kit, Peroxidase reagent (Vector laboratories #MP-7451) for 30 min at room temperature and washed further twice with PBS+0.05% Triton X-100. Staining was visualized using ImmPACT DAB Peroxidase Substrate Kit (Vector laboratories #SK-4105) according to the manufacturer's protocol and were counterstained with hematoxylin. Finally the slides were washed through ascending alcohol series that ended with Xylol and mounted with Surgipath Micromount Mounting Medium (Leica # 3801731).

3.4 Derivation of primary liver tumor cell lines

Liver tumors were resected with sterile instruments and washed in sterile PBS prior to digestion. Then tumor tissue was minced and resuspended in a mix of 4 mg/ml collagenase IV and dispase (w/v in sterile, serum free Dulbecco's Modified Eagle Medium (DMEM, Sigma)) at 37°C for 30min with gentle shaking. The dissociated tumor cells were then washed with complete DMEM (supplemented with 10% (v/v) fetal bovine serum (FBS) and 1% Penicillin/Streptomycin) and plated on collagen-coated plates (PurCol, Cell Systems; 0.05 mg/ml). Primary cultures were passaged until visibly free from other contaminating cell types.

3.5 Derivation of primary pancreatic tumor cell lines

Pancreatic tumors were dissected with sterile instruments, washed in sterile HBSS and were minced with a blade until chunks were about 1-2mm. Tumor tissues were resuspended in 1mg/ml Collagenase V (Sigma) (w/v in sterile, serum free HBSS with Ca/Mg) and incubated at 37°C for 30min with gentle shaking. The dissociated tumor

cells were then washed with PBS, resuspended in 0.25% Trypsin and incubated at 37°C for 5min to break up some extracellular matrix. Trypsin was then neutralized with complete DMEM. Before plated on collagen-coated plates, cells were further washed twice with complete medium. Primary cultures were passaged until the GFP positive population >90%.

3.6 Cell culture

All cell lines were maintained in complete DMEM at 37°C with 5% CO2. Liver and pancreatic cancer cells were split twice per week at a ratio of 1:30-40 and 1:5 correspondingly using collagen-coated plates. Myc; shKdm6a and KrasG12D; shKdm6a cells were cultivated in complete DMEM, with doxycycline (VWR; 1µg/ml) when applicable.

3.7 Virus production

For lentivirus production, HEK293T cells were plated one day before transfection into 10 cm plates and transfected when near confluence was reached using a plasmid mix of 2.5 µg pMD.2G, 8 µg psPAX2 (Addgene plasmid #12259 and # 12260, both were a gift from Didier Trono) and 10 µg pLenti CRISPR v2 harboring respective guides in 1000 µl serum free DMEM and 60 µl polyethylenimine (PEI, 1 µg/µl). The plasmid mix was then vortexed for 5, incubated at room temperature for 30 min incubation and added drop-wise to cells. 24h following the transfection, medium was exchanged and lentiviral supernatant was harvested 48 h post-transfection using 0.45 µm Cellulose Acetate Membrane filters (VWR) and stored at -80°C until use.

For Retrovirus production, HEK-gp-cells were also seeded out as for lentivirus production and transfected using a plasmid mix of 2.5 µg pMD.2G and 20 µg retroviral plasmid such as MLPe vector, pSIN, or pMSCV-rtTA3-PGK-Puro in 1000 µl serum free DMEM and 60 µl polyethylenimine (PEI, 1 µg/µl). The viruses were harvested as lentivirus.

3.8 Transduction

Target cells were plated on 10cm plate and one day following the plating, cells were transduced with viral supernatants in the presence of Polybrene (4 µg/ml). 2 days post-

transduction cells were selected with Puromycin (2 µg/ml), Blasticidin (10 µg/ml) or G418 (Neomycin; 1mg/ml) dependent on the plasmid.

3.9 Immunoblotting

Cells were harvested and lysed in cell lysis buffer (Cell Signaling Technology) supplemented with both protease (Complete Mini; Roche) and phosphatase inhibitors. To ensure lysis, cells were sonicated for 5 min in ice and subsequently centrifuged at 4˚C at 13,000rpm to collect protein lysates. Furthermore, protein lysates were equalized utilizing BCA protein assay (Thermo Scientific), equal amount of protein were mixed with Laemmli buffer (100 mM Tris-HCl pH 6.8, 5% glycerol, 2% SDS, 5% 2-mercaptoethanol) and boiled at 95°C for 5 min. Proteins were separated by SDS–PAGE, transferred onto PVDF membrane, and detected by immunoblotting using the appropriate antibodies. Image detection was performed with AlphaView software (ProteinSimple) using the Clarity Western ECL substrate Solution (Bio-Rad). The list of antibodies and their sources can be found in Table 3.

Table 4: Antibodies for Immunoblotting

Antigen	Dilution	Catalog number	Company
KDM6A (UTX)	1:1000	33510	CST
DEPTOR	1:1000	NBP1-49674	Novus Biological
TSC1	1:1000	6935	CST
TSC2	1:1000	4308	CST
pP70S6K T389	1:1000	9202	CST
pS6RP S235/6	1:1000	4858	CST
pS6RP S240/4	1:1000	5364	CST
S6RP	1:1000	2217	CST
P4EBP-1 T37/46	1:1000	2855	CST
4EBP-1	1:1000	9452	CST
Actin	1:20000	PA5-22325	Sigma
Vinculin	1:5000	V9131	Sigma
HRP-conjugated goat α-mouse	1:5000		Jackson Immuno Research
HRP-conjugated goat α-rabbit	1:5000		Jackson Immuno Research

3.17 Mutation detection by T7 assay

CRISPR/Cas9-mediated mutations were detected using the T7 endonuclease I (New England Biolabs). Briefly, genomic DNAs was isolated using Gentra Puregene Tissue Kit (Qiagen) in accordance to manufacturer's protocol. An approximately 700bp region surrounding the CRISPR/Cas9-targeted site was amplified using the Q5 Hot Start DNA polymerase (New England Biolabs), column-purified (Qiagen), and subjected to a series of melting & annealing cycles with the annealing temperature gradually lowered in each successive cycle. T7 endonuclease I was then added to selectively digest heteroduplex DNA. Digest products were visualized on a 2-3% agarose gel.
Alternatively, Sanger nucleotide sequencing analysis was performed on PCR products using a T7 primers to detect mutations.

Table 5: T7 primer sequences

Name	Sequence (5' – 3')
mKDM6A.1_F1	CAACAACTTTGTGCTGGTGCC
mKDM6A.1_R1	GTTTGCCTTACCTTGCCCAGCAG
mKDM6A.1_F2	CTACGAATCCCCCCCAGAGCT
mKDM6A.1_R2	GATCTCTCAAGAGAGCAAGCG
mKDM6A.2_F1	CTGACTCCTCACTAATGCAG
mKDM6A.2_R1	CATGCCCTGCTGGTTGAAGTGG
mKDM6A.2_F2	CCACGTGAATGTCTGGATTTC
mKDM6A.2_R2	GTAGCTCTATGGTGGCCAATC

3.18 Clonogenic assay

To assess cell survival and proliferation, 500 cells were plated in 6 well plates as triplicate. Both tetracycline inducible-shKdm6a or Kdm6a-cDNA expressing cells were grown in the presence or absence of doxycycline, and cells were fixed with methanol and stained with 0.05% crystal violet after 10 days.
For quantification, the amount of crystal violet taken up by the cells were dissolved in solubilization buffer (50% Methanol, 5% acetic acid and 0.1% SDS) and quantified in a spectrophotometer by reading the absorbance at 570nm.

3.19 Competition assay

To evaluate the effect of Kdm6a overexpression in cell proliferation/viability, Myc sgKdm6a cells expressing rtTA3 (GFP negative) were mixed with either GFP-positive Kdm6a overexpressing or control cells with 30:70 ratio. The GFP+/GFP− ratio were evaluated with Guava® easyCyte benchtop flow cytometer (Merck Millipore) over time in the presence or absence of doxycycline.

3.20 Apoptosis assay

Apoptosis was assessed in liver cancer cell lines via CellEvent™ Caspase-3/7 Green Detection Reagent (Invitrogen) according to manufacturer's protocol. Briefly, 10,000 cells were grown with and without doxycycline for 6 days in 6 well plate, trypsinized, and resuspended in complete DMEM. About 100,000 cells were incubated with 2 µM final concentration of CellEvent™ Caspase-3/7 Green Detection Reagent for 45 min at 37°C and subsequently analyzed with Guava® flow cytometer.

3.21 Drug treatment and cell viability assay

For assessment of cell sensitivity towards Torin1 (Cayman Chemical), cells were plated in 96 well plate one day prior to treatment and cell viabilities were assessed with CellTiter-Blue® (Promega) 72 hours following the drug treatment. The reagent was added into each well of 96 well plate with 1:10 dilution, incubated for 4 hours at 37 °C and fluorescent signal was recorded ($560_{Ex}/590_{Em}$) using FLUOstar Omega (BMG Labtech).

3.22 Quantitative reverse transcription PCR (qRT-PCR)

Total RNA was isolated using RNeasy Mini Kit (Qiagen) and Rnase-Free Dnase Set (Qiagen) in accordance to manufacturer's protocol. 1 µg of purified RNA was reverse transcribed using TaqMan® Reverse Transcription Reagents (Thermo Fisher Scientific) and diluted 1:20 before subjected to qPCR. For the qPCR reaction, cDNA was mixed with Power SYBR® Green Master Mix (Thermo Fisher Scientific) and target specific primers and performed in triplicate. Transcript levels were normalized to the levels of Tubulin mRNA expression and calculated using the deltaCt (ΔCt) method. qPCR was carried out using QuantStudio 3 Real-Time PCR system (Applied biosystems).

Table 6: qRT-PCR primer sequences

Name	Sequence (5' – 3')
mKDM6A_For	AAGGCTGTTCGCTGCTACG
mKDM6A_Rev	GGATCGACATAAAGCACCTCC
mTSC1_For	ACTCTCCCTTCTACCGAGACA
mTSC1_Rev	GAGGCTGCCGAATGAGTCTTC
mTSC2_For	GAGCTGATTAACTCGGTGGTC
mTSC2_Rev	GGCCAGGTCCCTTTCTTCC
mDEPTOR_For	ATAGACGGCACCATCTCAAAAC
mDEPTOR_Rev	GTCGGCTAATTTCTGCATGAGT
mTubulin_For	TCACTGTGCCTGAACTTACC
mTubulin_Rev	GGAACATAGCCGTAAACTGC

3.23 RNA sequencing and differential expression analysis

For RNA sequencing, total RNA from three independent tumor-derived cell lines (Myc; sgMll3 and Myc; sgp53) was isolated using RNeasy Mini Kit (Qiagen), QIAshredder Columns and Rnase-Free Dnase Set (Qiagen). RNA-Seq library construction and sequencing were performed according to protocols used by the integrated genomics operation (IGO) Core at MSKCC. 5-10 million reads were acquired per replicate sample. After removing adaptor sequences with Trimmomatic [126], RNA-seq reads were aligned to GRCh37.75(hg19) with STAR [127]. Genome wide transcript counting was performed by HTSeq to generate FPKM matrix [128]. Differentially expressed genes were identified by DESeq2 (v.1.8.2 ,package in R) and plotted in the volcano plot. The complete dataset is available at NCBI Gene Expression Omnibus (GSE85055).

3.24 CUT&RUN

Cleavage under target and release using nuclease (CUT&RUN) was performed as previously described by Skene et al. [129]. Briefly 250,000 Myc; TRE shKdm6a cells grown in the presence or absence of doxycycline were harvested and immobilized on activated Concanavalin A – coated beads at room temperature for 10 min, permeabilized with 0.025% Digitonin and incubated with antibody with rotation

overnight at 4°C. All the antibodies used in this study were diluted 1:100 for Cut&Run experiment and are listed in the Table7. Following the incubation, cells were incubated with the pA-MNase to a final concentration of 700 ng/ml at 4 °C for 1 hour, washed and digested upon Ca2+ addition at 0 °C for 30 min. To release the DNA-protein complex, cells were further incubated at 37 °C for 10 min and the supernatant was collected. The DNA fragments in the supernatant were then extracted using the spin column (Qiagen) and libraries were prepared using NEBNext Ultra II DNA library Kit for Illumina (New England Biolabs) following the manufacturer's protocol. The libraries were sequenced using HiSeq2500 (Illumina) in 25 bp paired-end rapid mode (library concentration of flowcell: 12pM, 1% PhiX spike-in) and HiSeq Rapid SBS Kit v2 (50 cycles; FC-402-402) was used for the HiSeq PE 25 R sequencing type.

Table 7: Antibodies for Cut&Run

Antigen	Catalog number	Company
KDM6A (UTX)	33510	CST
H3K27me3	9733	CST
H3K27ac	ab4729	Abcam
H3K4me1	ab8895	Abcam
H3K4me3	ab8580	Abcam
IgG	ab37415	Abcam

3.18 Human patient samples

Fifty HCCs and corresponding surrounding non-tumor liver tissues were used for the study. Liver tissues were collected at the Universities of Greifswald (Greifswald, Germany) and Regensburg (Regensburg, Germany). Institutional Review Board approval was obtained at local Ethical Committees of the Medical Universities of Greifswald (approval code: BB 67/10) and Regensburg (approval code 17-1015-101), in compliance with the Helsinki Declaration. Written informed consent was obtained from all individuals.

3.18.1 Immunohistochemistry

Human liver specimens were fixed overnight in 4% paraformaldehyde and embedded in paraffin. Sections were done at 5 µm in thickness. For immunohistochemical staining, slides were deparaffinized in xylene, rehydrated through a graded alcohol series, and rinsed in PBS. Antigen retrieval was performed in 10 mM sodium citrate buffer (pH 6.0) by placement in a microwave oven on high for 10 min, followed by a 20-min cool down at room temperature. After a blocking step with the 5% goat serum and Avidin-Biotin blocking kit (Vector Laboratories, Burlingame, CA, USA), the slides were incubated with the rabbit monoclonal anti-KDM6A (# 33510; Cell Signaling Technology, Danvers, MA, USA; dilution 1:100), anti-Deptor (# 11816; Cell Signaling Technology; dilution 1:100), and anti-phosphorylated RPS6 (# 2211; Cell Signaling Technology; dilution 1:3) primary antibodies overnight at 4 °C. Slides were then subjected to 3% hydrogen peroxide for 10 min to quench endogenous peroxidase activity and, subsequently, the biotin conjugated secondary antibody was applied at a 1:500 dilution for 30 min at room temperature. The immunoreactivity was visualized with the Vectastain Elite ABC kit (Vector Laboratories, Burlingame, CA, USA) and Vector NovaRed (Vector Laboratories) as the chromogen. Slides were counterstained with hematoxylin. Slides were evaluated semiquantitatively by comparing each tumor with its surrounding non-neoplastic counterpart, thus defining "high" and "low" the levels of a given protein in a HCC sample when compared to the corresponding non-tumorous counterpart.

3.18.2 Quantitative Reverse Transcription Real-Time PCR (qRT-PCR)

Gene Expression Assays for human UTX/KDM6A (ID# Hs00253500_m1), Deptor (Hs00961900_m1), and β-Actin (ID # 4333762T) genes were purchased from Applied Biosystems (Foster City, CA, USA). Quantitative values for each gene were calculated by using the PE Biosystems Analysis software and expressed as number target (NT). $NT = 2^{-\Delta Ct}$, wherein ΔCt value of each sample was calculated by subtracting the average Ct value of the target gene from the average Ct value of the β-Actin gene.

3.19 Cell lines, virus production for pooled CRISPR/Cas9 screening

Cells used in the pooled CRISPR/Cas9 were first lentivirally transduced with LentiCas9-Blast, followed by Blasticidin selection and assessed for stable Cas9

expression by western blotting. The epigenetic library used in this study was kindly provided by Lowe Lab, MSKCC and were cloned into the pUSEPR vector. This library was pooled together at equimolar ration and then used to generate lentivirus in HEK293T as described in virus production section above. Viral supernatants were collected 48 hour post-transfection and kept at -80°C.

3.19.1 Pooled CRISPR/Cas9 screening

Dilutions of this lentivirus correlated with RFP positivity in infected cells was tested and evaluated with FACS Fortessa (BD, Franklin Lakes) before the actual screening. To ensure that only one single sgRNA was transduced per cell, 30% of RFP-positive population was aimed 48h post-transduction. Total cells used in the screening were adjusted to achieve at least 1000-fold representation of each sgRNA in the initial cell population. The screening was performed in T175 flask to obtain the required cell numbers. Library transduced cells were subsequently selected with Puromycin for 4 days and splitted accordingly.

Genomic DNA was extracted with Gentra Puregene Tissue Kit (Qiagen) at the designated time points. To amplify the sgRNA cassette for sequencing and maintain the 1000X coverage of the sgRNA, 15 PCR reactions with each 2000 ng starting gDNA were amplified using the Q5 Polymerase for 20 cycles. PCR products were validated by agarose gel, pooled, and purified before subjected to sequencing. The primer sequences contain barcodes used in the PCR amplification are listed in Table 8.

The sequence data were mapped to the reference sgRNA library and read counts were then calculated for each individual sgRNA by CRISPR-AnalyzeR (DKFZ, Heidelberg). Differential representation of individual sgRNAs between initial and final timepoints were used to call the hit candidates.

Table 8: PCR primer sequences for CRISPR/Cas9 screening

Name	Sequence (5' – 3')
Reverse Primer	CAAGCAGAAGACGGCATACGAGATGTGACTGGAGTTCAGACGTGTG CTCTTCCGATCTTTTACCCCGCGCCACCTTCTCTAGG
Forward Primer #1	AATGATACGGCGACCACCGAGATCTACACTCTTTCCCTACACGACG CTCTTCCGATCTNNNNNNNNNCGGTTCAATTGTGGAAAGGACGAAA CACCG
Forward Primer #2	AATGATACGGCGACCACCGAGATCTACACTCTTTCCCTACACGACG CTCTTCCGATCTNNNNNNNNNGCTGGATTTTGTGGAAAGGACGAAA CACCG

Forward Primer #3	AATGATACGGCGACCACCGAGATCTACACTCTTTCCCTACACGACG CTCTTCCGATCTNNNNNNNNNTAACTCGGTTGTGGAAAGGACGAAA CACCG
Forward Primer #5	AATGATACGGCGACCACCGAGATCTACACTCTTTCCCTACACGACG CTCTTCCGATCTNNNNNNNNNATACTCAATTGTGGAAAGGACGAAA CACCG
Forward Primer #6	AATGATACGGCGACCACCGAGATCTACACTCTTTCCCTACACGACG CTCTTCCGATCTNNNNNNNNNGCTGAGAATTGTGGAAAGGACGAAA CACCG
Forward Primer #7	AATGATACGGCGACCACCGAGATCTACACTCTTTCCCTACACGACG CTCTTCCGATCTNNNNNNNNNATTGGAGGTTGTGGAAAGGACGAAA CACCG
Forward Primer #8	AATGATACGGCGACCACCGAGATCTACACTCTTTCCCTACACGACG CTCTTCCGATCTNNNNNNNNNTAGTCTAATTGTGGAAAGGACGAAA CACCG
Forward Primer #9	AATGATACGGCGACCACCGAGATCTACACTCTTTCCCTACACGACG CTCTTCCGATCTNNNNNNNNNCGGTGACCTTGTGGAAAGGACGAAA CACCG
Forward Primer #10	AATGATACGGCGACCACCGAGATCTACACTCTTTCCCTACACGACG CTCTTCCGATCTNNNNNNNNNTACAGAGGTTGTGGAAAGGACGAAA CACCG
Forward Primer #12	AATGATACGGCGACCACCGAGATCTACACTCTTTCCCTACACGACG CTCTTCCGATCTNNNNNNNNNTATGTCTTTTGTGGAAAGGACGAAA CACCG
Forward Primer #17	AATGATACGGCGACCACCGAGATCTACACTCTTTCCCTACACGACG CTCTTCCGATCTNNNNNNNNNCGTGAGCCTTGTGGAAAGGACGAAA CACCG
Forward Primer #18	AATGATACGGCGACCACCGAGATCTACACTCTTTCCCTACACGACG CTCTTCCGATCTNNNNNNNNNATCAGAGGTTGTGGAAAGGACGAAA CACCG

4. Results

4.1 KDM6A cooperates with c-MYC to drive liver tumorigenesis

To interrogate the function of Kdm6a CRISPR/Cas9 technology was applied to disrupt endogenous Kdm6a expression. In order to test appropriate sgRNAs, multiple single guide RNAs (sgRNA) targeting Kdm6a were designed using the http://crispr.mit.edu/ algorithm (MIT, Massachusetts), subsequently cloned into the pX330 plasmid, and were transfected into the murine fibroblast cell line 3T3. 3 days after transfection, genomic DNA was extracted, followed by targeted PCR-amplification and sgRNA-mediated genome editing was determined using T7 endonuclease-mediated digestion *in vitro*. T7 endonuclease digests double-strand DNA containing single nucleotide mismatches, such as those arising from pairing native DNA to CRISPR/Cas9-edited DNA. Shown in Figure 4.1 A is the T7 endonuclease-mediated digestion of Kdm6a locus specific PCR products following transfection with sgKdm6a-, but not with sgTp53-containing CRISPR/Cas9 plasmids. Sanger sequencing in combination with Inference of CRISPR Edit (ICE, Synthego, California) analyses further validated specific editing of the Kdm6a locus by sgKdm6a but not sgTp53 (Figure 4.1 B).

Two sgKdm6a targeting exon 1 (sgKdm6a.1) and exon 6 (sgKdm6a.2) were selected from our initial screen to further study the biological function of Kdm6a *in vivo*. To probe the function of Kdm6a on liver cancer development, we decided to choose a cancer prone background caused by enforced c-MYC expression. To this end, optimized hydrodynamic tail vein injection (HDTVi) technique was employed to deliver a plasmid cocktail solution containing a sleeping beauty transposon plasmid stably expressing human MYC (pT3-EF1a-MYC), a sgRNA-reconstituted pX330 CRISPR/Cas9 and a vector encoding the sleeping beauty transposase into the liver of C57/Bl6 wild-type mouse (Figure 4.1 C). In this condition, the plasmid cocktail injection was expected to generate a liver “tumor–initiating” cell population, where the transposon stably integrates MYC into the genome of host cells, and the pX330 CRISPR/CAS9 vector edits the targeted locus.

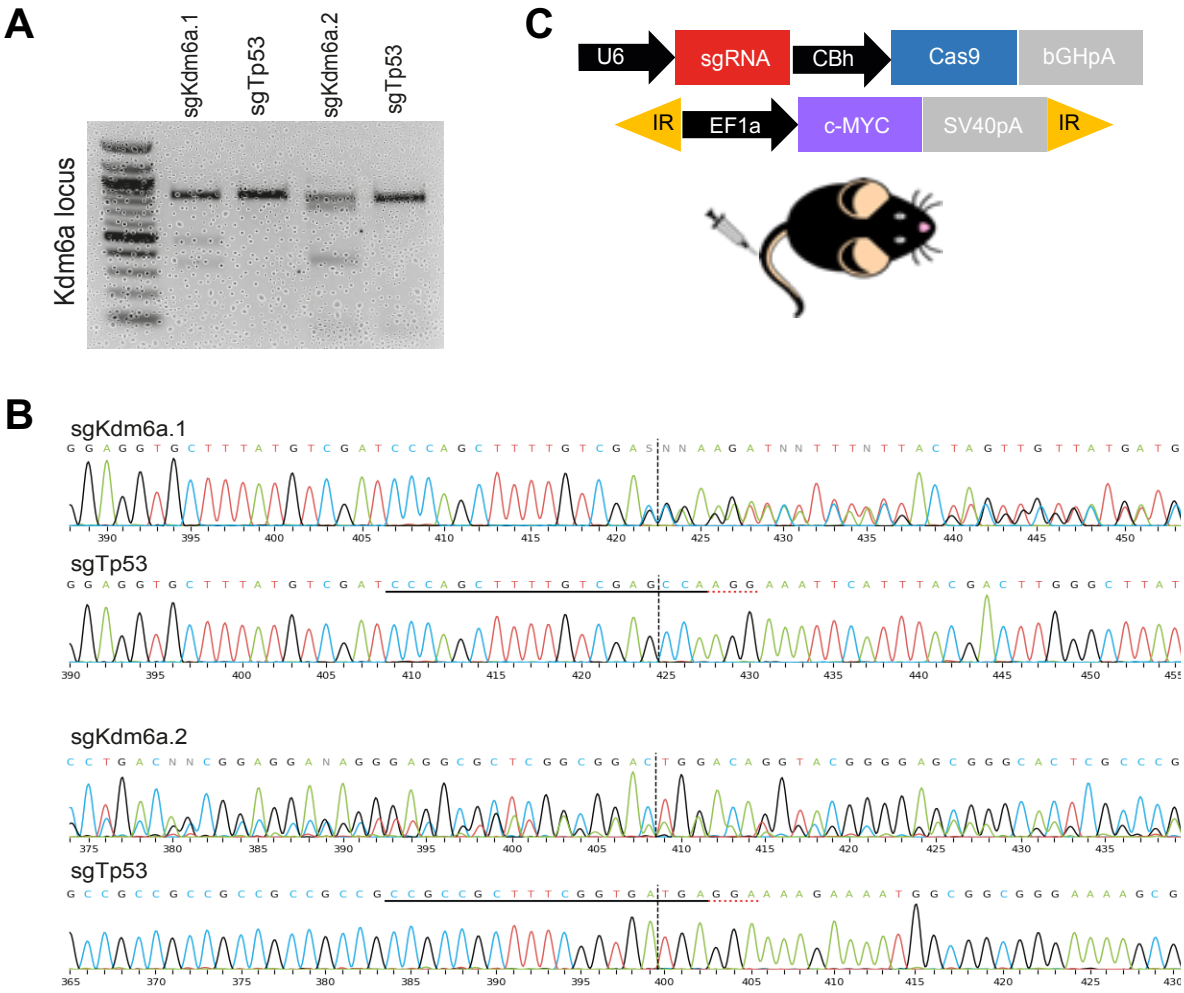

Figure 4.1 CRISPR/Cas9-mediated editing of Kdm6a. (A) Surveyor assay of PCR amplicons flanking predicted Kdm6a and Tp53 CRISPR cleavage sites. The ratio of intensity of the lower bands (containing indels) to that of the upper band (untargeted) provides an estimate of the efficiency of CRISPR/Cas cleavage at the Kdm6a and Tp53 loci. **(B)** Sanger sequencing of the CRISPR targeted Kdm6a locus . Dashed lines indicate the cutting site. **(C)** Vectors permitting transient expression of Cas9 and sgRNAs targeting KDM6A (top), and sleeping beauty transposon-based stable expression of c-MYC (bottom) were used to generate Myc; sgKdm6a liver tumor via HDTVi.

3 mice per group were monitored for up to 90 days on weekly basis and terminated immediately upon palpable liver tumors in accordance to the animal ethic permit. Mice receiving the sgRNA targeting Tp53 displayed high tumor burden in less than 50 days (Figure 4.2 A, Orange line). Likewise, the two independent sgKdm6a also induced rapid onset of tumors within a similar timeframe (Figure 4.2 A, Blue & Red lines). In contrast, all mice receiving the sgRNA GFP remained healthy during the course of the study (Figure 4.2 A, Black line).

Post mortem macroscopic inspection revealed the presence of multiple tumor nodules across the liver tissue of mice receiving sgTp53, sgKdm6a.1, or sgKdm6a.2

HDTVi (Figure 4.2 B). Histologic examination of tumor tissue using Hematoxylin & Eosin staining (HE) revealed abnormal growth of hepatocyte-like cells, a hallmark for hepatocellular carcinoma (HCC), for both groups (Figure 4.2 B). Parallel immunohistochemical (IHC) staining for Kdm6a reaffirmed loss of protein expression in sgKdm6a tumors, but not in sgTp53 tumors (Figure 4.2 B), validating editing efficiency of the selected sgRNAs *in vivo*. Importantly, no malignancy was be observed in the liver tissues of the control group (sgCntrl).

To gain further insights into the molecular functions of Kdm6a, primary cell lines were established from individual tumor nodules arising from each sgRNA. The established cell lines were annotated as Myc; sgKdm6a or Myc; sgTp53 for those derived from sgKdm6a- or sgTp53-derived liver tumors, respectively. Western blotting of Myc; sgKdm6a cell lines showed significant reduction (>95%) or absence of Kdm6a protein in comparison to Myc; sgTp53 cells (Figure 4.2 C).

Therefore, Kdm6a disruption by CRISPR/Cas9 leads to rapid liver tumor development in conjunction with enforced c-MYC expression, which is comparable to disruption of known tumor suppressor genes, such as Tp53.

To validate the specificity of the CRISPR/Cas9 system, a second orthogonal approach utilizing constitutive expression of shRNAs was pursued. First, a panel comprising 8 shRNAs targeting the 3'-untranslated region (3'-UTR) of Kdm6a were initially designed and tested using a constitutive retroviral expression system in murine 3T3 fibroblast cells. Using an shRNA targeting *Renilla* as a control, the two most potent shKdm6a were selected for subsequent testing *in vivo* (Figure 4.3 A). In order to guarantee stable expression *in vivo* shRNAs were cloned in a transposon-based plasmid was utilized, which allows stable integration of a GFP-fused shRNA under the control of the *EF1A* promoter (pT3-EF1a-GFP-miR-E) into the genome of host cells (Figure 4.3 B). This plasmid was co-delivered by HDTVi in conjunction with the same sleeping beauty transposon vector expressing human MYC as described above and liver cancer development was monitored (Figure 4.3 B).

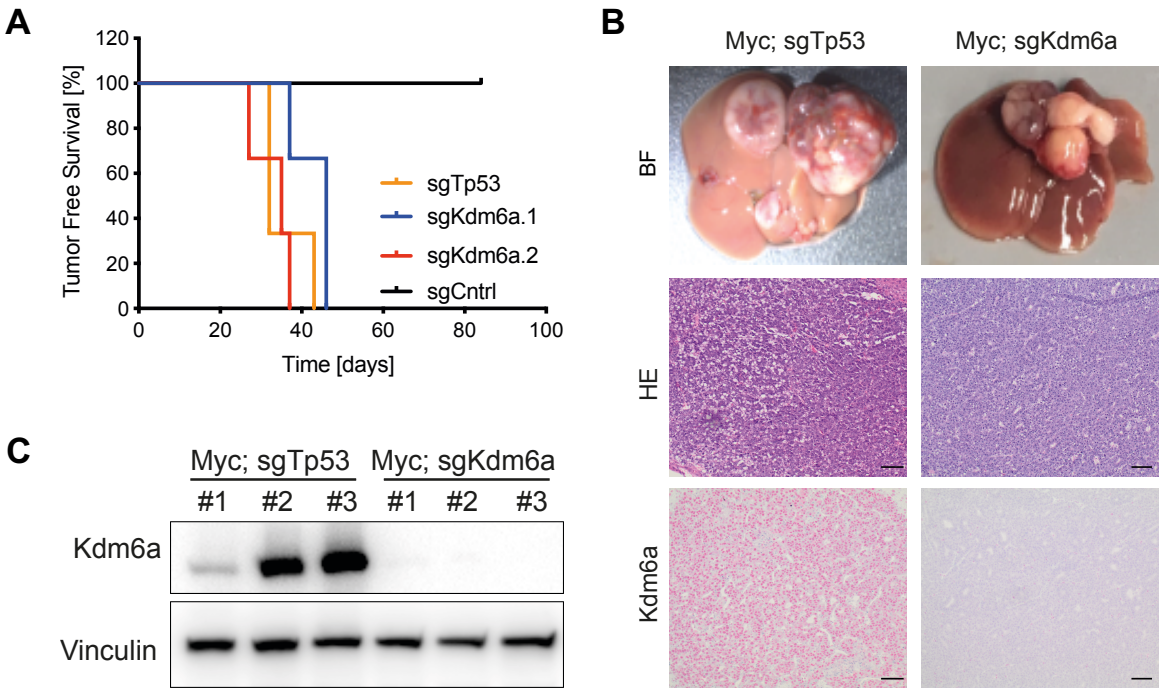

Figure 4.2 Kdm6a constrains c-MYC-driven tumorigenesis. (A) Tumor-free survival of mice injected with sgRNAs targeting Kdm6a, sgTp53, and sgCntrl. **(B)** Pathology of liver tumors generated by c-MYC overexpression and either Kdm6a or Tp53 knockout. Top, tumor nodules in Myc; sgTp53 and Myc; sgKdm6a injected mice. Middle, hematoxylin and eosin (HE) staining of liver tumors pictured above. Bottom, Kdm6a staining of corresponding tumors. Scale bar represent 50 µm. **(C)** Western blot analyses for Kdm6a in tumor derived cell lines from Myc;sgTp53 and Myc;sgKdm6a. Vinculin was used as loading control.

Following HDTVi, survival of the cohorts was investigated for up to 120 days. Whereas the two Kdm6a shRNAs robustly induced liver tumors among 10 mice tested for each shRNA (Figure 4.3 C, Blue & Red lines), mice treated with control shRenilla remained healthy throughout the course of observation (Figure 4.3 C, Black line). Similar to the previous CRISPR/Cas experiments, post-mortem examination of the two shKdm6a groups also revealed macroscopic tumor nodules across the liver tissue with histological characteristics of HCC (Figure 4.3 D & E). Importantly, sustained shRNA-mediated Kdm6a repression in tumor cells was confirmed due to GFP labelling of tumor tissue (Figure 4.3 D).

Thus, both CRISPR/Cas9 editing and shRNA mediated Kdm6a suppression consistently confirm a tumor-suppressive function of Kdm6a in the context of c-MYC-driven malignant transformation.

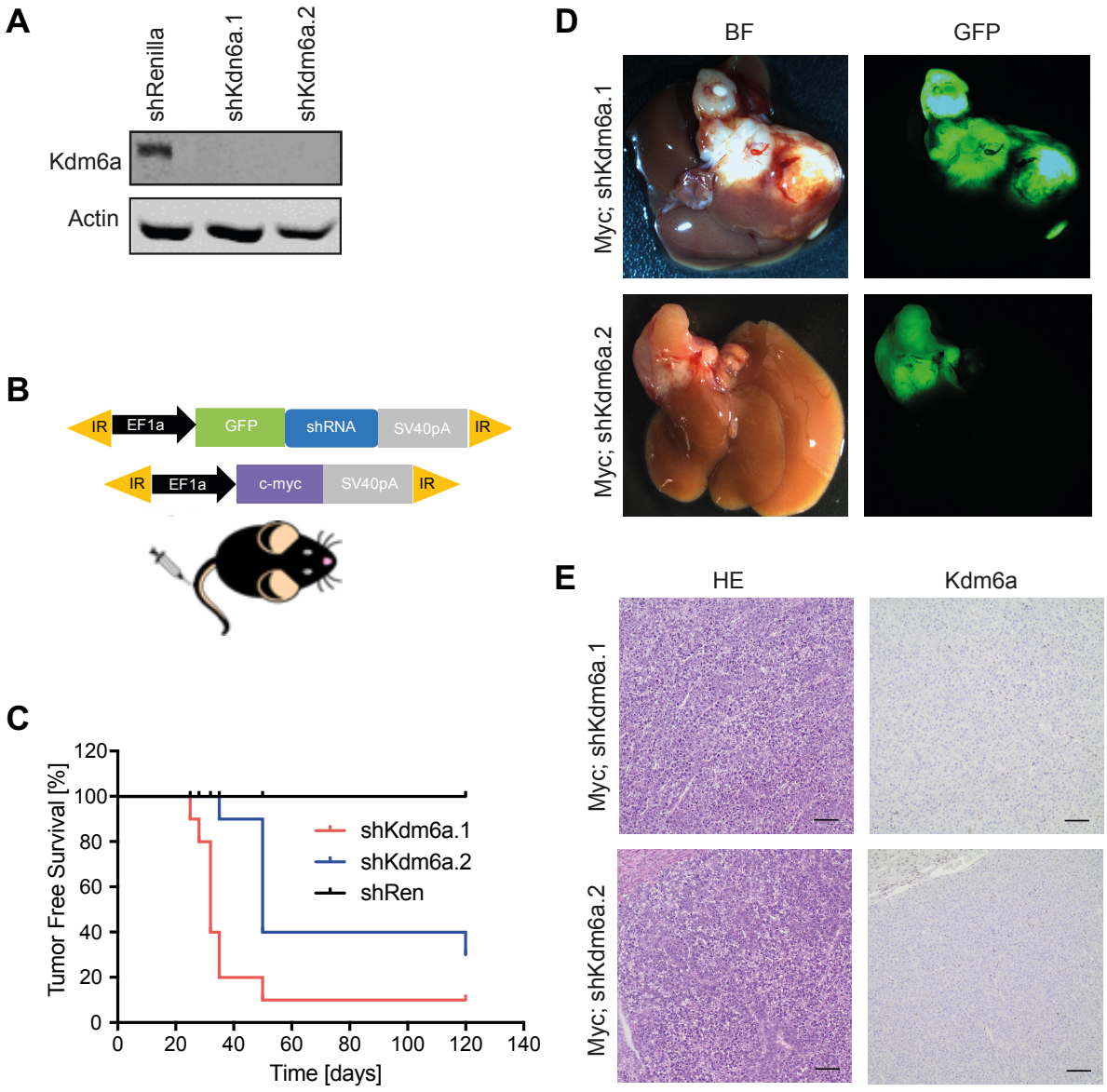

Figure 4.3 RNAi-mediated suppression of Kdm6a also promotes c-MYC-driven hepatocarcinogenesis. (A) Western blot analyses of Kdm6a knockdown by two different shRNAs. Actin was used as loading control. **(B)** Strategy for in vivo shRNA-mediated gene silencing in the setting of c-MYC overexpression. shRNAs targeting Kdm6a or Renilla were constitutively expressed and linked to GFP expression. **(C)** Tumor free survival of Myc; shKdm6a mice. **(D)** Tumor nodules observed in Myc; shKdm6a mice express shRNA-linked GFP. **(E)** Histopathology of Myc; shKdm6a liver tumors. Left, HE staining of liver tumors pictured above. Right, Kdm6a staining of corresponding tumors. Scale bar represent 50 µm.

4.2 Sustained Kdm6a loss is important for liver tumor maintenance

To address the question if sustained loss of Kdm6a is important for tumor maintenance, a tetracycline-inducible shRNA expression system was considered. For this, the validated shKdm6a.1 and shKdm6a.2 were subsequently cloned in a sleeping beauty transposon vector under tetracycline regulatory element (TRE) to allow for

tRFP-fused expression of shRNA in response to doxycycline (Tet-On; Figure 4.4 A). This vector was used in combination with a modified EF1a-MYC sleeping beauty transposon vector containing a reverse tet-transactivator (rtTA) (pT3-cMyc-IRES-rtTA3) to allow constitutive expression of rtTA3 (Figure 4.4 A). Using this Tet-On-shRNA system, precise control over endogenous Kdm6a expression can be achieved *in vivo* via feeding mice injected with these plasmids doxycycline-containing chow (Envigo Teklad, Indianapolis), which allows the expression of shKdm6a and subsequent suppression of Kdm6a protein.

To study whether sustained Kdm6a suppression is important for established tumors, we injected mice with these vectors and maintained them on doxycycline chow. Precise tumor growth was monitored not only by manual abdominal palpation but also by magnetic resonance imaging (MRI). Shown in Figure 4.4 B are representative MRI scans of liver lesions at the earliest possible time of detection (time 0; left panels, encircled in red), 2 weeks (middle panels), and 6 weeks following detection (right panels)). After tumor detection we stratified, tumor bearing mice were divided in two cohorts. One cohort was maintained on dox food. In the second cohort dox food was replaced by normal chow. Removal of doxycycline terminates the tRFP-fused shKdm6a expression and therefore allows for endogenous Kdm6a re-expression. Indeed, discontinuing dox-chow attenuated the tumor growth and prolonged the survival of this cohort dramatically in comparison to the control group fed continuously with doxycycline-containing chow (Figure 4.4.B & C). Similar to previous post-mortem examinations, macroscopic tumor nodules labelled with fluorescent proteins were observed in mouse livers receiving continuous doxycycline chow. In contrast, lesions extracted from mice receiving normal food showed little to no RFP labelling (Figure 4.4. D) and IHC staining also confirmed the Kdm6a expression in liver (Figure 4.5 E).

Additionally, we generated also primary cell lines from animals maintained on dox food. Accordingly, these set of cell lines were annotated as Myc; TRE shKdm6a.1 or the Myc; TRE sKdm6a.2 where the number refers to the different shKdm6a used to generate the liver tumor. Of note, these cell lines were maintained and propagated in continuous presence of doxycycline in culture.

Overall, findings from this set of experiment demonstrate that sustained Kdm6a suppression is important for tumor maintenance.

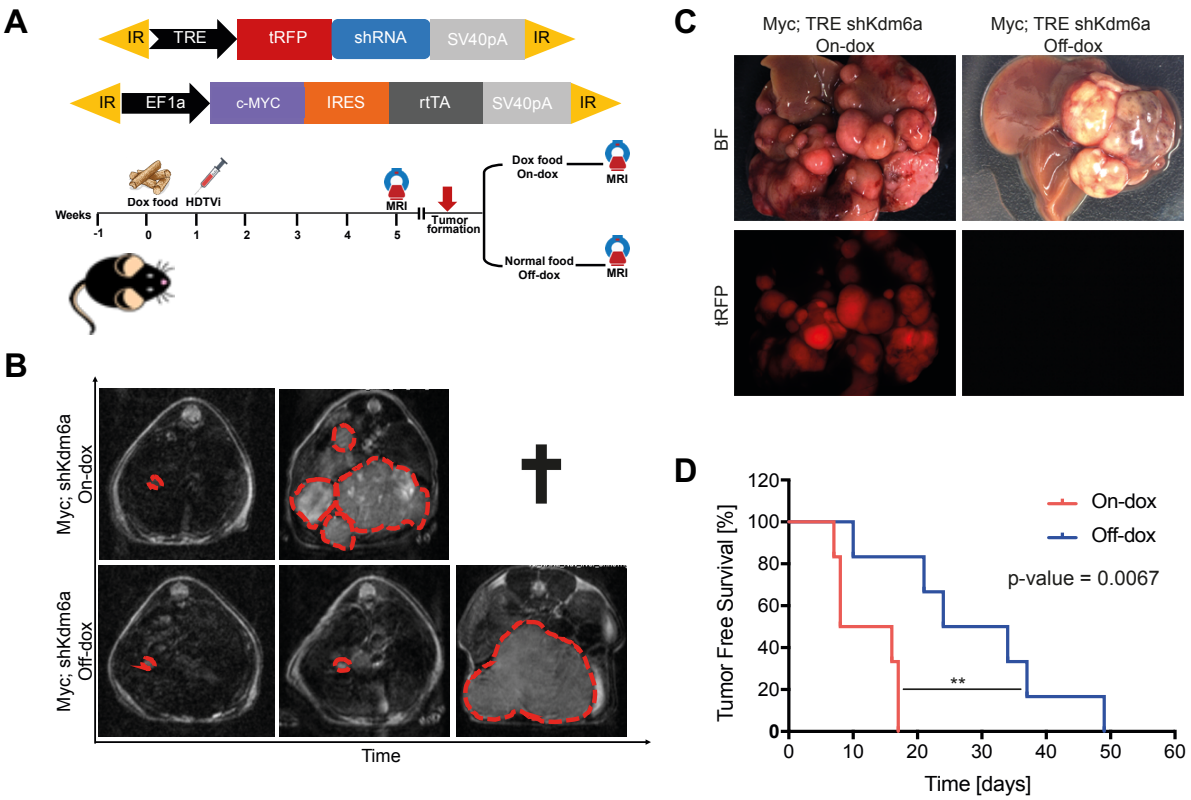

Figure 4.4 Endogenous Kdm6a re-expression restrains tumor progression. (A) Schematic view of the dox-inducible shKdm6a-mediated knockdown mice (Myc; TRE shKdm6a) and MRI experiment setting. **(B)** Representative MRI scan of Myc; TRE shKdm6a liver tumors (marked in red). **(C)** Tumor nodules observed in Myc; TRE shKdm6a mice express shRNA-linked tRFP. **(D)** Tumor-free survival of Myc; TRE shKdm6a mice in the presence (red line; Off-dox) or absence (blue line; On-dox) of Kdm6a.

4.3 Pro-apoptotic effect of Kdm6a

4.3.1 Endogenous Kdm6a re-expression induces apoptosis

To further analyze the molecular mechanisms of Kdm6a induced tumor suppressive functions, experiments were performed utilizing the above described primary cell lines. Immediate following the cell lines establishment, intact tetracycline-regulatory elements for shKdm6a were initially re-examined at both protein and mRNA levels. To do so, cell lines were cultured in absence of doxycycline for up to 6 days prior to harvest for Western blotting or RNA extraction. Cells cultured in presence of doxycycline served as reference for Kdm6a baseline expression in this experiment. Both Western blotting and qRT-PCR analyses showed restored levels of endogenous Kdm6a protein and mRNA in the two Myc; TRE shKdm6a cell lines upon doxycycline withdrawal from the culture (Figure 4.5 A & B). Noticeably, the doxycycline withdrawal condition appeared to reduce cell numbers significant for both of the Myc; TRE

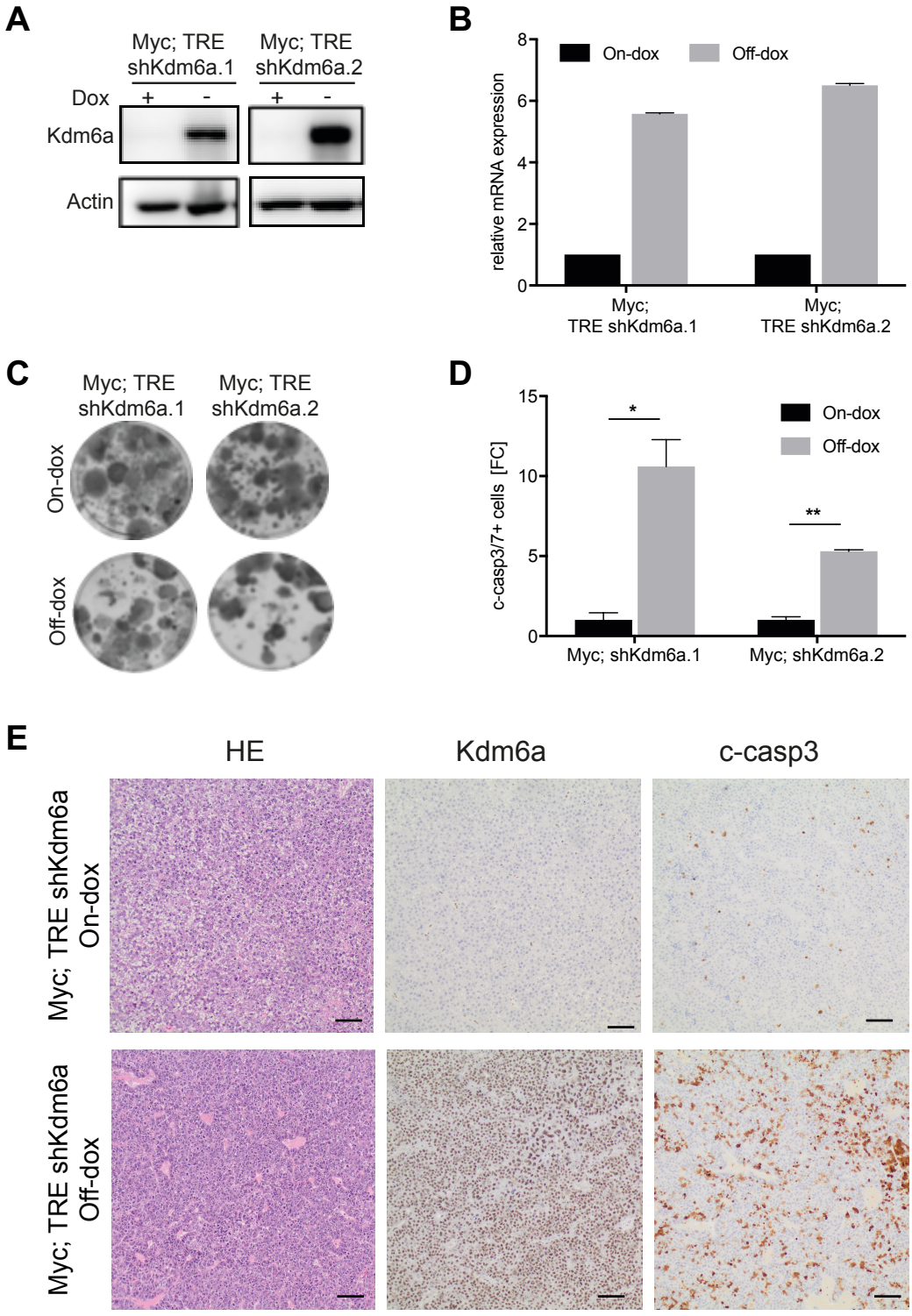

Figure 4.5 Kdm6a re-expression induces apoptosis. (A) Western blot analyses before (On-dox) and after (Off-dox) Kdm6a restoration in Myc; TRE shKdm6a cell lines expressing two independent Kdm6a shRNAs. Actin served as a loading control. (B) Quantitative PCR for Kdm6a expression in Myc; TRE shKdm6a cell lines with and without doxycycline. (C) Colony formation assay of indicated cell lines with or without doxycycline for 10 days. (D) Active caspase-3/7 labeling in Myc; TRE shKdm6a cell lines grown for 6 days with and without dox. Error bars represent mean ± SD from triplicates. **p<0.01 *p<0.05 (unpaired two-tailed t-test). FC=fold change. (E) IHC stainings of Myc; TRE shKdm6a liver tumors. Scale bar represent 50 µm.

shKdm6a cell lines. To assess this in a more quantitative manner, colony forming capacities of the cell lines were followed for up to 10 days in presence or absence of doxycycline. Crystal violet stained of the fixed colonies indeed confirmed reductions in overall cell numbers upon doxycycline withdrawal (Figure 4.5 C).

To account for the observed phenotypes, changes in cell apoptosis due to caspases activation were analyzed. Accordingly, processing of fluorochrome/quencher-conjugated DEVD peptide, a generic substrate for caspases 3/7, was used as a readout parameter to indicate caspase activation. Endogenous Kdm6a re-expression consistently increased the processing of the DEVD peptide in the two Myc; TRE shKdm6a cell lines *in vitro* (Figure 4.5 D), indicating increased apoptosis. Moreover, utilizing tumor tissues of our *in vivo* experiment, we observed increased numbers of tumor cells positively stained with activated cleaved caspase-3 in tumor lesion re-expressing Kdm6a (i.e. alternating doxycycline and no-doxycycline chow diet), while minimal cleaved caspase-3-positive cells were detected in tumors with Kdm6a knockdown (Figure 4.5 E).

4.3.2 Kdm6a overexpression cause apoptosis *in vitro*

To independently validate our results in another cell line model, Kdm6a was exogenously re-expressed in CRISPR/Cas knockout cell lines (Myc; sgKdm6a) using tetracycline-inducible vectors. Myc; sgKdm6a cell lines were first retrovirally transduced with pMSCV-rtTA3-PGK-Puro to create a stable cell line expressing rtTA. Subsequently, these cell lines were transduced for a second time with TRE-based vectors expressing the cDNA of Kdm6a, pSIN-TRE-KDM6A-PGK-Venus (Figure 4.6 A). Cells that were transduced with this inducible vector system constitutively express Venus (fluorescent proteins) and a Neomycin (G418) resistance cassette and allow the expression of KDM6A cDNA in an inducible manner. As control, we also transduced the rtTA-expressing cells with the same vector construct without the Kdm6a cDNA, pSIN-TRE-linker-PGK-Venus (Figure 4.6 A). Utilizing these cell lines, Kdm6a expression can be induced upon doxycycline addition as shown in western blots at different time points (Figure 4.6 B) and phenotypic alterations caused by Kdm6a can be assessed.

In agreement with our previous findings in the shRNA-based re-expression model, Myc; sgKdm6a cell lines with Kdm6a overexpression depleted significantly

over time compared to parental cell lines in competition assays (Figure 4.6 C), indicating a negative effect of Kdm6a expression on cell growth. Furthermore, less colonies were observed in clonogenic assay when Myc; sgKdm6a cells were cultured in doxycycline-containing medium (On-dox; Kdm6a overexpression) relative to cells that were cultured in standard medium (Off-dox, Kdm6a-null) (Figure 4.6 D, E). Increase of Caspase activity was also detected upon Kdm6a overexpression and quantified by the flow cytometry (Figure 4.6 F).

In summary, Kdm6a re-expression leads to retardation of cell growth due to induction of apoptosis *in vitro* and *in vivo*.

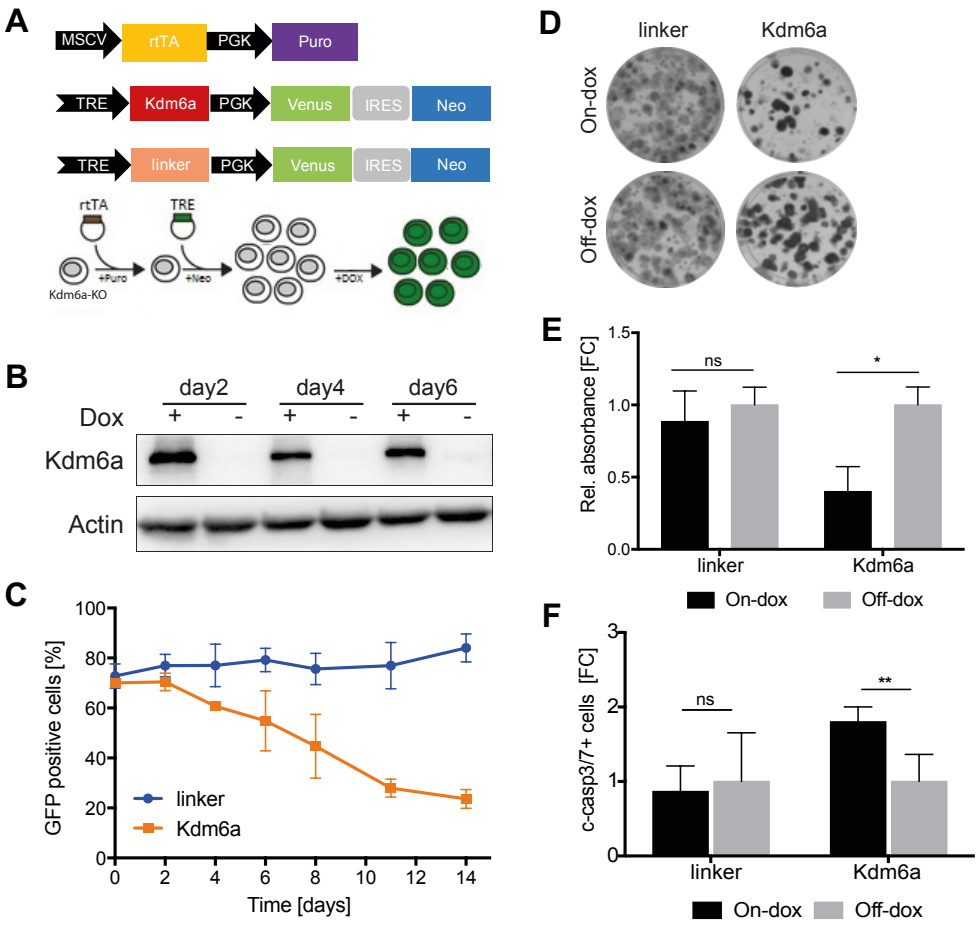

Figure 4.6 Kdm6a overexpression causes apoptosis in Kdm6a-deficient cells. (A) Top, vector constructs expressing rtTA and doxycycline-inducible vectors to overexpress either Kdm6a or linker (control) which is linked to GFP expression. Bottom, schematic workflow to generate rescue cell lines in Myc; sgKdm6a cell lines. **(B)** Western blot analyses of Kdm6a overexpression in Myc;sgKdm6a cell line with or without doxycycline at different time points. Actin was used as loading control. **(C)** Competition assay of Myc; sgKdm6a with Kdm6a (orange line) or without Kdm6a (blue line) over 14 days. **(D)** Colony formation assay of Myc; sgKdm6a cell lines with or without Kdm6a cultured with or without doxycycline for 10 days. **(E)** Colorimetric quantification of colony formation assay. Values are mean ± SD of three replicates. * $p<0.05$ (unpaired two-tailed t-test). **(F)** Active caspase-3/7 labeling in the indicated cell lines grown for 6 days with and without doxycycline. Error bars represent mean ± SD from triplicates. ** $p<0.01$ (unpaired two-tailed t-test). FC=fold change.

4.4 Deciphering molecular function of Kdm6a as tumor suppressor

4.4.1 Loss of KDM6A leads to transcriptional and epigenetic changes

To delineate the molecular mechanism of Kdm6a, we compared the global transcriptomes of three independently derived Myc; sgKdm6a cell lines to three independent Myc; sgTp53 cells. The RNA-seq analysis revealed a significant amount of differentially regulated genes upon Kdm6a knockout (Figure 4.7 A). With the threshold p-value<0.05 and 1< log2FC <-1, 910 genes were identified to be down-regulated and 330 were up-regulated when Kdm6a expression is disrupted as shown in the volcano plot. Downstream processing of these differentially expressed genes with Ingenuity Pathway Analysis (IPA) was used to determine pathways influenced by Kdm6a and revealed activation of certain metabolic and protein translation pathways such as glycolysis, oxidative phosphorylation, EIF2 signaling, mTOR signaling and regulation of eIF4 and p70S6K signaling (Figure 4.7 B).

Consistently, Gene Set Enrichment Analysis (GSEA) of global gene expression profiles also showed a marked upregulation of mTORC1 signaling pathway among others upon Kdm6a knockout (Figure 4.7 C). This led us to look further into mTOR pathway components, especially components implicated in mTORC1 signaling. Based on the transcriptomic expression data, negative regulators of mTORC1 such as Tsc1/2 and Deptor were downregulated in Kdm6a knockout cells while several translation initiation factors and ribosomal proteins were upregulated (Figure 4.7 D). In agreement with this, activation of mTORC1 signaling-related genes was also validated in Myc; TRE shKdm6a cell lines, as Kdm6a re-expression in Myc; TRE shKdm6a cell lines led to repression of PI3K/Akt/mTOR signaling pathway via upregulation of negative regulators. These findings together indicate the loss of Kdm6a leads to transcriptional changes related to mTOR pathway activation.

To further understand the underlying mechanism for these gene expression changes, we performed Cut&Run epigenetic profiling for Kdm6a and several histone marks in Myc; TRE shKdm6a cell line with or without the Kdm6a expression. Cut&Run profiles of Kdm6a revealed specific binding of Kdm6a after endogenous re-expression. We annotated Kdm6a peaks according to specific regulatory elements (Suppl. Fig 1) and found that 22.5% of Kdm6a peaks clustered in proximity of transcriptional start

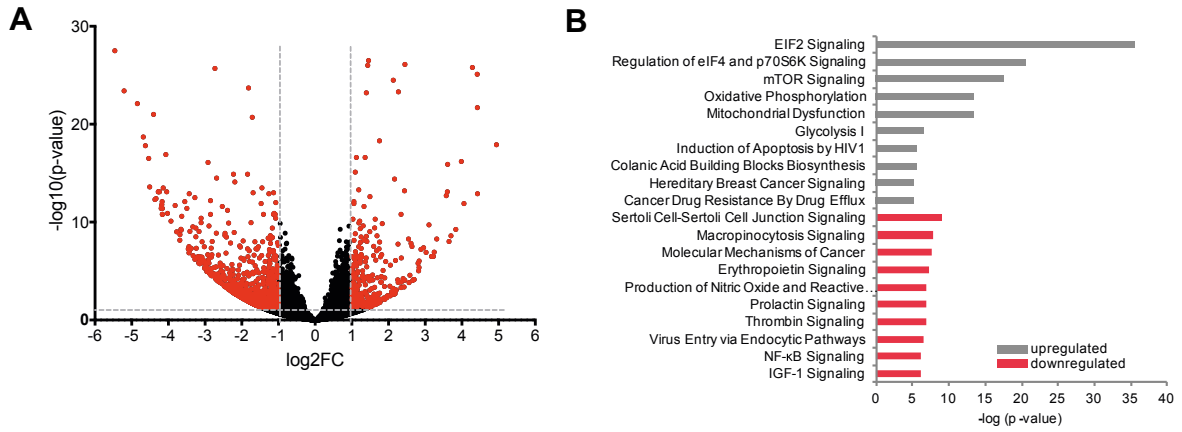

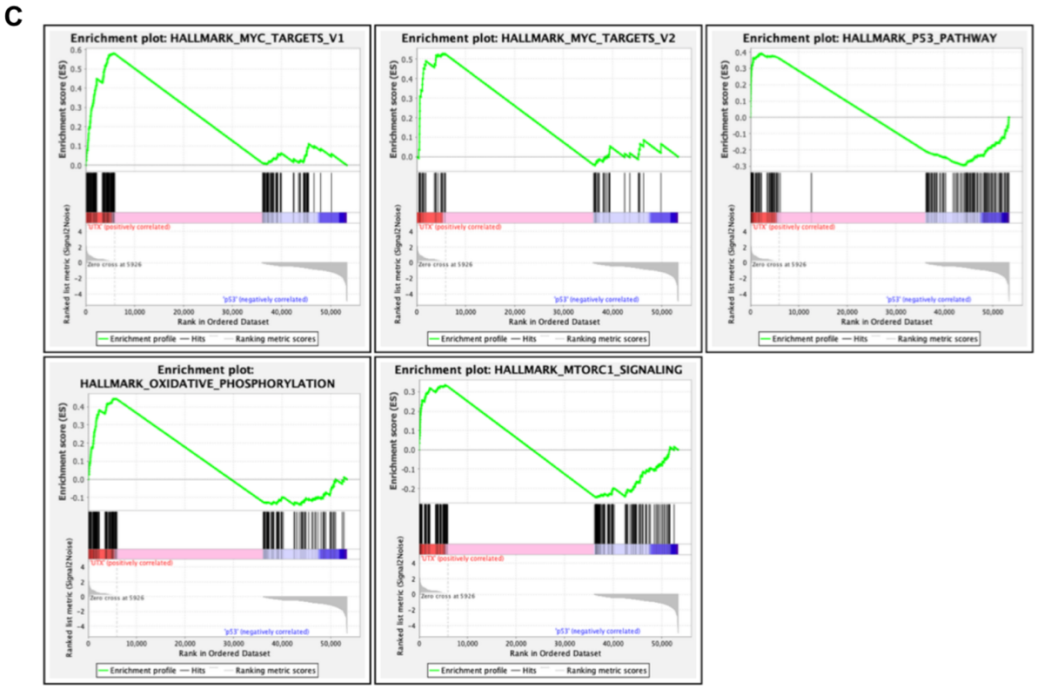

Table: Gene sets enriched in phenotype UTX (3 samples)

	GS follow link to MSigDB	GS DETAILS	SIZE	ES	NES	NOM p-val	FDR q-val	FWER p-val	RANK AT MAX	LEADING EDGE
1	HALLMARK_MYC_TARGETS_V1	Details ...	195	0.58	0.98	0.625	1.000	0.751	5828	tags=62%, list=11%, signal=69%
2	HALLMARK_MYC_TARGETS_V2	Details ...	58	0.53	0.90	0.611	1.000	0.841	5323	tags=43%, list=10%, signal=48%
3	HALLMARK_P53_PATHWAY	Details ...	195	0.39	0.86	0.737	1.000	0.841	2234	tags=26%, list=4%, signal=27%
4	HALLMARK_OXIDATIVE_PHOSPHORYLATION	Details ...	178	0.44	0.83	0.924	0.814	0.841	5693	tags=53%, list=11%, signal=60%
5	HALLMARK_MTORC1_SIGNALING	Details ...	192	0.33	0.67	0.925	0.878	0.841	5332	tags=35%, list=10%, signal=39%

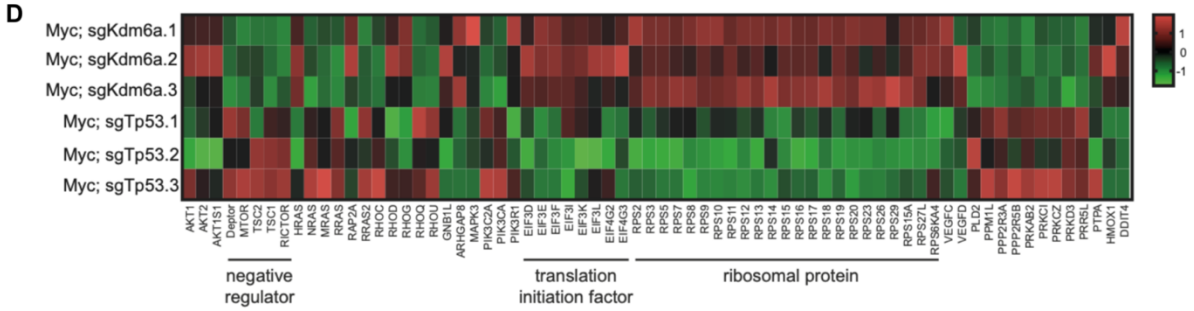

For figure legend, see next page.

sites (TSS). These analyses provided us with more than 1000 genes in which Kdm6a binding can be found throughout the genome. Amongst those genes, Kdm6a peaks were also be observed in the TSS of mTORC1 negative regulators genes such as Deptor and Tsc2 (Figure 4.8 B) but also in Kdm6a gene itself, suggesting possible self-regulatory function.

Moreover, global profile analyses of different histone marks H3K4me1, H3K4me3, H3K27ac and H3K27me3 near Kdm6a peaks revealed distinct areas of enrichment and depletion between cells with (Off-dox) and without (On-dox) Kdm6a expression. Given the Kdm6a was physically associated with genomic regions marked by H3K27me3 and its disruption in some studies was linked with increased global or locus-specific level of H3K27 methylation, we expected changes in H3K27 methylation level upon Kdm6a alteration. But surprisingly, the level of H3K27me3 in our model did not change upon Kdm6a expression while enhancer marks such as H3K27ac and H3K4me1 were increased upon Kdm6a disruption. Furthermore, histone marks indicating active TSS, H3K4me3, were depleted globally when Kdm6a were repressed (Figure 4.8 A). Of note, profile analyses of Kdm6a and the histone marks far from the Kdm6a peaks, did not show any significant alterations. This together points to the effects of Kdm6a on the histone modification landscape.

Figure 4.7 Kdm6a loss leads to distinct transcriptional changes.

(A) Volcano plot of differentially expressed genes revealed by RNA sequencing of three independent Myc; sgKdm6a and Myc; sgTp53 liver tumor-derived cell lines. Genes with more than 2-fold expression change and exceeding p-adjusted < 0.05 are color-labeled. **(B)** Top ten affected canonical pathways from RNA-seq data based on Ingenuity Pathway Analysis. **(C)** GSEA plots of hallmark pathways, which are altered in Myc; sgKdm6a cell lines. Table at the bottom shows the corresponding GSEA scores for each pathway. **(D)** Heatmap of differentially regulated genes specifically in mTOR pathway in Myc; sgKdm6a and Myc; sgTp53 cell lines.

4.4.2 KDM6A-deficient cells show hyperactivation of mTORC1 signaling

Following the lead from our transcriptomic and epigenetic profiling, the regulatory nature of Kdm6a on the mTOR pathway, especially mTORC1 signaling were validated by western blotting. To date, the serine/threonine kinase mTOR, is classified into two distinct evolutionarily conserved multiprotein complexes: the mTOR complex 1 (mTORC1) and the mTOR complex 2 (mTORC2). These two complexes are known to have different subcellular localization, downstream substrates, and sensitivity toward rapamycin [130, 131]. mTORC1 is known to phosphorylate 4E-BP1, p70S6K and subsequently S6RP, which promotes protein translation (Suppl. Fig 2). Of note, the DEPTOR (DEP domain-containing mTOR-interacting protein) subunit that can be found in both mTOR complexes has also been shown to negatively regulate mTORC1 in addition to the TSC complexes [132].

Using the Myc; TRE shKdm6a cell lines, we observed a positive relationship between Kdm6a and mTOR repressive proteins including Deptor, Tsc1, and Tsc2 (Figure 4.9 A). This relationship was also seen in CRISPR/Cas9 knockout cell lines where expression of Deptor, Tsc1 and Tsc2 were significantly lower in Myc; sgKdm6a cell lines compared to Myc; Tp53 cell lines (Figure 4.9 B). This correlation between Kdm6a and different mTORC1 negative regulators was also reflected on transcriptional level (Figure 4.9 C and D).

Additionally, phosphorylation of pS6RP (both S235/6 and S240/4) and pP70S6K (T389) in Myc; TRE shKdm6a were significantly reduced over different time points when Kdm6a expression was restored in these cells, indicating a possible Kdm6a-dependent regulation of this pathway in tumorigenesis (Figure 4.9 E). This result was consistent with activation of mTORC1 signaling upon Kdm6a disruption both in fresh tissues and in paraffin section of Myc; TRE shKdm6a liver tumor tissues by western blot (Figure 4.9 F) and IHC staining respectively (Figure 4.9 G).

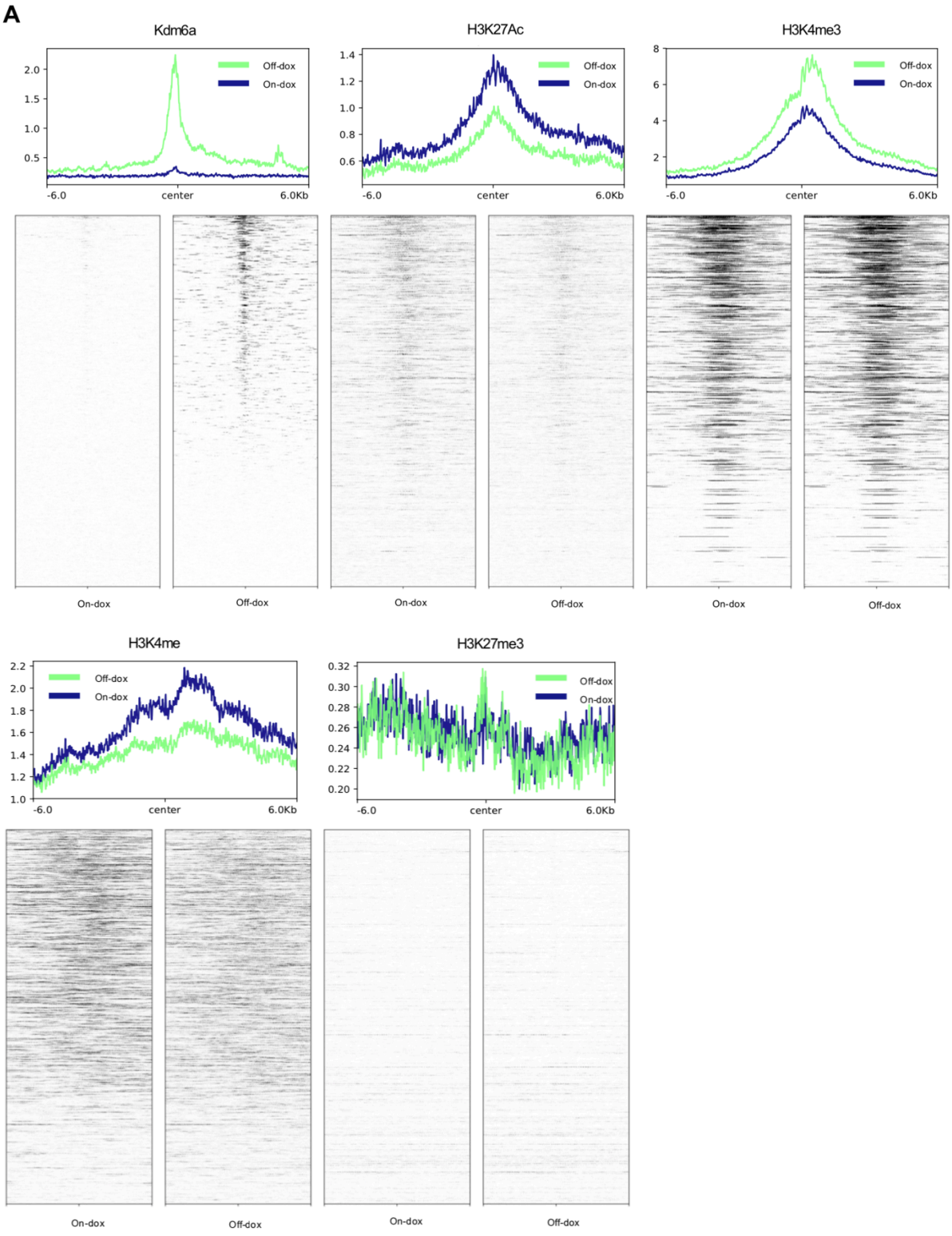

Figure continued on next page.

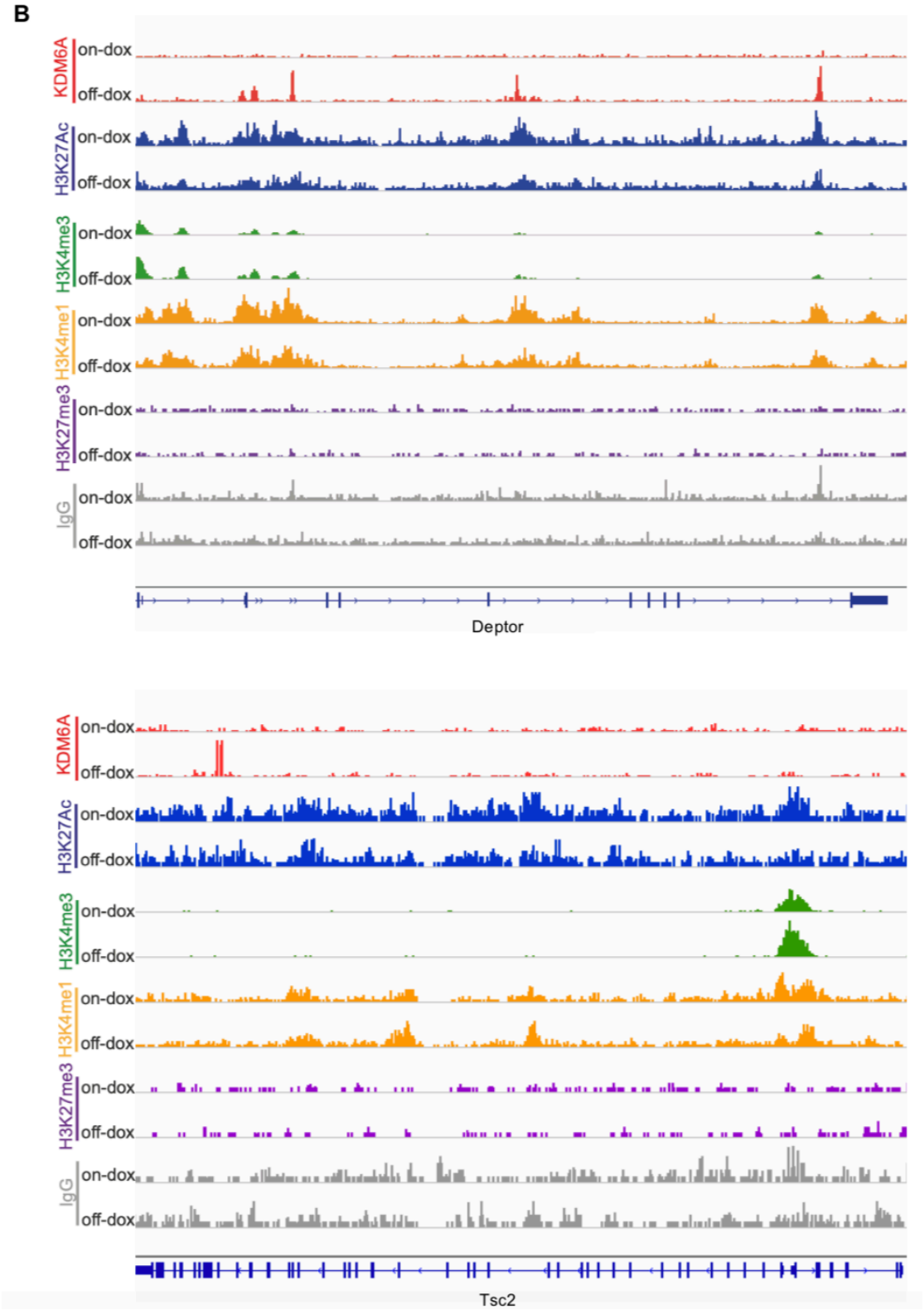

Figure 4.8 Genome wide profiling of histone modifications and Kdm6a. (A) Global profile plots (top) and heatmaps (bottom) of Kdm6a and histone modifications (H3K4me3, H3K4me1, H3K27Ac, H3K27me3) from Cut&Run signals in Myc; TRE shKdm6a cell line line in the presence (Off-dox) or absence (On-dox) of KDM6A sorted by Kdm6a signal. **(B)** KDM6A, H3K27Ac, H3K4me3, H3K4me1, and H3K27me3 occupancies at Deptor (top) and Tsc2 (bottom) loci in the Myc; TRE shKdm6a liver tumor-derived cell line.

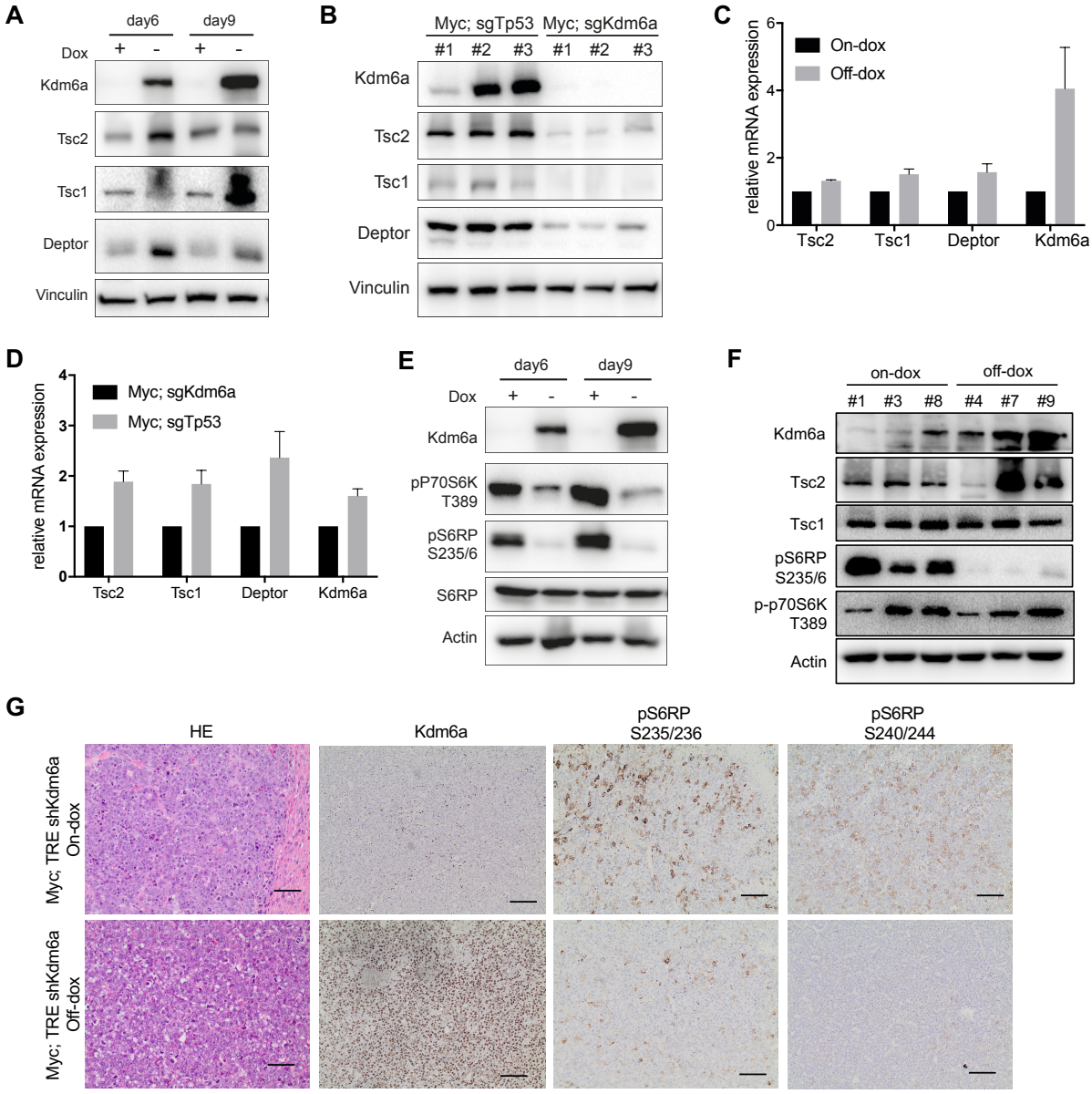

Figure 4.9 Kdm6a loss hyperactivates mTOR signaling. (A) Time course western blot analysis in one of Myc; TRE shKdm6a cell line for mTOR negative regulators in the presence (Off-dox) or absence (On-dox) of Kdm6a. **(B)** Western blot of mTOR negative regulators in three independent Myc; sgKdm6a and Myc; sgTp53 cell lines. **(C)** Quantitative PCR for Tsc2, Tsc1 and Deptor mRNA expression in Myc; TRE shKdm6a cell line with and without doxycycline. **(D)** mRNA expression of Tsc2, Tsc1 and Deptor in Myc; sgKdm6a and Myc; sgTp53 cell lines. Western blot analysis in one of Myc; TRE shKdm6a cell line **(E)** and in tumor tissues **(F)** for mTORC1 signaling. **(G)** Representative images of Kdm6a and pS6RP expressing cells detected by immunohistochemistry in murine livers at endpoint of experiment with or without doxycycline. Scale bar represent 50 μm.

4.4.3 Kdm6a regulates mTORC1 signaling through Deptor

To validate the identified Kdm6a-Deptor circuitry, we hypothesized that knockout of Deptor could rescue Kdm6a re-expression triggered phenotypes. In this regard, caspase3/7 activity was used as a phenotypic readout, since Kdm6a re-expression not only reduced mTORC1 signaling, but also promoted caspase3/7 activity (Figure 4.10 A). Deptor was targeted by CRISPR/Cas9 technology with two different sgRNAs and an empty vector as control in Myc; TRE shKdm6a cell lines. Those cells were then cultured in either normal (Off-dox) or doxycycline-containing (On-dox) medium and assessed for their caspase3/7 activity. In accordance with our previous findings, caspase 3/7 activity in control cells was significantly increased in Off-dox condition where Kdm6a was re-expressed compared to On-dox condition. However, when Deptor was knocked out, the caspase3/7 activity in Off-dox condition was partially rescued (Figure 4.10 B). This can be linked to abrogation of mTORC1 repression associated with Kdm6a re-expression as shown in Figure 4.10 C. Specifically, the Myc; TRE shKdm6a cell line with Deptor knockout did not exhibit a prominent downregulation of mTORC1 signaling pathway upon Kdm6a re-expression.

Given the phenotypic relationship between Kdm6a and Deptor, we tested whether Deptor overexpression can abrogate tumorigenesis of Myc; sgKdm6a tumors in murine livers as describe in section 4.1 before. To this end, 5 mice were hydrodynamically injected with pT3-EF1a-MYC, pX330-sgKdm6a, transposon-based vector expressing Deptor cDNA under *EF1a* promoter (pT3-EF1a-Deptor-IRES-GFP) and the sleeping beauty transposase (Figure 4.10 D). As control, another cohort with the equal number of mice (5) was injected with empty vector (pT3-EF1a-linker-IRES-GFP) and expected to mimic the similar tumor incidence as shown in Figure 4.2 A.

Depicted in Figure 4.10 E, only three out of five control mice with Myc; sgKdm6a develop tumor within 20 weeks and mice with Deptor overexpression did not develop liver tumor at all. Although the difference was not significant (p-value = 0.0788), mice with the Deptor overexpression showed a better tumor-free survival over the observation period compared to the control mice (Figure 4.10 E).

This together indicate the hyperactivation of mTORC1 signaling upon Kdm6a disruption and the increased caspases activity by Kdm6a re-expression can be rescued partially by Deptor knockout. Whereas Deptor overexpression could possibly abrogate the Myc; sgKdm6a tumorigenesis *in vivo*.

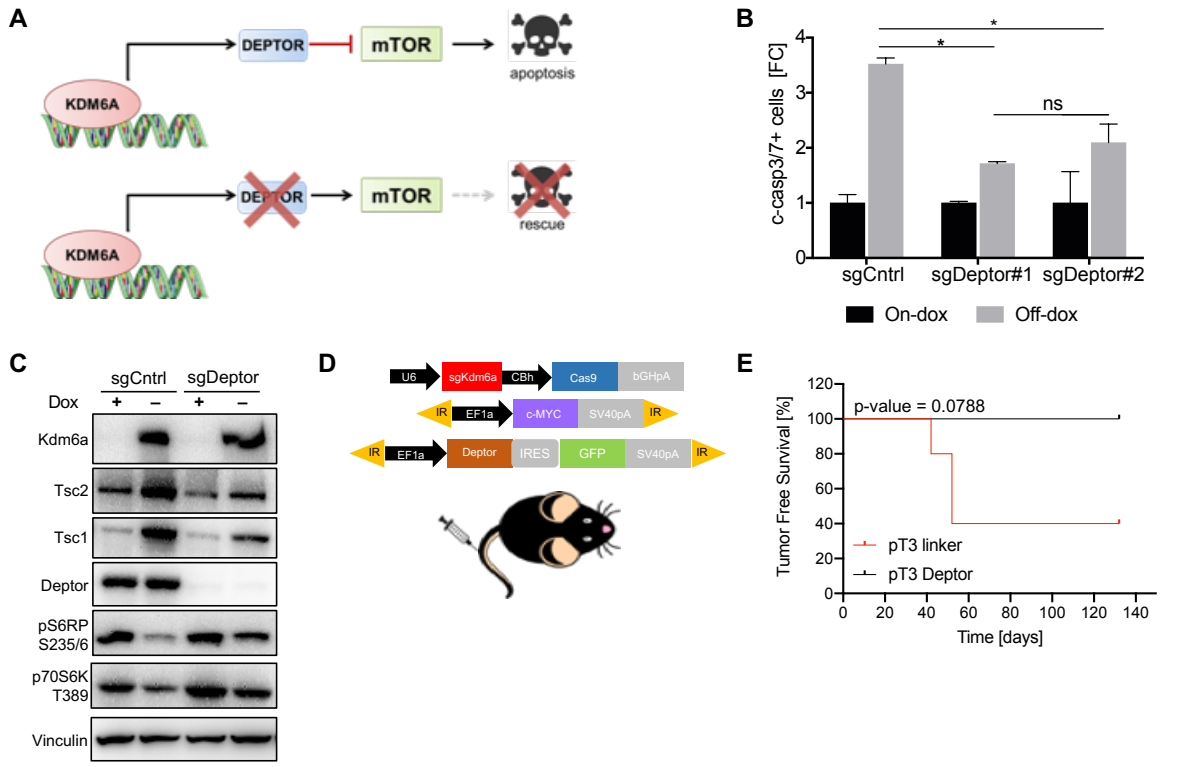

Figure 4.10 Deptor disruption can partially rescue apoptosis caused by Kdm6a expression. (A) Schematic view of apoptosis rescue by Deptor knockout. **(B)** Caspase-3/7 assay in Myc; TRE shKdm6a cells expressing either sgRNAs targeting Deptor or empty vector as control at 6 days timepoint. Error bars represent mean ± SD from triplicates. *P<0.05 (unpaired two-tailed t-test). **(C)** Western blot for mTOR signaling in Myc; TRE shKdm6a cell line with either sgRNAs targeting Deptor or empty vector as control. **(D)** Schematic view of in vivo rescue experiment with Deptor overexpression in Myc; sgKdm6a tumors. **(E)** Tumor free survival of Myc; sgKdm6a mice with Deptor overexpression (pT3 Deptor, red line) or without Deptor expression (pT3 linker, black line).

4.4.4 KDM6A expression correlates with DEPTOR expression in human HCC

To extend our observations to human liver cancer we analyzed the expression patterns of KDM6A, DEPTOR and the activity of mTORC1 in human HCC and normal liver tissue.

A HCC tissue microarray (TMA) collected by Institute of Pathology, Heidelberg was immunohistochemically stained for KDM6A and evaluated for staining intensity. The TMA comprises of 720 representative tissue distributed on 7 slides with 40 histologically normal livers, 188 cirrhotic livers and 476 HCCs. Individual Kdm6a immunohistochemical stains were quantified and scored as following: 0 = unstained, 1 = weakly, 2 = moderately and 3 = strongly positive. As shown in Figure 4.11 A, almost 40% of HCC tissues were scored 0 in the quantification. In contrast, absence

of KDM6A staining in normal liver and cirrhotic tissues was significantly lower than in HCC, with less than 10%, indicating the prevalence of KDM6A loss in HCC.

An independent HCC cohort was collected from the Institute of Pathology, Regensburg consisting of 50 HCC tissue and the adjacent normal tissue. This cohort was used to validate the correlation between KDM6A and mTORC1 signaling in patients. IHC staining for KDM6A, DEPTOR, and pS6RP were performed and the cohort was classified according to their KDM6A expression, either KDM6A low or high. Analyses of the IHC stains confirmed that KDM6A expression was linked to DEPTOR expression, which led to inhibition of mTORC1 signaling characterized by reduced pS6RP signal (Figure 4.11 B). Statistical significance of those correlations was also tested by Fisher's exact test in contingency tables. Shown also in Figure 4.12 B, IHC staining of KDM6A was positively correlated with DEPTOR protein expression (p-value<0.0001), albeit not significantly correlated with pS6RP (p-value = 0.1512). Accordingly, qRT-PCR of KDM6A and DEPTOR in HCC and normal liver tissue reasserted the positive correlation between KDM6A and DEPTOR in HCC but not in the surrounding normal liver tissue (Figure 4.11 C and D).

In line with our finding, TCGA whole genome sequencing data from publicly available datasets also revealed linear relationship between KDM6A and DEPTOR across different cancer types including HCC (Figure 4.11 E and F).

Thus, these data confirms that KDM6A loss hyperactivates mTORC1 signaling in human HCC samples via DEPTOR.

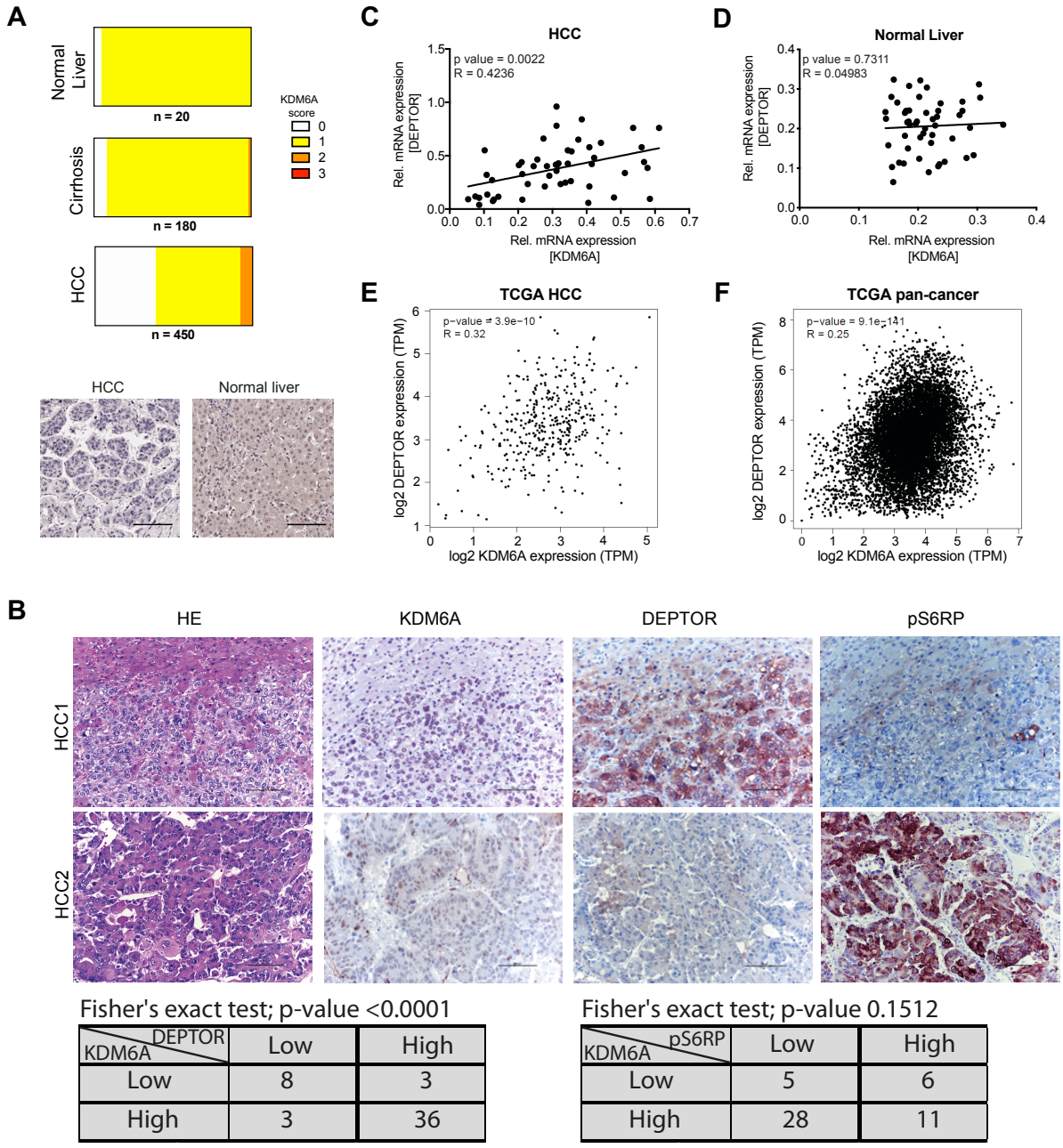

Fisher's exact test; p-value <0.0001

KDM6A \ DEPTOR	Low	High
Low	8	3
High	3	36

Fisher's exact test; p-value 0.1512

KDM6A \ pS6RP	Low	High
Low	5	6
High	28	11

Figure 4.11 KDM6A expression correlates with DEPTOR expression in human HCC. (A) Top, proportion of patient samples with KDM6A loss (score = 0) in the TMAs classified into normal liver tissues, cirrhotic tissues and HCCs. Bottom, representative Kdm6a staining in the TMAs. Scale bar represent 50 µm. **(B)** Immunohistochemical staining of HE, KDM6A, DEPTOR and pS6RP in two representative HCC patients. Scale bar represent 20 µm. Table below shows the significance of the correlation between KDM6A/DEPTOR and KDM6A/pS6RP. Correlation between KDM6A and DEPTOR expression in HCC **(C)** and in normal liver **(D)** of clinical cohort consisting 50 patients. Correlation between KDM6A and DEPTOR from publicly available data in HCC **(E)** and pan-cancer **(F)**.

4.5 Kdm6a-deficient tumors are susceptible to mTOR inhibition

Given our findings so far implied that Kdm6a-deficient tumors show elevated mTOR pathway activity, we next asked whether Kdm6a-deficient tumors are more sensitive to mTOR inhibitors compared to Kdm6a proficient tumors. To address this question, cells were treated with specific drugs targeting mTOR in various concentrations and cell viability was assessed 72 hours post-treatment using CellTiter-Blue® Assay. To be precise, CellTiter-Blue reagent measured the metabolic capacity of cells, where viable cells are able to reduce a redox dye, resazurin, into a quantifiable fluorescent product, resorufin. Nonviable cells will lose the ability to convert resazurin and do not generate any signal.

Using the doxycycline-inducible shKdm6a model system, Kdm6a loss increased the effect of mTOR inhibitors including Torin1, Rapamycin and Onatasertib (Figure 4.12 A). Quantitative comparison of their IC_{50} values showed 2 to 10-fold higher sensitivity in absence of Kdm6a. Strikingly, this susceptibility was only observed for mTOR inhibitors but not for PI3K inhibitors such as Copanlisib and Dactolisib (Figure 4.12 B).

From this set of experiment, we can conclude that Kdm6a-deficient cell lines are more sensitive to mTOR inhibition and that inhibition of mTOR upstream pathways including the PI3K pathway do not affect Kdm6a-deficient tumors.

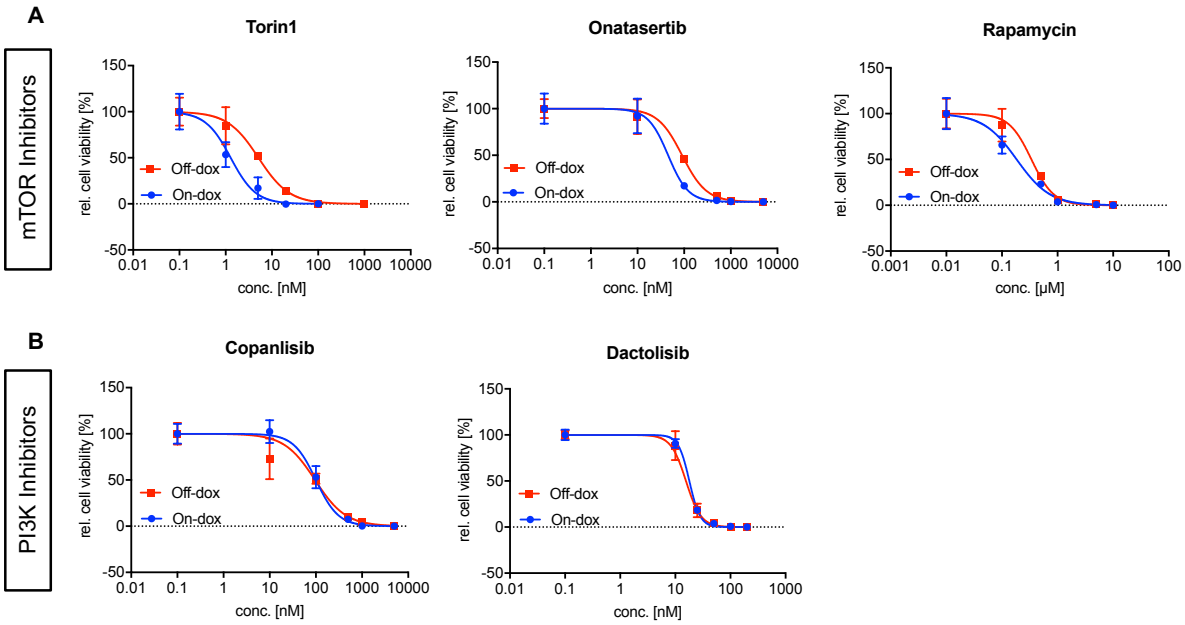

Figure 4.12 Kdm6a-deficient tumors are susceptible to mTOR inhibition. Dose response curve of different mTOR inhibitors (A) and PI3K inhibitors (B) in Myc; TRE shKDM6A cells in the presence (red line; Off-dox) or absence (blue line; On-dox) of Kdm6a.

4.6 Epigenetic vulnerabilities of Kdm6a-deficient cells

4.6.1 pooled CRISPR/Cas9 screening

Since Kdm6a is a histone modifier and its mutation caused altered H3K4-me1, H3K4-me3, H3K27-Ac epigenetic landscape (Figure 4.8 A), we asked the question whether Kmd6a-deficient tumors would exhibit specific epigenetic vulnerabilities. Using CRISPR/Cas9-based screening with an epigenetic modifiers-focused sgRNA library, we aimed to reveal genes which are essential for Kdm6a-deficient tumor cells. The focused sgRNA library targets 600 known and putative epigenetic modifier genes, which each targeted by 6 independent sgRNA. Three independent Myc; sgKdm6a and Myc; sgTp53 tumor-derived cell lines (Figure 4.2) were stably transduced with Cas9 and used for the screening as biological triplicates. The lentiviral library pool was transduced into those cells lines in a manner that each sgRNA was represented in at least 1000 cells throughout the screening. After puromycin selection (T0), changes in sgRNA representation following 15 population doublings (T15) were quantified using deep sequencing of sgRNA guide strands amplified from genomic DNA of transduced cells as described before (Figure 4.13 A).

The correlation of normalized sgRNA reads present in the replicates at T0 was close to 1 but substantially decreased by T15 within the same replicate. The decrease in correlation could be associated to changes in sgRNA representation in the library (Figure 4.13 B). Using the scoring criterion of greater than twofold average depletion in at least two independent biological replicates, we were able to identify several hits from both Myc; sgKdm6a and Myc; sgTp53 cell lines. These included the positive control sgRNAs targeting essential genes such as Rpa1 and Pcna (Figure 4.13 C). For a “hit” to undergo further analysis, we required that at least three out of six independent sgRNAs targeting a particular gene were identified in the primary screen. Genes fulfilling these criteria included the Actr5 (Actin Related Protein 5), Hdac3 (histone deacetylase 3) and Phf23 (PHD Finger Protein 23) (Figure 4.13 C).

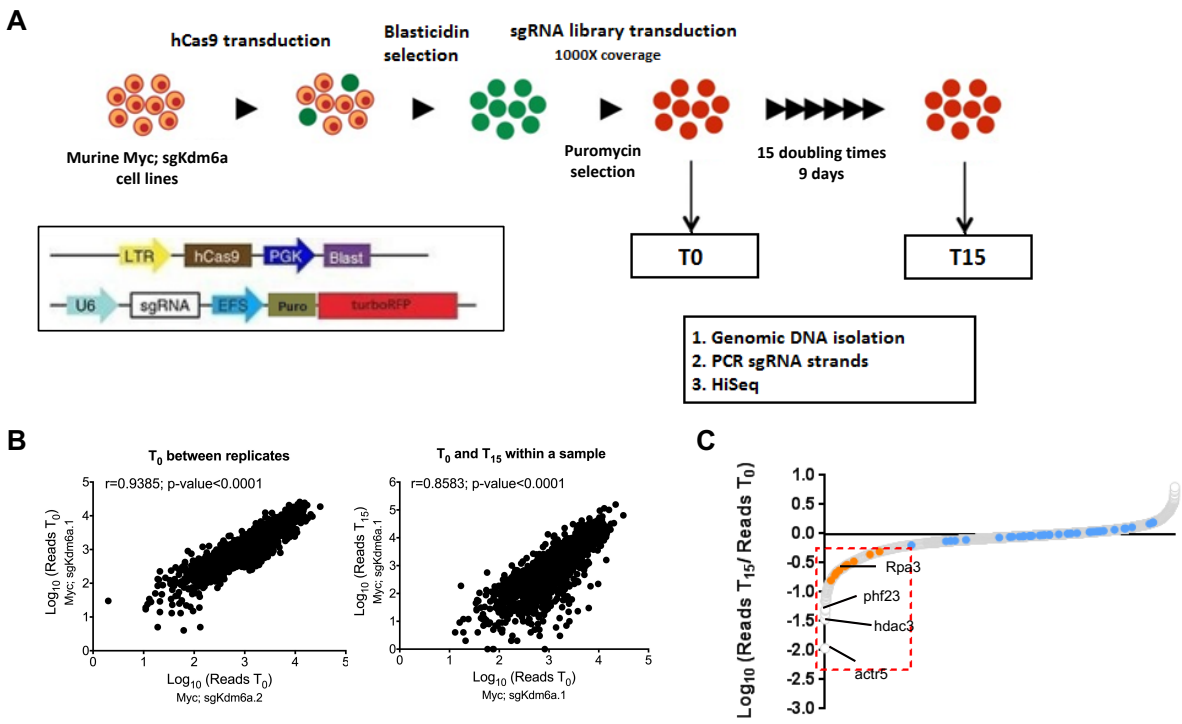

Figure 4.13 Pooled CRISPR/Cas9 screening. (A) Schematic view of the screening strategy. **(B)** Representative scatter plots illustrating the correlation of normalized reads per sgRNA between replicates at the beginning of the experiment (left) and replicates at different time points (right). **(C)** Pooled negative selection screening results in Myc; sgKdm6a cell lines (3 biological replicates). Red dotted box indicates the hit selection criteria.

4.6.2 Hits validation

Hits from the CRISPR/Cas9 screening were further validated *in vitro* employing a flow cytometry-based competition assay. For this purpose, two sgRNAs for each candidate from were selected from the initial lentiviral library and expressed as GFP-fused sgRNA using the pLKO-U6-EFs-GFP-P2A-Blasticidin plasmid. An additional sgRNA was also added using the CHOPCHOP algorithm (Bergen, Norway) to exclude any algorithm-specific effect. Rpa3 and Rosa26 were used as positive and negative control respectively.

Despite differences in the kinetic, hit candidates were depleted over time in Myc; sgKdm6a cell lines, but not in Myc; sgTp53 cell lines (Figure 4.14 A). This observation thus, implied possible specific vulnerability of Kdm6a deficiency. Amongst the 18 hit candidates, sgRNA targeting of Hdac3 in the Myc; sgKdm6a cells led to a rapid depletion of the edited population comparable to the positive control, Rpa3. T7 endonuclease assay validated CRISPR/Cas9 genome editing efficiency of the sgHdac3 in the targeted gene locus (Figure 4.14 B). Using Tet-On shHdac3

(Figure 4.14 C) induced downregulation of Hdac3 expression, we further validated the vulnerability of the Myc; sgKdm6a cells (Figure 4.14 D) on Hdac3. This susceptibility of Kdm6a-deficient cells towards Hdac3 can also be confirmed in Myc; TRE shKdm6a cell lines. Kdm6a-deficient cells which were cultured in On-dox condition were significantly affected by Hdac3 disruption while cells with Kdm6a expression were less affected (Figure 4.14E).

These sets of experiments strongly imply dependence of Kdm6a-deficient tumor cells on Hdac3 gene expression, which may represents a novel therapeutic strategy.

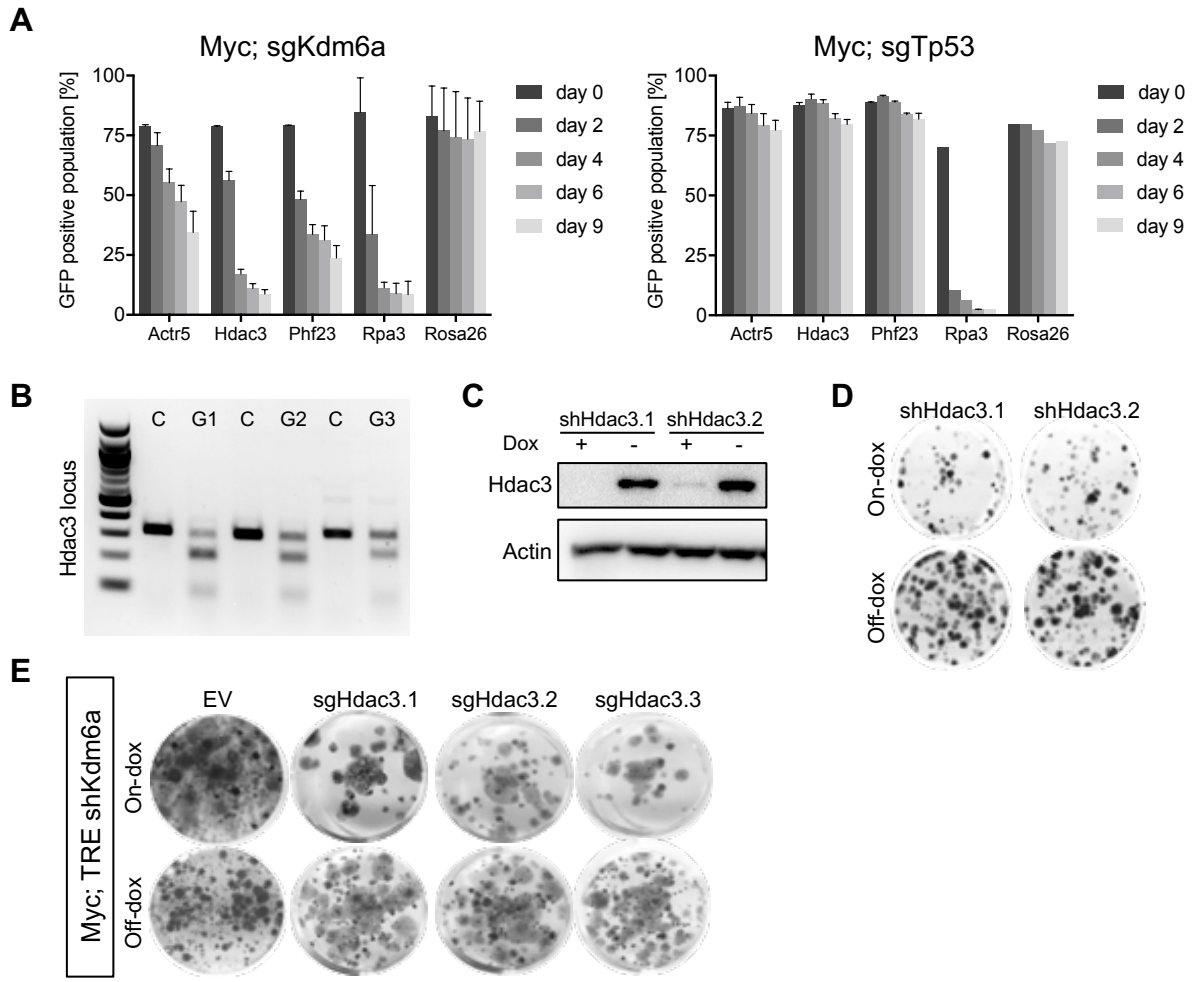

Figure 4.14 Kdm6a-deficient cells are vulnerable to Hdac3 depletion. (A) Negative selection competition assay that plots the percentage of GFP+ cells over time following transduction with the indicated sgRNAs in Myc; sgKdm6a and Myc; sgTp53 cell lines. Rpa3 and Rosa26 were used as positive and negative control respectively. (B) Surveyor assay of PCR amplicons flanking predicted Hdac3 cleavage sites. C = control, G = guide. (C) Western blot analyses of Hdac3 knockdown by two different shRNAs. Actin was used as loading control. (D) Colony formation assay of Myc; sgKdm6a cell line with indicated shRNAs with or without doxycycline after 10 days. (E) Colony formation assay of Myc; TRE shKdm6a cell line with three different sgRNAs against Hdac3 after 10 days with (lower row) or without (upper row) Kdm6a.

4.7 Loss of KDM6A with Kras^{G12D} leads to PDAC

In parallel to our Myc-driven HCC mouse model, we further validated Kdm6a function in a Kras^{G12D}-driven ESC-based pancreatic cancer mouse model under tetracycline-driven regulation as described before (Figure 4.15 A). The targeting vector used for this ESC-GEMM consists of the dox-inducible shRNAs against Kdm6a or Renilla as control, which are coupled to GFP as a reporter.

Consistently, doxycycline induction of shKdm6a led to development of the pancreatic ductal adenocarcinoma (PDAC) over the course of 70 weeks (Figure 4.15 B, blue & red lines). Importantly, littermates with Renilla-targeting shRNA did not develop any macroscopic malignancy throughout the course of observation (Figure 4.15 B, Black line). Gross post-mortem examination of the two shKdm6a groups revealed GFP-labelled macroscopic cyst and malignant tumor growth of pancreatic ducts (Figure 4.15 C), which could be traced back to the ESC line expressing the GFP-fused shKdm6a. IHC stainings for Kdm6a reaffirmed loss of Kdm6a protein expression in the PDAC but not in the normal pancreas of shRenilla group (Figure 4.15 D). Of note, IHC staining for GFP demonstrated expression and sequestration of GFP-fused shRenilla with endogenous Kdm6a in these samples. Although there was no macroscopic malignancy observed in shRenilla group upon post-mortem examination, IHC staining of the shRenilla pancreas showed pre-malignant pancreatic intraepithelial neoplasia (Figure 4.15 D).

Hence, our ESC-based model with Kras^{G12D} activation coupled with Kdm6a repression in murine pancreas induced the PDAC while the activation of Kras^{G12D} alone did not lead to PDAC but the pre-malignant PanIN as described in the literatures.

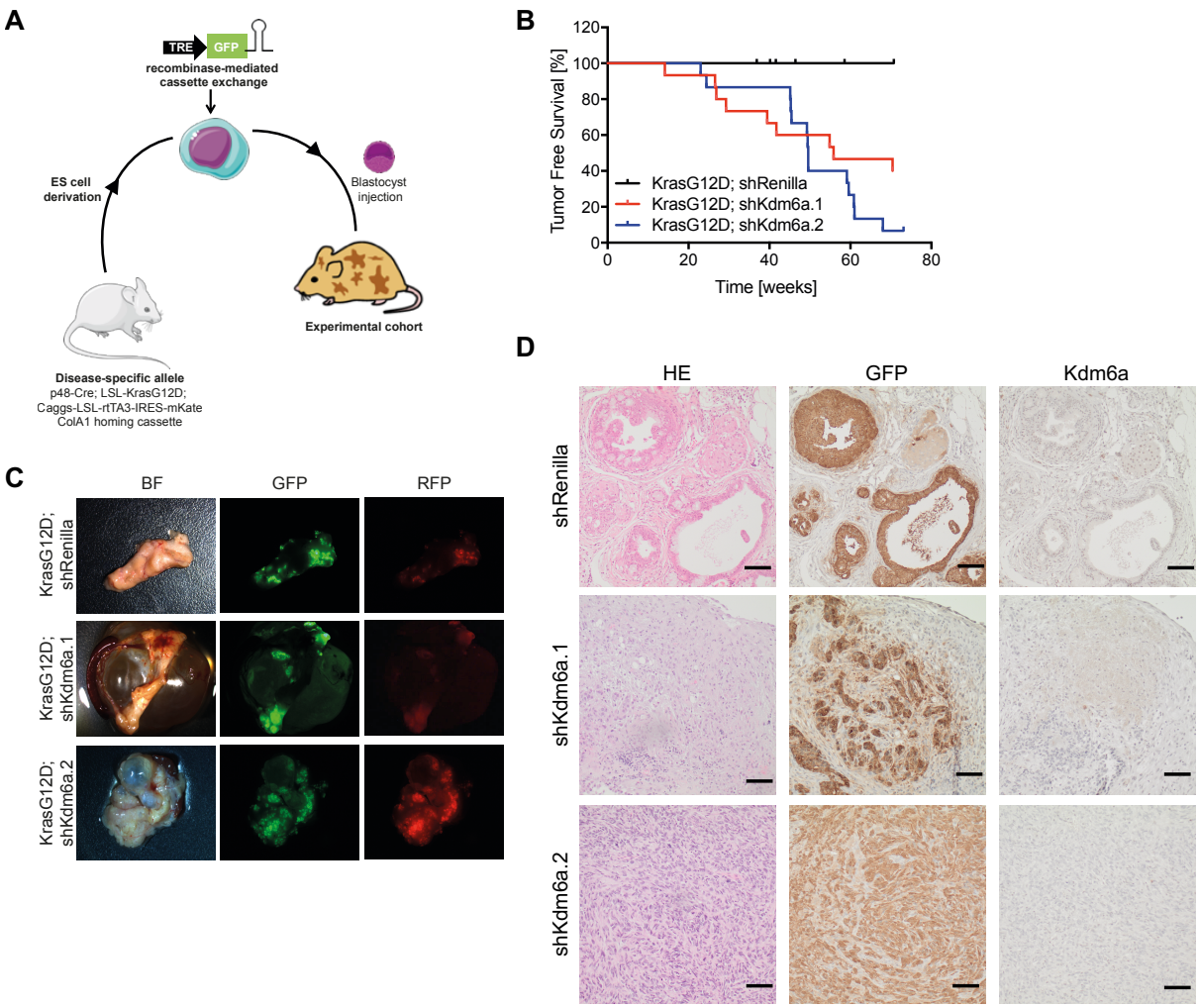

Figure 4.15 Loss of Kdm6a with KrasG12D leads to PDAC. (A) Schematic for generating ESC-based PDAC mouse model. **(B)** Tumor free survival of KrasG12D; shKdm6a mice (blue and red lines) and KrasG12D; shRenilla (black line) mice as control. **(C)** Tumor nodules with cyst or normal pancreas observed in KrasG12D; shKdm6a and KrasG12D; shRenilla mice express shRNA-linked GFP and rtTA3-linked RFP. **(D)** Immunohistochemical staining of HE, GFP and Kdm6a, in KrasG12D; shKdm6a and KrasG12D; shRenilla mice.

To investigate whether Kdm6a also exerts similar molecular function in the Kras^{G12D} driven PDAC, primary cell lines were established from the both of Tet-ON shKdm6a PDAC tumors under continuous presence of doxycycline.

Similar to the experiments in Myc-driven HCC cell lines, loss of Kdm6a in Kras^{G12D} PDAC activated mTORC1 signaling characterized by increased pS6RP and pP70S6K signals in western blotting (Figure 4.16 A). Additionally, the positive correlation between Kdm6a and the negative regulators of mTORC1 including Deptor and Tsc2, was confirmed. Given the hyperactivation of mTORC1 signaling is consistent, we tested the sensitivity of these cells towards mTOR inhibition. Indeed, Kdm6a-deficient pancreatic tumor cell also displayed increased susceptibility to

mTOR inhibitors, such as Torin1 (Figure 4.16 B). Cells with Kdm6a disruption were 10 times more sensitive to Torin1 treatment compared to Kdm6a proficient cells, at least *in vitro*.

Collectively, the Tet-On shKdm6a; Kras^{G12D} PDAC recapitulates the tumor-suppressive function of Kdm6a via mTOR regulation, independent of the oncogenic background.

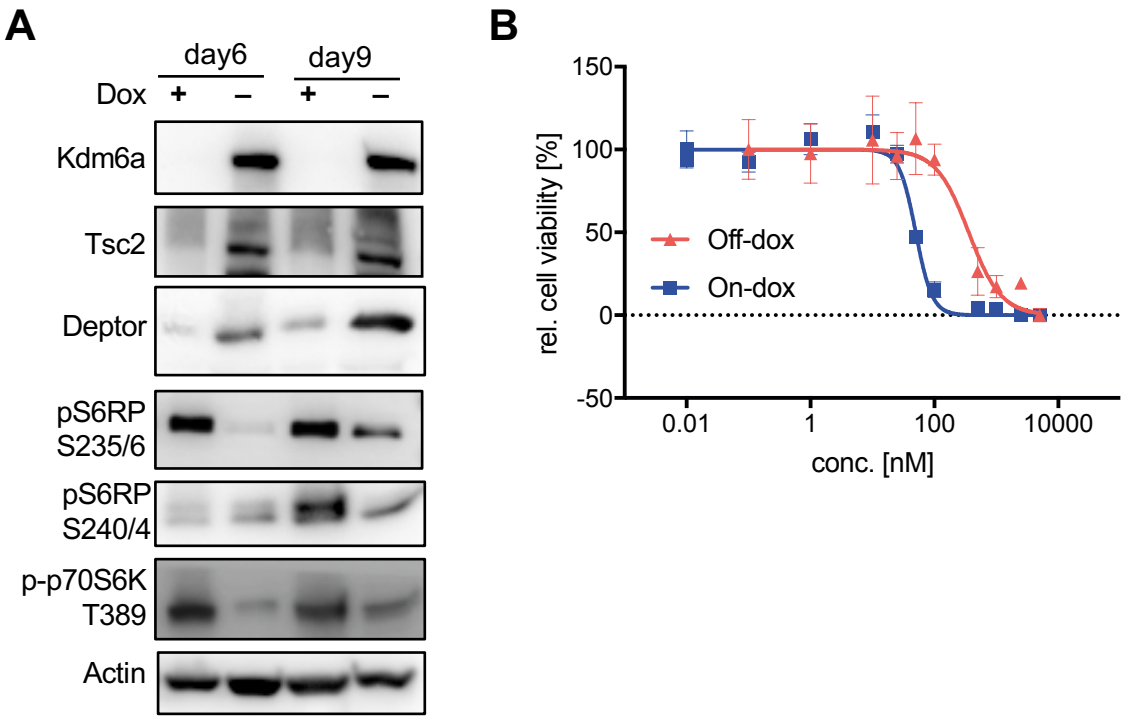

Figure 4.16 Kdm6a loss with Kras^{G12D} activates mTOR signaling and is accompanied with sensitivity to mTOR inhibitors. (A) Western blot for mTOR signaling in KrasG12D; shKdm6a cell line in the presence (Off-dox) or absence (On-dox) of Kdm6a. **(B)** Dose response curve of Torin1 in KrasG12D; shKdm6a cell in the presence (red line; Off-dox) or absence (blue line; On-dox) of Kdm6a.

5. Discussion

In this present study, we reveal an important tumor suppressive function for the histone demethylase Kdm6a in c-MYC-driven liver cancer and $Kras^{G12D}$-driven pancreatic cancer. We demonstrate that disruption of Kdm6a by CRISPR/Cas9 or RNA interference leads to hyperactivation of mTORC1 signaling. Subsequent RNA-seq and Cut&Run analyses uncovered a direct regulatory mechanism of Kdm6a on mTOR via regulation of negative regulatory proteins of mTOR signaling, such as Deptor. Conversely, endogenous Kdm6a re-expression diminishes mTORC1 activity via Deptor and attenuates tumor growth of established Kdm6a-deficient tumors. Accordingly, Kdm6a-deficient tumors exhibit increased sensitivity to mTORC1 inhibition.

5.1 Kdm6a is a tumor suppressor in liver cancer

Current literature perceives Kdm6a as a putative tumor suppressor. This perspective is mostly derived from reports that Kdm6a is frequently mutated across different cancer types and in many cases these mutations are loss-of-function mutations or are deleterious. Notably, more than 30% of urothelial carcinoma exhibit Kdm6a inactivating mutations [58] and its loss results in aberrant activation of PRC2-regulated transcriptional repression [133]. The tumor suppressive function of Kdm6a was also extensively studied in leukemia, especially in T-ALL, where Kdm6a-loss in T-ALL promotes Notch-dependent proliferation [88].

Yet, several studies have also attributed pro-oncogenic functions to Kdm6a, for example in breast cancer [134, 135], prostate cancer [136], and cervical cancer [137]. Specifically, Kdm6a was shown to be associated directly with the steroid hormone receptor such as estrogen- or androgen- receptor and permitting steroid hormone dependent gene transcriptions [135, 136], which in turn promote growth and invasion of breast and prostate cancer. In cervical cancer, the high-risk human papillomaviruses (HPVs) E7 expressing cells were found to be addicted to Kdm6a expression and the $p21^{CIP1}$ mediated suppression of replication stress [137].

Based on our human HCC data, we observed a loss of KDM6A expression in about 30% of HCC based on IHC staining while only less than 5% of normal liver tissue showed no expression of KDM6A. This observation indicates that KDM6A could play a tumor suppressive role in liver cancer as tumor cells select for loss of its expression.

However, the cause of this reduced expression is not reflected in sequencing data from public databases (TCGA) where only 3% of liver malignancies show KDM6A genomic alterations, which would be associated with low or absent protein expression. As not only genetic changes can lead to changes in gene expression it is worth speculating that the observed changes might be due to epigenetic changes influencing Kdm6a expression on transcription levels or that reduced protein levels are caused on translational or post-translational levels.

Furthermore, our functional analyses clearly demonstrated that Kdm6a acts as a tumor suppressor in the context of oncogenic signals, such as c-MYC and $Kras^{G12D}$, in liver and pancreatic cancer respectively. These findings are in line with many other tumor types as indicated above. By applying inducible RNA-interference, we also found that Kdm6a was not only essential for tumor initiation but also exhibits an important role in tumor maintenance. While we were able to confidently confirm the tumor suppressive properties of Kdm6a in the context of c-MYC and $Kras^{G12D}$ in the present study, the cooperativity with other oncogenes and/or tumor suppressor genes in liver and pancreatic cancer will be subject for future studies. The HDTVi method will be instrumental and could be easily applied to efficiently test different combinations of oncogenes or tumor suppressor genes frequently deregulated in liver malignancies, such as β-Catenin or Tp53, in combination with Kdm6a knockout in mice. It will be interesting, if Kdm6a will act as a tumor suppressor in these genetic contexts or if it might act pro-tumorigenic as described in other tumor types.

5.2 Molecular function of Kdm6a in tumor suppression

Initially, the tumor suppressive function of Kdm6a has been linked to its demethylase activity on the H3K27. In T-ALL, excessive H3K27me3 was shown to cause Notch-dependent growth advantage and inactivation of Retinoblastoma (Rb) [75, 138]. In comparison, our epigenetic profiling revealed minimal alteration of the global H3K27me3 level upon Kdm6a disruption, implying possible demethylase-independent tumor suppressor functions of Kdm6a. Moreover, specifically in genes where we found Kdm6a binding, such as Deptor and Tsc1 or Tsc2, H3K27me3 levels also did not differ significantly in condition with or without Kdm6a expression. However, this H3K27me3 profile was analyzed globally and it is possible that the demethylase activity of Kdm6a acts in specific loci. Though, to completely rule out the contribution

of demethylase activity of Kdm6a in tumor suppression, it would be tempting to perform experiments with catalytically-dead versions of Kdm6a and assess its tumor suppressive capacity.

Of note, the loss of Kdm6a increased the global levels of H3K4me1 and H3K27ac, which are widely accepted as enhancer markers. In line with our findings, Andricovich et al. reported minimal alteration in signal intensity and distribution of H3K27me3 together with aberrant activation of super-enhancers regulating ΔNp63, MYC, and RUNX3 oncogenes upon the loss of Kdm6a in squamous-like pancreatic cancer [94]. The non-catalytic properties of Kdm6a as tumor suppressor was also confirmed by Gozdecka et al. and Ezponda et al. in leukemia [92, 139]. Specifically in acute myeloid leukemia (AML) Kdm6a disruption showed only minor changes in H3K27me3 but significant and bidirectional alterations in H3K27ac and a predominant loss of H3K4me1 that led to maintenance of pro-oncogenic E-twenty-six (ETS) and repression of tumor-suppressive GATA transcriptional programs [139]. Interestingly, in human multiple myeloma (MM), loss of Kdm6a does also not affect global H3K27me3 levels, but leads to abnormal PRC2-mediated repression and regulation of MLL2/KMT2D target genes [92].

5.2 Loss of Kdm6a is essential for c-MYC driven tumorigenesis

Our transcriptomic analyses revealed regulation of different pathways including EIF2 signaling, eIF4 and p70S6K signaling, mTOR signaling and oxidative phosphorylation (Figure 4.7 B) in Kdm6a-deficient tumor cells. We focused on the mTOR pathway due to its important implications in tumorigenesis and its potential as chemotherapeutic target in clinical settings. Lei et al. previously reported increased p-Akt and p-mTOR level through increased methylation at the Pten promoter in neural stem cell upon loss of Kdm6a [140]. However, loss of Kdm6a in our c-MYC mouse model neither changed the H3K27-me3 levels on the Pten promoter nor transcriptional levels of Pten. Furthermore, there was also no increased sensitivity towards PI3K inhibition in Kdm6a-deficient tumor cells. Thus, these findings suggest that hyperactivation of mTORC1 signaling in our Kdm6a-deficient liver tumors is likely to be Pten-independent. Nevertheless, Kdm6a-dependent Pten regulation was described in a developmental context without other genetic interventions while our study was performed in a disease/tumorigenesis context that involved expression of other

oncogenes. Therefore, it would be interesting to assess mTORC1 signaling activity upon Kdm6a deletion in developmental models or under physiological conditions in the liver as described by Lei and colleagues. Moreover, it would be also tempting to examine whether Pten expression in our Myc; TRE shKdm6a mouse model could rescue the Kdm6a phenotype.

Through RNA-seq and Cut&Run data analysis, we found that Kdm6a negatively regulates mTORC1 activity through Deptor, a known mTOR negative regulator of mTOR, in our c-MYC driven liver tumor by positively regulating Deptor at mRNA and protein levels (Figure 4.9 A and B). Interestingly, Liu et al. showed recently that mTORC1 signaling is indispensable for c-MYC driven tumorigenesis and disruption of Raptor, the unique member of the mTORC1 complex, strongly inhibits c-MYC-driven liver tumor formation [141]. Moreover, this dependency of c-MYC oncogenic activity to mTOR pathway was also described by Pourdehnad et al. in lymphomas where mTOR-dependent phosphorylation of 4EBP1 is essential for c-MYC driven tumor initiation and maintenance [142]. Hence, these observations might explain the synergistic effect of c-MYC and Kdm6a in our model, where loss of Kdm6a leads to hyperactivated mTORC1 signaling, which is essential for c-MYC driven hepatocarcinogenesis. Moreover, in previous HDTVi experiments we also found a strong synergistic effect of c-MYC with either myr-Akt expression or Pten knockout to induce liver tumors. Both Akt and Pten are known to be upstream of mTORC1 signaling but can also feed in other signaling nodes. Thus, it would be of significant interest to further examine, if these tumors are also largely dependent on mTORC1 signaling like Kdm6a-deficient tumors or depend also on inhibition of other downstream signaling nodes.

5.3 Kdm6a re-expression induces apoptosis

While c-MYC is an established oncogene, c-MYC over-expression alone is insufficient to drive malignant transformation in our model. In fact, in the early 1990s Evan and colleagues discovered induction of apoptosis by c-MYC in fibroblast where cells with enforced c-MYC expression undergo apoptosis following growth factor withdrawal [17]. Subsequently, Cleveland and colleagues described that c-MYC overexpression triggered interleukin-3-dependent apoptosis in 32Dcl3 myeloid progenitor cells [18]. Research on the involvement of c-MYC in apoptosis has been extensive and studies have identified several associated pathways that mediate the apoptotic responses

including activation of $p19^{ARF}$- p53-driven apoptosis due to increase in transcriptional burden and genomic stability [143, 144]. Loss or downregulation of Kdm6a enables c-MYC-driven hepatocellular carcinogenesis, while re-expression of Kdm6a appeared to lead to activated caspase 3-driven cell death in our c-MYC driven liver tumors. While we are yet to determine the precise mechanisms for caspase3 activation, our RNA-seq data implied minimal activation of the established c-MYC driven $p19^{ARF}$- p53 cellular apoptosis response as described by Zindy et al. despite functional p53 in Kdm6a-deficient cell lines indicated by clear p53 induction in response to doxorubicin (data not shown).

Interestingly, our RNA-seq data from Myc; TRE shKdm6a cell lines documented significant induction of Fas (CD95) transcripts upon Kdm6a re-expression. Fas was first described by Nagata et al. as a death receptor that belongs to the tumor necrosis factor receptor superfamily [145, 146]. Interaction of Fas with its ligand FasL induces the recruitment of Fas-associated protein with death domain (FADD), which leads to activation of apoptosis-initiating proteases, such as caspase-8. The activation of caspase-8 can subsequently induce apoptosis through various molecules including caspase-3 and caspase-7 [147]. This might explain the mechanisms of increased caspase activation upon Kdm6a re-expression in our study.

Beside from what was mentioned before, a study by Wendel et al. featured mTORC1 inhibition in c-MYC-driven lymphoma model induces apoptosis and reverses chemo-resistance [148]. In context of liver malignancies, mTOR inhibition was also shown to increase cell apoptosis in YAP/TAZ-driven hepatoblastoma assessed by the increased caspase-3 activity and apoptosis was induced by downregulation of pro-survival proteins such as Survivin as well as upregulation of pro-apoptotic protein such as Bak [149]. Moreover, it was previously demonstrated that in c-MYC-driven liver cancer, E2F1 exerted an anti-apoptotic property through the mTOR pathway [150]. Altogether these findings further suggest an important role of mTOR signaling in preventing apoptosis, which could also explain our observation of increased apoptosis upon Kdm6a re-expression in our Myc; TRE shKdm6a model.

5.4 Therapeutic possibilities of Kdm6a-deficient tumors

Due to its known demethylase activity on the H3K27, studies have related the tumor suppressive function of Kdm6a to its catalytic function and subsequently found that

inhibition of its counterpart Ezh2, a known H3K27 methylase, to arrest Kdm6a-deficient tumor growth. This vulnerability of Kdm6a-deficient tumors to Ezh2 inhibitors, such as GSK126, has been confirmed in bladder cancer [133], lung cancer [151], multiple myeloma [92], and T-cell acute lymphoblastic leukemia [87]. Although we did not perform Ezh2 inhibitor treatment in our study, CRISPR/Cas9 mediated knockout of Ezh2 or Eed in Kdm6a-deficient tumors did not affect their proliferation or viability assessed by competition assay (data not shown). In addition, H3K27me3 level were unaltered upon Kdm6a expression and its tumor suppressive function appears to be independent of its demethylase activity, at least in our models. Hence we did not expect increased sensitivity towards Ezh2 inhibitors.

Considering the dependency of Kdm6a-deficient tumors towards mTORC1 signaling, we examined the specific toxicity of mTOR inhibitors in KDM6A-deficient cells. As expected, increased sensitivity towards three different mTOR inhibitors Rapamycin, Torin1 and Onatasertib was observed in Kdm6a-deficient cells but not in Kdm6a proficient cells, suggesting the regulation of mTORC1 signaling by Kdm6a leads to a specific vulnerability. Since there are some FDA-approved mTOR inhibitors available, the therapeutic potential of mTOR inhibitors such as Rapamycin using Rapamune (Pfizer) in Kdm6a-deficient tumors needs to be assessed further, especially using *in vivo* experiments to confirm the observed vulnerability of Kdm6a-deficient tumor cells *in vitro*.

5.5 Loss of Kdm6a exerts specific vulnerability towards Hdac3

To further account for the apparent Kdm6a tumor suppressive activity, we investigated whether Kdm6a-deficient tumors exhibit particular dependency on certain epigenetic genes. Our CRISPR/Cas9 screening and subsequent validation identified Hdac3 as a novel vulnerability for the Kdm6a-deficient tumors. Whereas both, Kdm6a and Hdac3, play direct roles in post-translational histone modification, the link between the two genes has yet to be explored.

Hdac3 is an enzyme that catalyzes deacetylation of histones and non-histone proteins [152]. Although it is widely accepted as a specific lysine deacetylase enzyme, it is not much known which histone marks or which substrates Hdac3 deacetylates. To date, there are two studies describing that Hdac3 removes acetyl groups from H3K27 [153] and H3K9 [154] and thus repressing proximal gene expression. Since histone

deacetylation is a mechanism of epigenetic gene repression, Hdac3 is also important in transcriptional regulation, cell cycle progression, and developmental events. In order to completely understand the mechanism how Hdac3 disruption in Kdm6a-deficient cells leads to lethality, one would need to perform epigenetic profiling to evaluate changes in the epigenetic landscape upon Hdac3 repression/deletion.

There was one study in 2018 by Watanabe et al. that demonstrated specific vulnerability of KDM6A knockout in PDAC cells to HDAC inhibitors through enrichment of H3K27ac in CDKN1A locus [95]. However, our findings cannot recapitulate this and we find only minimal alterations of H3K27ac in Cdkn1a. However, this study certainly differs in liver cells versus pancreatic cells and mouse cells versus human cells. Moreover, the HDAC inhibitor used in this study is not specific for HDAC3 and instead targets multiple HDACs at the same time.

Reported studies in literature also describe Hdac3 as a class I histone deacetylase with regulatory functions in lipid metabolism [155, 156], transcriptional regulation [157] and inflammatory responses [158] via both of its deacetylase activity as well as in a complex with other proteins [159]. HDAC3 had been reported to form a complex with NCoR and SMRT (NCoR2) to abrogate inflammatory cell response via repression of JNK pathway [160]. The JNK pathway, however, is also known to promote cell death via upregulation of pro-apoptotic genes via the transactivation of c-Jun or by directly modulating the activities of mitochondrial pro- and anti-apoptotic proteins through distinct phosphorylation events [161]. Relevant to this observation, our Cut&Run experiment established binding of Kdm6a to NCoR2 genes. Moreover, gene dependency analysis using publicly available DepMap database revealed significant Kdm6a dependency to NCoR in multiple cancer such as gastric, colorectal, skin, bile duct, and blood cancer (depmap.org). Taken these observations together, one could speculate that Kdm6a may exert its tumor suppressive function via JNK-mediated cell death. Specifically, loss or downregulation of Kdm6a may cooperate with HDAC3/NCoR/SMRT complex to repress JNK-activated cell death mechanisms.

On the other hand, studies also demonstrated that Hdac3 binds to and deacetylates Akt, which leads to activation of its kinase activity in acute myeloid leukemia and in atherosclerosis development [162, 163]. In leukemia, Hdac3 expression is frequently reported to cause chemo-resistance due to activation of PI3K/Akt signaling pathway [162, 164]. This activation of PI3K/Akt signaling by Hdac3 was also confirmed in atherosclerosis [165]. Based on these findings it is tempting to

speculate that disruption of Hdac3 in Kdm6a-deficient cells will lead to its dissociation with Akt and thus decrease the kinase activity of Akt. This downregulation of Akt signaling could also affect mTORC1 signaling, which we found Kdm6a-deficient cells are strongly dependent on. Of course further studies will be needed to proof this relation between Hdac3 and mTORC1 signaling in Kdm6a-deficient tumors.

Finally, for the future therapeutic possibilities, it will be very important to also evaluate the sensitivity of Kdm6a-deficient cells to pharmacological inhibition of Hdac3 . There are already a few FDA-approved Hdac inhibitors available for clinical use but there is also one selective Hdac3 inhibitor, RGFP966, that can be used in this regard. Additionally, a combination treatment with mTOR inhibitor and Hdac3 inhibitor would be interesting in order to perform any possible synergistic effect between both inhibitors.

5.6 Tumor suppressive function of Kdm6a beyond liver cancer

In order to study the molecular function of Kdm6a in another genetic context, we developed an ESC-based PDAC model with oncogenic $Kras^{G12D}$ mutation. This $Kras^{G12D}$ mutation together with Kdm6a disruption in murine pancreata reflects the genetic condition of a subset of PDAC patients [166]. Using our PDAC model, we demonstrated that downregulation of Kdm6a together with $Kras^{G12D}$ led to pancreatic malignancies through hyperactivation of mTORC1 signaling. As a consequence, these tumors were also very sensitive to mTOR inhibitors, such as Torin1, at least *in vitro*. Interestingly, cooperation between $Kras^{G12D}$ and Kdm6a in tumor initiation and maintenance was shown before in lung and pancreatic cancer, where loss of Kdm6a contributes to tumorigenesis in these genetic contexts [94, 151, 167]. In these settings Wu et al. described that Kdm6a loss led to deregulation of PRC2 target genes while Andricovich and colleagues demonstrated that loss of Kdm6a caused aberrant activation of super enhancers [94, 151]. Although further *in vivo* experiments confirming the efficacy of mTOR inhibitor in Kdm6a-deficient tumor are still needed, our novel findings might serve as new therapeutic strategy for lung and pancreatic cancer patients with Kdm6a loss.

6. Supplementary Data

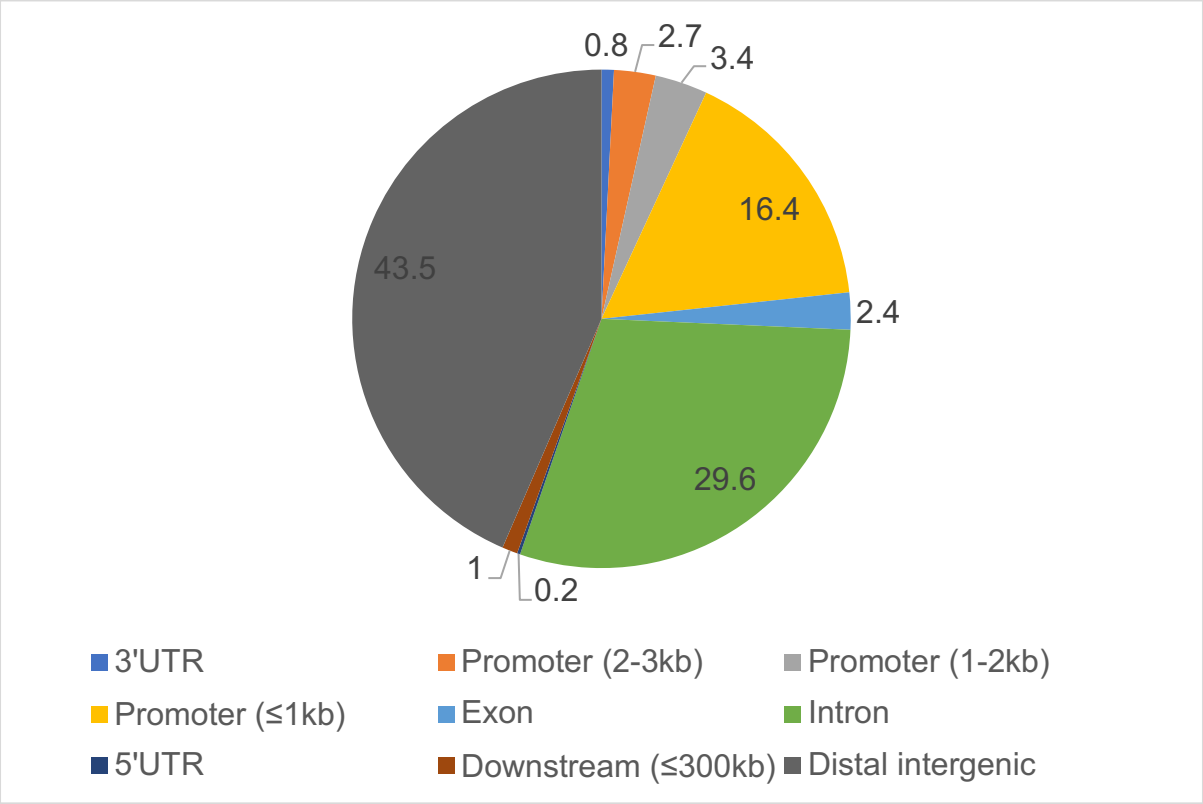

Suppl. Figure 1 Binding sites of Kdm6a genome-wide based on Cut&Run profiling.

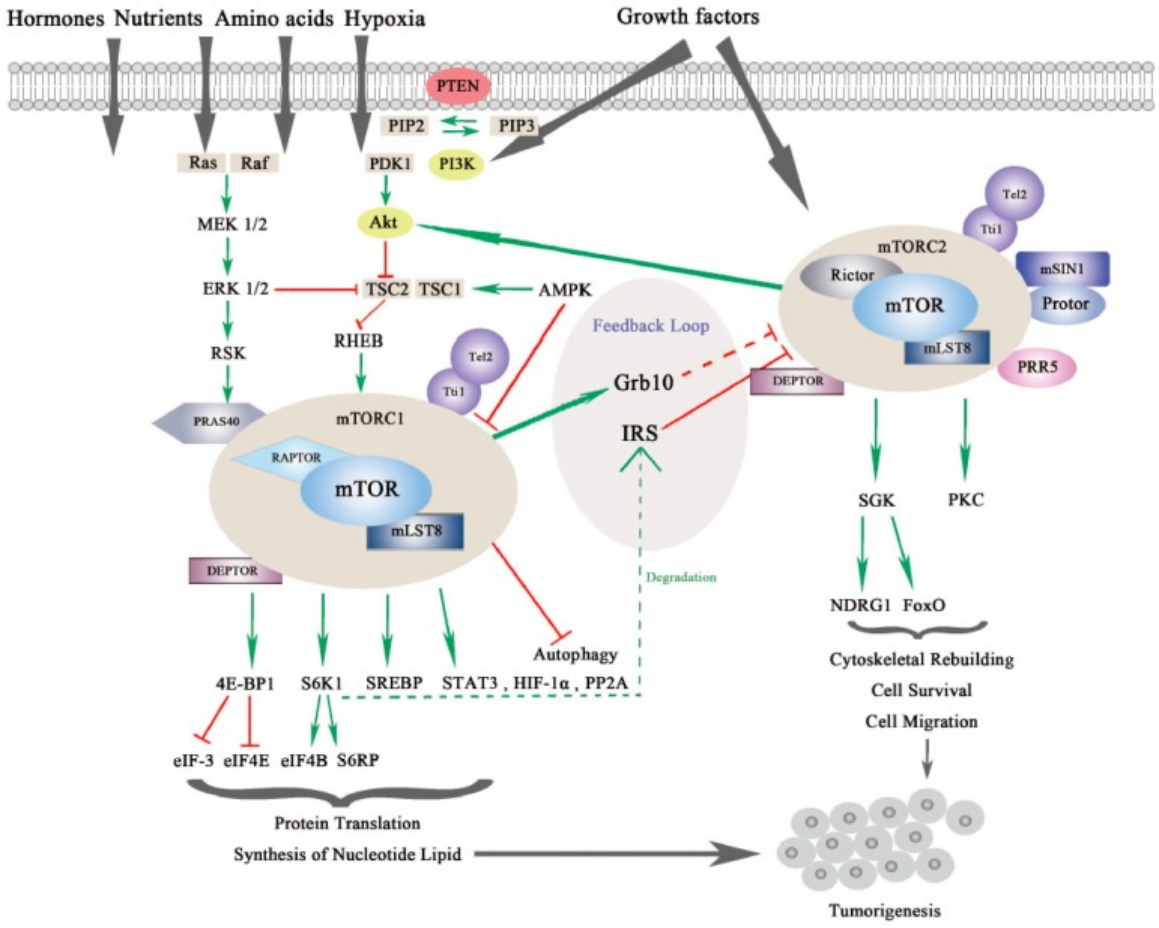

Suppl. Figure 2 The mTOR complexes and signaling pathway of mTORC1 and mTORC2;Unmodified taken from Tian et al. [130].

7. Bibliography

1. (US), N.I.o.H., *Biological Sciences Curriculum Study.* , in *NIH Curriculum Supplement Series [Internet]*. 2007: Bethesda (MD). p. https://www.ncbi.nlm.nih.gov/books/NBK20362/.
2. Institute, N.C., *Defining Cancer* 17 September 2007.
3. Organization, W.H., *Cancer*. 12 September 2018.
4. Vogelstein, B. and K.W. Kinzler, *The multistep nature of cancer.* Trends Genet, 1993. **9**(4): p. 138-41.
5. Yi, K. and Y.S. Ju, *Patterns and mechanisms of structural variations in human cancer.* Experimental & molecular medicine, 2018. **50**(8): p. 98-98.
6. Meyerson, M., S. Gabriel, and G. Getz, *Advances in understanding cancer genomes through second-generation sequencing.* Nat Rev Genet, 2010. **11**(10): p. 685-96.
7. Hanahan, D. and R.A. Weinberg, *The Hallmarks of Cancer.* Cell, 2000. **100**(1): p. 57-70.
8. Hanahan, D. and Robert A. Weinberg, *Hallmarks of Cancer: The Next Generation.* Cell, 2011. **144**(5): p. 646-674.
9. Fouad, Y.A. and C. Aanei, *Revisiting the hallmarks of cancer.* American journal of cancer research, 2017. **7**(5): p. 1016-1036.
10. Watson, I.R., et al., *Emerging patterns of somatic mutations in cancer.* Nature reviews. Genetics, 2013. **14**(10): p. 703-718.
11. Zhu, K., et al., *Oncogenes and tumor suppressor genes: comparative genomics and network perspectives.* BMC genomics, 2015. **16 Suppl 7**(Suppl 7): p. S8-S8.
12. Feitelson, M.A., et al., *Genetic mechanisms of hepatocarcinogenesis.* Oncogene, 2002. **21**(16): p. 2593-2604.
13. Nevzorova, Y.A., et al., *Overexpression of c-myc in hepatocytes promotes activation of hepatic stellate cells and facilitates the onset of liver fibrosis.* Biochimica et Biophysica Acta (BBA) - Molecular Basis of Disease, 2013. **1832**(10): p. 1765-1775.
14. Bournet, B., et al., *KRAS G12D Mutation Subtype Is A Prognostic Factor for Advanced Pancreatic Adenocarcinoma.* Clinical and translational gastroenterology, 2016. **7**(3): p. e157-e157.
15. *KRAS(G12D) Gene Dosage Drives Pancreatic Tumor Evolution and Progression.* Cancer Discov, 2018. **8**(3): p. 265.
16. Pelengaris, S., M. Khan, and G. Evan, *c-MYC: more than just a matter of life and death.* Nature Reviews Cancer, 2002. **2**(10): p. 764-776.
17. Evan, G.I., et al., *Induction of apoptosis in fibroblasts by c-myc protein.* Cell, 1992. **69**(1): p. 119-28.
18. Askew, D.S., et al., *Constitutive c-myc expression in an IL-3-dependent myeloid cell line suppresses cell cycle arrest and accelerates apoptosis.* Oncogene, 1991. **6**(10): p. 1915-22.
19. Kress, T.R., A. Sabò, and B. Amati, *MYC: connecting selective transcriptional control to global RNA production.* Nature Reviews Cancer, 2015. **15**(10): p. 593-607.
20. Felsher, D.W. and J.M. Bishop, *Transient excess of MYC activity can elicit genomic instability and tumorigenesis.* Proceedings of the National Academy of Sciences of the United States of America, 1999. **96**(7): p. 3940-3944.
21. Vafa, O., et al., *c-Myc Can Induce DNA Damage, Increase Reactive Oxygen Species, and Mitigate p53 Function: A Mechanism for Oncogene-Induced Genetic Instability.* Molecular Cell, 2002. **9**(5): p. 1031-1044.

22. Thorgeirsson, S.S. and E. Santoni-Rugiu, *Transgenic mouse models in carcinogenesis: interaction of c-myc with transforming growth factor alpha and hepatocyte growth factor in hepatocarcinogenesis.* Br J Clin Pharmacol, 1996. **42**(1): p. 43-52.
23. Freimuth, J., et al., *Application of magnetic resonance imaging in transgenic and chemical mouse models of hepatocellular carcinoma.* Molecular Cancer, 2010. **9**(1): p. 94.
24. Ju, H.L., et al., *Transgenic mouse models generated by hydrodynamic transfection for genetic studies of liver cancer and preclinical testing of anti-cancer therapy.* Int J Cancer, 2016. **138**(7): p. 1601-8.
25. di Magliano, M.P. and C.D. Logsdon, *Roles for KRAS in pancreatic tumor development and progression.* Gastroenterology, 2013. **144**(6): p. 1220-9.
26. Spaargaren, M., J.R. Bischoff, and F. McCormick, *Signal transduction by Ras-like GTPases: a potential target for anticancer drugs.* Gene Expr, 1995. **4**(6): p. 345-56.
27. Scheffzek, K., et al., *The Ras-RasGAP complex: structural basis for GTPase activation and its loss in oncogenic Ras mutants.* Science, 1997. **277**(5324): p. 333-8.
28. Sherr, C.J., *Principles of tumor suppression.* Cell, 2004. **116**(2): p. 235-46.
29. Sun, W. and J. Yang, *Functional mechanisms for human tumor suppressors.* J Cancer, 2010. **1**: p. 136-40.
30. Wang, L.H., et al., *Loss of Tumor Suppressor Gene Function in Human Cancer: An Overview.* Cell Physiol Biochem, 2018. **51**(6): p. 2647-2693.
31. Stracquadanio, G., et al., *The importance of p53 pathway genetics in inherited and somatic cancer genomes.* Nat Rev Cancer, 2016. **16**(4): p. 251-65.
32. Olivier, M., et al., *The IARC TP53 database: New online mutation analysis and recommendations to users.* Human Mutation, 2002. **19**(6): p. 607-614.
33. Joosten, S.C., et al., *Epigenetics in renal cell cancer: mechanisms and clinical applications.* Nature Reviews Urology, 2018. **15**(7): p. 430-451.
34. Chen, Z., et al., *Epigenetic Regulation: A New Frontier for Biomedical Engineers.* Annual Review of Biomedical Engineering, 2017. **19**(1): p. 195-219.
35. Angiolilli, C., et al., *New insights into the genetics and epigenetics of systemic sclerosis.* Nature Reviews Rheumatology, 2018. **14**(11): p. 657-673.
36. Smith, Z.D. and A. Meissner, *DNA methylation: roles in mammalian development.* Nat Rev Genet, 2013. **14**(3): p. 204-20.
37. Zhou, V.W., A. Goren, and B.E. Bernstein, *Charting histone modifications and the functional organization of mammalian genomes.* Nat Rev Genet, 2011. **12**(1): p. 7-18.
38. Esteller, M., *Epigenetics in cancer.* N Engl J Med, 2008. **358**(11): p. 1148-59.
39. Seles, M., et al., *Current Insights into Long Non-Coding RNAs in Renal Cell Carcinoma.* Int J Mol Sci, 2016. **17**(4): p. 573.
40. Chi, P., C.D. Allis, and G.G. Wang, *Covalent histone modifications--miswritten, misinterpreted and mis-erased in human cancers.* Nat Rev Cancer, 2010. **10**(7): p. 457-69.
41. Kandoth, C., et al., *Mutational landscape and significance across 12 major cancer types.* Nature, 2013. **502**(7471): p. 333-339.
42. Berger, S.L., et al., *An operational definition of epigenetics.* Genes Dev, 2009. **23**(7): p. 781-3.
43. Khan, M.I., et al., *Targeting epigenome with dietary nutrients in cancer: Current advances and future challenges.* Pharmacol Res, 2018. **129**: p. 375-387.

44. Takai, D. and P.A. Jones, *Comprehensive analysis of CpG islands in human chromosomes 21 and 22.* Proceedings of the National Academy of Sciences, 2002. **99**(6): p. 3740-3745.
45. Rodriguez-Paredes, M. and M. Esteller, *Cancer epigenetics reaches mainstream oncology.* Nat Med, 2011. **17**(3): p. 330-9.
46. Feinberg, A.P., R. Ohlsson, and S. Henikoff, *The epigenetic progenitor origin of human cancer.* Nature Reviews Genetics, 2006. **7**(1): p. 21-33.
47. Kanwal, R. and S. Gupta, *Epigenetic modifications in cancer.* Clinical genetics, 2012. **81**(4): p. 303-311.
48. Kouzarides, T., *Chromatin modifications and their function.* Cell, 2007. **128**(4): p. 693-705.
49. Portela, A. and M. Esteller, *Epigenetic modifications and human disease.* Nat Biotechnol, 2010. **28**(10): p. 1057-68.
50. Dalgliesh, G.L., et al., *Systematic sequencing of renal carcinoma reveals inactivation of histone modifying genes.* Nature, 2010. **463**(7279): p. 360-3.
51. Cao, K. and A. Shilatifard, *Enhancers in Cancer: Genetic and Epigenetic Deregulation*, in *Encyclopedia of Cancer (Third Edition)*, P. Boffetta and P. Hainaut, Editors. 2019, Academic Press: Oxford. p. 559-568.
52. Funato, K. and V. Tabar, *Histone Mutations in Cancer.* Annual Review of Cancer Biology, 2018. **2**(1): p. 337-351.
53. Sarthy, J.F. and S. Henikoff, *Bringing Oncohistones into the Fold.* Cancer Discovery, 2019. **9**(10): p. 1346-1348.
54. Nacev, B.A., et al., *The expanding landscape of 'oncohistone' mutations in human cancers.* Nature, 2019. **567**(7749): p. 473-478.
55. Hu, D., et al., *The MLL3/MLL4 Branches of the COMPASS Family Function as Major Histone H3K4 Monomethylases at Enhancers.* Molecular and Cellular Biology, 2013. **33**(23): p. 4745-4754.
56. Smith, E., C. Lin, and A. Shilatifard, *The super elongation complex (SEC) and MLL in development and disease.* Genes Dev, 2011. **25**(7): p. 661-72.
57. Piunti, A. and A. Shilatifard, *Epigenetic balance of gene expression by Polycomb and COMPASS families.* Science, 2016. **352**(6290): p. aad9780.
58. Wang, L. and A. Shilatifard, *UTX Mutations in Human Cancer.* Cancer Cell, 2019. **35**(2): p. 168-176.
59. Ong, C.K., et al., *Exome sequencing of liver fluke-associated cholangiocarcinoma.* Nat Genet, 2012. **44**(6): p. 690-3.
60. Song, Y., et al., *Identification of genomic alterations in oesophageal squamous cell cancer.* Nature, 2014. **509**(7498): p. 91-5.
61. Watanabe, Y., et al., *Frequent alteration of MLL3 frameshift mutations in microsatellite deficient colorectal cancer.* PLoS One, 2011. **6**(8): p. e23320.
62. Fujimoto, A., et al., *Whole-genome sequencing of liver cancers identifies etiological influences on mutation patterns and recurrent mutations in chromatin regulators.* Nat Genet, 2012. **44**(7): p. 760-4.
63. Gu, D.L., et al., *Target genes discovery through copy number alteration analysis in human hepatocellular carcinoma.* World J Gastroenterol, 2013. **19**(47): p. 8873-9.
64. Sze, C.C. and A. Shilatifard, *MLL3/MLL4/COMPASS Family on Epigenetic Regulation of Enhancer Function and Cancer.* Cold Spring Harbor perspectives in medicine, 2016. **6**(11): p. a026427.

65. Kanda, H., et al., *The Drosophila ortholog of MLL3 and MLL4, trithorax related, functions as a negative regulator of tissue growth.* Mol Cell Biol, 2013. **33**(9): p. 1702-10.
66. Lee, J., et al., *A tumor suppressive coactivator complex of p53 containing ASC-2 and histone H3-lysine-4 methyltransferase MLL3 or its paralogue MLL4.* Proc Natl Acad Sci U S A, 2009. **106**(21): p. 8513-8.
67. Kantidakis, T., et al., *Mutation of cancer driver MLL2 results in transcription stress and genome instability.* Genes Dev, 2016. **30**(4): p. 408-20.
68. Hong, S., et al., *Identification of JmjC domain-containing UTX and JMJD3 as histone H3 lysine 27 demethylases.* Proc Natl Acad Sci U S A, 2007. **104**(47): p. 18439-44.
69. Arcipowski, K.M., C.A. Martinez, and P. Ntziachristos, *Histone demethylases in physiology and cancer: a tale of two enzymes, JMJD3 and UTX.* Curr Opin Genet Dev, 2016. **36**: p. 59-67.
70. Li, X., et al., *UTX is an escape from X-inactivation tumor-suppressor in B cell lymphoma.* Nature Communications, 2018. **9**(1): p. 2720.
71. Greenfield, A., et al., *The UTX gene escapes X inactivation in mice and humans.* Hum Mol Genet, 1998. **7**(4): p. 737-42.
72. Dunford, A., et al., *Tumor-suppressor genes that escape from X-inactivation contribute to cancer sex bias.* Nat Genet, 2017. **49**(1): p. 10-16.
73. Hong, S., et al., *Identification of JmjC domain-containing UTX and JMJD3 as histone H3 lysine 27 demethylases.* Proceedings of the National Academy of Sciences, 2007. **104**(47): p. 18439-18444.
74. Walport, L.J., et al., *Human UTY(KDM6C) is a male-specific N-methyl lysyl demethylase.* J Biol Chem, 2014. **289**(26): p. 18302-13.
75. Herz, H.M., et al., *The H3K27me3 demethylase dUTX is a suppressor of Notch- and Rb-dependent tumors in Drosophila.* Mol Cell Biol, 2010. **30**(10): p. 2485-97.
76. Lee, M.G., et al., *Demethylation of H3K27 Regulates Polycomb Recruitment and H2A Ubiquitination.* Science, 2007. **318**(5849): p. 447-450.
77. Sengoku, T. and S. Yokoyama, *Structural basis for histone H3 Lys 27 demethylation by UTX/KDM6A.* Genes Dev, 2011. **25**(21): p. 2266-77.
78. Wang, C., et al., *UTX regulates mesoderm differentiation of embryonic stem cells independent of H3K27 demethylase activity.* Proceedings of the National Academy of Sciences, 2012. **109**(38): p. 15324-15329.
79. Wang, S.-P., et al., *A UTX-MLL4-p300 Transcriptional Regulatory Network Coordinately Shapes Active Enhancer Landscapes for Eliciting Transcription.* Molecular cell, 2017. **67**(2): p. 308-321.e6.
80. Shpargel, K.B., et al., *UTX and UTY demonstrate histone demethylase-independent function in mouse embryonic development.* PLoS Genet, 2012. **8**(9): p. e1002964.
81. Vandamme, J., et al., *The C. elegans H3K27 demethylase UTX-1 is essential for normal development, independent of its enzymatic activity.* PLoS Genet, 2012. **8**(5): p. e1002647.
82. Miller, S.A., S.E. Mohn, and A.S. Weinmann, *Jmjd3 and UTX play a demethylase-independent role in chromatin remodeling to regulate T-box family member-dependent gene expression.* Molecular cell, 2010. **40**(4): p. 594-605.
83. Seenundun, S., et al., *UTX mediates demethylation of H3K27me3 at muscle-specific genes during myogenesis.* EMBO J, 2010. **29**(8): p. 1401-11.

84. Shpargel, K.B., et al., *KDM6 demethylase independent loss of histone H3 lysine 27 trimethylation during early embryonic development.* PLoS Genet, 2014. **10**(8): p. e1004507.
85. Welstead, G.G., et al., *X-linked H3K27me3 demethylase Utx is required for embryonic development in a sex-specific manner.* Proc Natl Acad Sci U S A, 2012. **109**(32): p. 13004-9.
86. Wang, C., et al., *UTX regulates mesoderm differentiation of embryonic stem cells independent of H3K27 demethylase activity.* Proc Natl Acad Sci U S A, 2012. **109**(38): p. 15324-9.
87. Van der Meulen, J., et al., *The H3K27me3 demethylase UTX is a gender-specific tumor suppressor in T-cell acute lymphoblastic leukemia.* Blood, 2015. **125**(1): p. 13-21.
88. Ntziachristos, P., et al., *Contrasting roles of histone 3 lysine 27 demethylases in acute lymphoblastic leukaemia.* Nature, 2014. **514**(7523): p. 513-7.
89. Mar, B.G., et al., *Sequencing histone-modifying enzymes identifies UTX mutations in acute lymphoblastic leukemia.* Leukemia, 2012. **26**(8): p. 1881-1883.
90. Jankowska, A.M., et al., *Mutational spectrum analysis of chronic myelomonocytic leukemia includes genes associated with epigenetic regulation: UTX, EZH2, and DNMT3A.* Blood, 2011. **118**(14): p. 3932-3941.
91. van Haaften, G., et al., *Somatic mutations of the histone H3K27 demethylase gene UTX in human cancer.* Nat Genet, 2009. **41**(5): p. 521-523.
92. Ezponda, T., et al., *UTX/KDM6A Loss Enhances the Malignant Phenotype of Multiple Myeloma and Sensitizes Cells to EZH2 inhibition.* Cell reports, 2017. **21**(3): p. 628-640.
93. Nickerson, M.L., et al., *Concurrent alterations in TERT, KDM6A, and the BRCA pathway in bladder cancer.* Clin Cancer Res, 2014. **20**(18): p. 4935-48.
94. Andricovich, J., et al., *Loss of KDM6A Activates Super-Enhancers to Induce Gender-Specific Squamous-like Pancreatic Cancer and Confers Sensitivity to BET Inhibitors.* Cancer Cell, 2018. **33**(3): p. 512-526.e8.
95. Watanabe, S., et al., *Loss of KDM6A characterizes a poor prognostic subtype of human pancreatic cancer and potentiates HDAC inhibitor lethality.* Int J Cancer, 2019. **145**(1): p. 192-205.
96. van Haaften, G., et al., *Somatic mutations of the histone H3K27 demethylase gene UTX in human cancer.* Nature Genetics, 2009. **41**(5): p. 521-523.
97. Bhatia, S.N., et al., *Cell and tissue engineering for liver disease.* Science translational medicine, 2014. **6**(245): p. 245sr2-245sr2.
98. Gordillo, M., T. Evans, and V. Gouon-Evans, *Orchestrating liver development.* Development, 2015. **142**(12): p. 2094-2108.
99. Ryerson, A.B., et al., *Annual Report to the Nation on the Status of Cancer, 1975-2012, featuring the increasing incidence of liver cancer.* Cancer, 2016. **122**(9): p. 1312-1337.
100. Mann, D.A., *Epigenetics in liver disease.* Hepatology, 2014. **60**(4): p. 1418-25.
101. Goeppert, B., et al., *Global alterations of DNA methylation in cholangiocarcinoma target the Wnt signaling pathway.* Hepatology, 2014. **59**(2): p. 544-54.
102. Lee, S., et al., *Aberrant CpG island hypermethylation along multistep hepatocarcinogenesis.* The American journal of pathology, 2003. **163**(4): p. 1371-1378.
103. Liu, M., L. Jiang, and X.-Y. Guan, *The genetic and epigenetic alterations in human hepatocellular carcinoma: a recent update.* Protein & cell, 2014. **5**(9): p. 673-691.
104. Bakiri, L. and E.F. Wagner, *Mouse models for liver cancer.* Molecular Oncology, 2013. **7**(2): p. 206-223.

105. Murakami, H., et al., *Transgenic Mouse Model for Synergistic Effects of Nuclear Oncogenes and Growth Factors in Tumorigenesis: Interaction of c-myc and Transforming Growth Factor α in Hepatic Oncogenesis.* Cancer Research, 1993. **53**(8): p. 1719-1723.
106. Suda, T. and D. Liu, *Hydrodynamic Gene Delivery: Its Principles and Applications.* Molecular Therapy, 2007. **15**(12): p. 2063-2069.
107. *High Levels of Foreign Gene Expression in Hepatocytes after Tail Vein Injections of Naked Plasmid DNA.* Human Gene Therapy, 1999. **10**(10): p. 1735-1737.
108. Kamimura, K., et al., *Image-Guided Hydrodynamic Gene Delivery: Current Status and Future Directions.* Pharmaceutics, 2015. **7**(3): p. 213-23.
109. Ivics, Z., et al., *Molecular Reconstruction of Sleeping Beauty, a Tc1-like Transposon from Fish, and Its Transposition in Human Cells.* Cell, 1997. **91**(4): p. 501-510.
110. Dupuy, A.J., et al., *Mammalian mutagenesis using a highly mobile somatic Sleeping Beauty transposon system.* Nature, 2005. **436**(7048): p. 221-226.
111. Logsdon, C.D. and B. Ji, *The role of protein synthesis and digestive enzymes in acinar cell injury.* Nature Reviews Gastroenterology & Hepatology, 2013. **10**(6): p. 362-370.
112. Leung, P.S., *Overview of the pancreas.* Adv Exp Med Biol, 2010. **690**: p. 3-12.
113. Ryan, D.P., T.S. Hong, and N. Bardeesy, *Pancreatic Adenocarcinoma.* New England Journal of Medicine, 2014. **371**(11): p. 1039-1049.
114. Morris, J.P., S.C. Wang, and M. Hebrok, *KRAS, Hedgehog, Wnt and the twisted developmental biology of pancreatic ductal adenocarcinoma.* Nature Reviews Cancer, 2010. **10**(10): p. 683-695.
115. Hezel, A.F., et al., *Genetics and biology of pancreatic ductal adenocarcinoma.* Genes Dev, 2006. **20**(10): p. 1218-49.
116. Brat, D.J., et al., *Progression of pancreatic intraductal neoplasias to infiltrating adenocarcinoma of the pancreas.* Am J Surg Pathol, 1998. **22**(2): p. 163-9.
117. Lee, J.W., et al., *Genetically Engineered Mouse Models of Pancreatic Cancer: The KPC Model (LSL-Kras(G12D/+) ;LSL-Trp53(R172H/+) ;Pdx-1-Cre), Its Variants, and Their Application in Immuno-oncology Drug Discovery.* Current protocols in pharmacology, 2016. **73**: p. 14.39.1-14.39.20.
118. Hingorani, S.R., et al., *Preinvasive and invasive ductal pancreatic cancer and its early detection in the mouse.* Cancer Cell, 2003. **4**(6): p. 437-50.
119. Aguirre, A.J., et al., *Activated Kras and Ink4a/Arf deficiency cooperate to produce metastatic pancreatic ductal adenocarcinoma.* Genes Dev, 2003. **17**(24): p. 3112-26.
120. Westphalen, C.B. and K.P. Olive, *Genetically engineered mouse models of pancreatic cancer.* Cancer journal (Sudbury, Mass.), 2012. **18**(6): p. 502-510.
121. Hingorani, S.R., et al., *Trp53R172H and KrasG12D cooperate to promote chromosomal instability and widely metastatic pancreatic ductal adenocarcinoma in mice.* Cancer Cell, 2005. **7**(5): p. 469-83.
122. Saborowski, M., et al., *A modular and flexible ESC-based mouse model of pancreatic cancer.* Genes & development, 2014. **28**(1): p. 85-97.
123. Hsu, P.D., et al., *DNA targeting specificity of RNA-guided Cas9 nucleases.* Nature Biotechnology, 2013. **31**(9): p. 827-832.
124. Pelossof, R., et al., *Prediction of potent shRNAs with a sequential classification algorithm.* Nat Biotechnol, 2017. **35**(4): p. 350-353.
125. Dickins, R.A., et al., *Probing tumor phenotypes using stable and regulated synthetic microRNA precursors.* Nature Genetics, 2005. **37**(11): p. 1289-1295.

126. Bolger, A.M., M. Lohse, and B. Usadel, *Trimmomatic: a flexible trimmer for Illumina sequence data.* Bioinformatics, 2014. **30**(15): p. 2114-20.
127. Dobin, A., et al., *STAR: ultrafast universal RNA-seq aligner.* Bioinformatics, 2013. **29**(1): p. 15-21.
128. Anders, S., P.T. Pyl, and W. Huber, *HTSeq--a Python framework to work with high-throughput sequencing data.* Bioinformatics, 2015. **31**(2): p. 166-9.
129. Skene, P.J., J.G. Henikoff, and S. Henikoff, *Targeted in situ genome-wide profiling with high efficiency for low cell numbers.* Nature Protocols, 2018. **13**(5): p. 1006-1019.
130. Tian, T., X. Li, and J. Zhang, *mTOR Signaling in Cancer and mTOR Inhibitors in Solid Tumor Targeting Therapy.* International journal of molecular sciences, 2019. **20**(3): p. 755.
131. Shimobayashi, M. and M.N. Hall, *Making new contacts: the mTOR network in metabolism and signalling crosstalk.* Nat Rev Mol Cell Biol, 2014. **15**(3): p. 155-62.
132. Peterson, T.R., et al., *DEPTOR is an mTOR inhibitor frequently overexpressed in multiple myeloma cells and required for their survival.* Cell, 2009. **137**(5): p. 873-886.
133. Ler, L.D., et al., *Loss of tumor suppressor KDM6A amplifies PRC2-regulated transcriptional repression in bladder cancer and can be targeted through inhibition of EZH2.* Sci Transl Med, 2017. **9**(378).
134. Kim, J.-H., et al., *UTX and MLL4 coordinately regulate transcriptional programs for cell proliferation and invasiveness in breast cancer cells.* Cancer research, 2014. **74**(6): p. 1705-1717.
135. Xie, G., et al., *UTX promotes hormonally responsive breast carcinogenesis through feed-forward transcription regulation with estrogen receptor.* Oncogene, 2017. **36**(39): p. 5497-5511.
136. Morozov, V.M., et al., *Inhibitor of H3K27 demethylase JMJD3/UTX GSK-J4 is a potential therapeutic option for castration resistant prostate cancer.* Oncotarget, 2017. **8**(37): p. 62131-62142.
137. Soto, D.R., et al., *KDM6A addiction of cervical carcinoma cell lines is triggered by E7 and mediated by p21CIP1 suppression of replication stress.* PLoS Pathog, 2017. **13**(10): p. e1006661.
138. Wang, J.K., et al., *The histone demethylase UTX enables RB-dependent cell fate control.* Genes Dev, 2010. **24**(4): p. 327-32.
139. Gozdecka, M., et al., *UTX-mediated enhancer and chromatin remodeling suppresses myeloid leukemogenesis through noncatalytic inverse regulation of ETS and GATA programs.* Nat Genet, 2018. **50**(6): p. 883-894.
140. Lei, X. and J. Jiao, *UTX Affects Neural Stem Cell Proliferation and Differentiation through PTEN Signaling.* Stem cell reports, 2018. **10**(4): p. 1193-1207.
141. Liu, P., et al., *A functional mammalian target of rapamycin complex 1 signaling is indispensable for c-Myc-driven hepatocarcinogenesis.* Hepatology (Baltimore, Md.), 2017. **66**(1): p. 167-181.
142. Pourdehnad, M., et al., *Myc and mTOR converge on a common node in protein synthesis control that confers synthetic lethality in Myc-driven cancers.* Proceedings of the National Academy of Sciences of the United States of America, 2013. **110**(29): p. 11988-11993.
143. Zindy, F., et al., *Myc signaling via the ARF tumor suppressor regulates p53-dependent apoptosis and immortalization.* Genes Dev, 1998. **12**(15): p. 2424-33.

144. Hoffman, B. and D.A. Liebermann, *Apoptotic signaling by c-MYC.* Oncogene, 2008. **27**(50): p. 6462-6472.
145. Nagata, S. and P. Golstein, *The Fas death factor.* Science, 1995. **267**(5203): p. 1449-56.
146. Nagata, S., *Apoptosis by Death Factor.* Cell, 1997. **88**(3): p. 355-365.
147. Yamada, A., et al., *Dual Role of Fas/FasL-Mediated Signal in Peripheral Immune Tolerance.* Frontiers in Immunology, 2017. **8**(403).
148. Wendel, H.-G., et al., *Survival signalling by Akt and eIF4E in oncogenesis and cancer therapy.* Nature, 2004. **428**(6980): p. 332-337.
149. Liu, P., et al., *Central role of mTORC1 downstream of YAP/TAZ in hepatoblastoma development.* Oncotarget, 2017. **8**(43): p. 73433-73447.
150. Ladu, S., et al., *E2F1 inhibits c-Myc-driven apoptosis via PIK3CA/Akt/mTOR and COX-2 in a mouse model of human liver cancer.* Gastroenterology, 2008. **135**(4): p. 1322-1332.
151. Wu, Q., et al., *In vivo CRISPR screening unveils histone demethylase UTX as an important epigenetic regulator in lung tumorigenesis.* Proc Natl Acad Sci U S A, 2018. **115**(17): p. E3978-e3986.
152. Zhang, X., et al., *Histone deacetylase 3 (HDAC3) activity is regulated by interaction with protein serine/threonine phosphatase 4.* Genes & development, 2005. **19**(7): p. 827-839.
153. Hatzi, K., et al., *A hybrid mechanism of action for BCL6 in B cells defined by formation of functionally distinct complexes at enhancers and promoters.* Cell reports, 2013. **4**(3): p. 578-588.
154. Mullican, S.E., et al., *Histone deacetylase 3 is an epigenomic brake in macrophage alternative activation.* Genes Dev, 2011. **25**(23): p. 2480-8.
155. Knutson, S.K., et al., *Liver-specific deletion of histone deacetylase 3 disrupts metabolic transcriptional networks.* Embo j, 2008. **27**(7): p. 1017-28.
156. Feng, D., et al., *A circadian rhythm orchestrated by histone deacetylase 3 controls hepatic lipid metabolism.* Science, 2011. **331**(6022): p. 1315-9.
157. Emmett, M.J. and M.A. Lazar, *Integrative regulation of physiology by histone deacetylase 3.* Nature Reviews Molecular Cell Biology, 2019. **20**(2): p. 102-115.
158. Chen, X., et al., *Requirement for the histone deacetylase Hdac3 for the inflammatory gene expression program in macrophages.* Proc Natl Acad Sci U S A, 2012. **109**(42): p. E2865-74.
159. Sun, Z., et al., *Deacetylase-independent function of HDAC3 in transcription and metabolism requires nuclear receptor corepressor.* Mol Cell, 2013. **52**(6): p. 769-82.
160. Zhang, J., et al., *The N-CoR-HDAC3 nuclear receptor corepressor complex inhibits the JNK pathway through the integral subunit GPS2.* Mol Cell, 2002. **9**(3): p. 611-23.
161. Dhanasekaran, D.N. and E.P. Reddy, *JNK signaling in apoptosis.* Oncogene, 2008. **27**(48): p. 6245-6251.
162. Long, J., et al., *Targeting HDAC3, a new partner protein of AKT in the reversal of chemoresistance in acute myeloid leukemia via DNA damage response.* Leukemia, 2017. **31**(12): p. 2761-2770.
163. Zampetaki, A., et al., *Histone deacetylase 3 is critical in endothelial survival and atherosclerosis development in response to disturbed flow.* Circulation, 2010. **121**(1): p. 132-42.
164. Zhang, L., et al., *Bakkenolide A inhibits leukemia by regulation of HDAC3 and PI3K/Akt-related signaling pathways.* Biomed Pharmacother, 2016. **83**: p. 958-966.

165. Martin, D., et al., *Unspliced X-box-binding protein 1 (XBP1) protects endothelial cells from oxidative stress through interaction with histone deacetylase 3.* The Journal of biological chemistry, 2014. **289**(44): p. 30625-30634.
166. Bailey, P., et al., *Genomic analyses identify molecular subtypes of pancreatic cancer.* Nature, 2016. **531**(7592): p. 47-52.
167. Speirs, C.K., et al., *Inactiviation of the Histone H3K27 Demethylase UTX/KDM6A Gene Cooperates with Activated KRAAS in a Lung Carcinogenisis Model Evaluated by MicroPET-CT Imaging.* International Journal of Radiation Oncology • Biology • Physics, 2015. **93**(3): p. S73.

Acknowledgement

I have come to realize that I have spent some of the best and most challenging years of my adult life doing my PhD and I could not have arrived to this moment without the great support of my colleagues, friends and family. Thanks for keep me going! ☺

First and foremost, I would like to express my sincere gratitude to Dr. med. Darjus Felix Tschaharganeh for giving me a unique opportunity to carry out my PhD in his group. Words cannot express how grateful I am for the trust, the guidance and the freedom both personally and scientifically throughout this time. I remembered those days when I just started in his lab, I was surprised that the one-month-old lab was completely up and running. I saw you working at the bench with your energy and enthusiasms, always had an open ear and provided all the supports that I needed as a freshman. You still have not changed despite the lab size growing exponentially. Thank you for inspiring me, for the motivation, for the-pat-in-the-back, for the summer BBQs, and many more. I hope that I met at least your bare minimum expectation as your first PhD student, if not, even better to do your proud…. In a case, I am embarrassing you, you don't have to tell me ☺…..

I would also like to acknowledge my TAC members, Prof. Dr. Ralf Bartenschlager, Prof. Dr. Frank Lyko and Dr. Kyung-Min Noh for the continuous supports from the beginning, the helpful discussions, valuable feedbacks, inputs, and especially being available even during the Covid-19 pandemic. I also want to thank you for your willingness to be part of my PhD-examination committee.

On this occasion, I also wish thank Prof. Dr. Matthias Heikenwälder for the insightful discussion and help with our murine tissue processing/embedding/sectioning for histology. Your passion for science and perspective have inspired me as a research scientist .

I am also thankful to Dr. Pavlo Lutsik and Kersten Breuer from the computational cancer epigenomics for all their extensive support in bioinformatical analysis of the Cut&Run data. In addition, I would like to thank Dr. Agnes Hotz-Wagenblatt for her help in organizing and structuring all our sequencing data but also other computational supports.

Many thanks also goes to Dr. Ana Banito who not only guided me in Cut&Run experiment but also helped me in solving different kind of difficulties along the line. I

remembered how passionate you were about this new technique, that you went to try the Cut&Run and the ChIP-seq side by side and how excited you were to see the techniques was more superior. It is very inspiring and I am grateful that I was able to learn it from you. This Cut&Run experiment contributed an essential part in this project and without this data, the project would not come together as what it is today. Thank you also for the occasional coffee time despite your busy schedule as a PI – I really enjoy our small chit-chat.

A very special thank you goes to Lena for all the countless supports and help in the lab, be it on the weekdays, or the weekends and holidays. Needless to say that without you, neither I would finish nor this project come this far. Thank you for being there during the bad days, thank you for always listening to me and thank you for everything you did throughout your time in and outside the lab. Despite your constant sarcasms, you have become one of my best friend. I am looking forward to our regular coffee date, the Thermomix session and continuing our friendship.

I also thank Lisa and Luise for their technical assistance during my PhD time and all the apprentices and students that had also contributed directly to this work, starting from Christian, Christina, Julia, Aga, and Ellen Yung. Special mentioned for the fellow PhD students, with whom I shared the many hours, ups-downs, and the “Darjus-is-watching-you”. Without you all, my PhD will not be the same. Moreover, despite being in two different buildings, thank you Stephan and Katrin for being my discussion buddies, helping with the proofreading and the silly-together time in ATV. That always lighten up my day. ☺

Finally, I would like to thank my friends outside the lab: Claudia, Anke, Patrick, Anik and Jonas for distracting me from work and remind me there is life outside the lab. I wish I could spend more time with you guys.

Last but not least, Aldwin, my fiancé… you are absolutely my everything throughout this PhD journey and there is no way I could have made it this far without you. There were time when I almost gave up, when I hit the wall and frustrated, you were the one that keep me going, keep me motivated and support me no matter what. I am also incredibly grateful for my family, papa dan mama yang senantiasa memberikan support, kebebasan, dan semuanya. Tanpa support dari papa dan mama, tidak mungkin aku bisa study di Jerman dan juga menempuh jalur PhD ini. To my sisters, Sharleen and Selwyn, thank you for being great listener to all my complaints and mumblings, Thank you!